University of Stavanger

Faculty of Science and Technology

MASTER'S THESIS

Study program/ Specialization: **MSc Petroleum Engineering / Drilling Technology**	Spring semester, 2013 **Open** / Restricted access
Writer: **Sigurd Lund**	…… (Writer's signature)
Faculty supervisor: **Bernt S. Aadnøy** External supervisor(s):	
Title of thesis: **Experimental Circulation Loss Study**	
Credits (ECTS): **30**	
Key words: Circulation Loss Elastoplastic fracturing model Drilling fluid optimization LCM in OBM	Pages: …86…… + enclosure: …3 pages Stavanger, …….. Date/year

Acknowledgement

During the this thesis work I have learned a lot, both when it comes to planning and conducting laboratory experiments as well as what it takes to land a thesis like this. I would have no chance to complete my work without all the people that have helped me. For that I am truly grateful.

MI-Swaco has been very accommodating and helpful in any way. From MI-Swaco I would like to thank Arne Askø, Bjørn Bleie, Jorunn Øvsthus and Beathe Pettersen for taking their time to supervise me, and let me use their laboratory facilities.

Statoil has shown a real interest in my work and provided information and feedback all the way. Tomasz Wroblewski and Tor Henry Omland have been good help and motivation. Their open mind and critical questions have helped me along.

UiS has provided facilities and experienced personnel for me. My supervisor, Prof. Bernt S. Aadnøy, has been a great motivator and a good discussion partner. This thesis would be nothing without Aadnøy's feedbacks and thoughts. Assoc. Prof Mesfin Belayneh and Sivert Drangeid have supervised me for my laboratory experiments. Their knowledge has been indispensable for me.

Abstract

Circulation losses could occur during any operation that involves pumping into a well. As of today, it is recognized as one of the most costly drilling problems. In some situation it might be hard to stop, and usually takes precious rig time to deal with the problem. In order to mitigate the risk of circulation loss solid particles are used in the active drilling fluid, known as lost circulation materials (LCM). These materials have a tendency to increase the fracture gradient of the well. Circulation losses occur in different ways, however, the type of loss that is treatable with LCM are those related to fractures in the wellbore wall. LCMs in the active drilling fluid will create bridges at the fractures; seal them off and stop/reduce the losses.

Numerous of studies have been conducted for water-based drilling fluids, but not so many on oil based fluids. One of the big differences between water and oil based fluids is that the friction between the LCM particles tend to be less for oil based fluids opposed to water based fluids. Due to this reason, the bridges created with an oil-based fluid are, somewhat, more unstable than bridges formed by a water based fluids.

Experiments in this thesis are divided into two parts. Part I attacks the problem of finding a suitable particle size distribution (PSD) for bridging. A theoretical PSD was proposed, but test results showed that the theoretical PSD was not very suitable for bridging purposes. However, an interesting observation was made. As the concentration of smaller particles increases, the fluid seemed to perform better in terms of bridging. The bigger particles form some sort of a framework at the fracture mouth, whereas the smaller particles fills the voids between the bigger particles. This indicates that smaller particles are also important in order to achieve good bridging properties.

The bridging properties of four different materials are tested as LCM in oil based drilling fluid in part II of the experimental part of this work. CaCO3, LC-Lube, Feldspar and Quartz were tested in a bridge apparatus. A couple of different observations were made. Firstly, CaCO3 mixed with LC-Lube (Graphite) has shown to be suitable for creating bridges in water-based systems. In this study, CaCO3 and LC-Lube did not show promising results, not separately or in a mix. On the other hand, Quartz and Feldspar had good results, and was able to withstand a high average pressure for a wide spectrum of fracture openings. This was the case even for reasonably small concentration of the materials mixed in the drilling fluid. Both of these materials had good bridging capabilities with a concentration of 39kg/m3. At a fracture opening of 500-micron, Quartz proved to be 400% better in terms of average test pressure than CaCO3. Generally, particles at the upper part of Mohs scale of hardness performed better than particles at the lower part of Mohs scale. This observation is in line with the recently developed Elastoplastic fracture model from the University of Stavanger.

Synergy between the materials was also tested. No good combinations were found. All materials acted better as LCM separately opposed to being in a mixture with any of the other materials.

Table of Content

List of Figures

List of Tables

Abbreviations

ECD	Equivalent circulation density
LCM	Lost circulation material
LOT	Leak-off test
XLOT	Extended leak-off test
PSD	Particle size distribution
OBM	Oil based mud
WBM	Water based mud
MWD	Measurement While Drilling
FCS	Fracture Closure Stress
BOP	Blowout preventer
IPT	Ideal Packing Theory

Nomenclature

σ_h	Minimum horizontal stress	psi | bar
σ_H	Maximum horizontal stress	psi | bar
σ_v	Vertical/Overburden stress	psi | bar
ν	Poisson's ratio	-
β	Biot's constant	-
P_o	Pore pressure	psi | bar
P_w	Well pressure	psi | bar
ρ_b	Formation bulk density	-
g	Gravitational constant	ft/s^2 | m/s^2
γ	Formation average specific gravity	-
d	Depth	m | ft
τ	Shear stress	psi | bar
ϒ	Shear strain	-
ε	Normal strain	-
G	Modulus of rigidity	psi | bar
E	Young's Modulus of elasticity	psi | bar
P_{wf}	Fracture pressure	psi | bar
D, d	Diameter	m | in
w	Fracture width	m | in

1 Introduction

1.1 Background of the Thesis

During drilling, numerous of situations could occur such as stuck pipe, circulation losses, issues with tools, downhole communication problems etc. These problems happen due to different reasons, but a common consequence is a potentially very high cost.

This thesis concerns circulation losses and how preventive measures can be used in order to avoid lost circulation. Losses could happen in different ways. Fluid might escape into the formation when drilling into a high permeability rock layer, cavernous zones or through natural or induced fractures. It is often hard to tell the cause behind losses, hence, it is also challenging to determine the right action to stop losses. Choosing the wrong action might cause additional issues. This is one of the reasons why circulation losses are one of the most costly problems to stop.

However, preventive methods could, if not eliminate, at least reduce the risk of circulation loss. Oil companies around the world have different procedures to do this, but most of them use the same principal. It is common practice to use lost circulation material (LCM) either in the active drilling fluid or in LCM pills that are pumped into the hole when entering a challenging formation or when losses have occurred. LCM is also used in cement to avoid fracturing during cementing operations. LCMs are particles that are mixed in the drilling fluid or mixed as a pre-blended LCM pill. These particles will create bridges at the fractures that will seal off the fracture, avoiding further fracture growth.

Recent studies at the University of Stavanger suggest a new theory on how LCM heals already existing and induced fractures. The new theory is called the Elastoplastic fracture model. In order to predict the fracture gradient in a well, the well-known Kirsch equations are used. However, it is a known fact that these equations underestimate the fracture pressure in many situations. The Elastoplastic fracture model offers a method to predict a more reliable fracture gradient because it takes the mud cake's plastic deformation into account, in addition to the elastic deformation of the rock formation (Kirsch). The theory has been tested for water based mud systems, but there are still a lot of research and testing remains, especially for oil based mud system. If the theory proves to be trustworthy, its application could potentially save oil companies millions of dollars annually.

1.2 Objective of Work

Oil-based field mud will be used in this study to investigate its bridging capabilities. The main idea is to use four different materials will be tested as lost circulation materials (LCM). The following four materials will be used as LCM:

- Quartz
- Feldspar

- CaCO3
- LC-Lube (Graphite)

These four particles will be tested bot separately and in combination with each other.

This study will also investigate the performance a theoretical particle size distribution (PSD). The theoretical PSD is based upon the theory of sphere packing, where the smaller particles in the mix could fit into voids between the bigger particles.

2 Theory

2.1 Introduction

Figure 2.1 shows a pressure plot for a well. During drilling, the pressure in the well has to be in balance with the formation pressure. If the density of the drilling fluid is too low, there is a risk that the bottom hole pressure becomes less than the pore – or collapse pressure of the formation and could result in well control problems. It might cause problems like stuck pipe or hole cleaning issues. On the other hand, a too high mud density might cause the bottom hole pressure to exceed the fracture pressure of the formation. This will cause the formation to crack up and the drilling fluid can escape into the rock formation. In the industry, this is referred to as lost circulation, and is sometimes extremely costly to stop.[1]

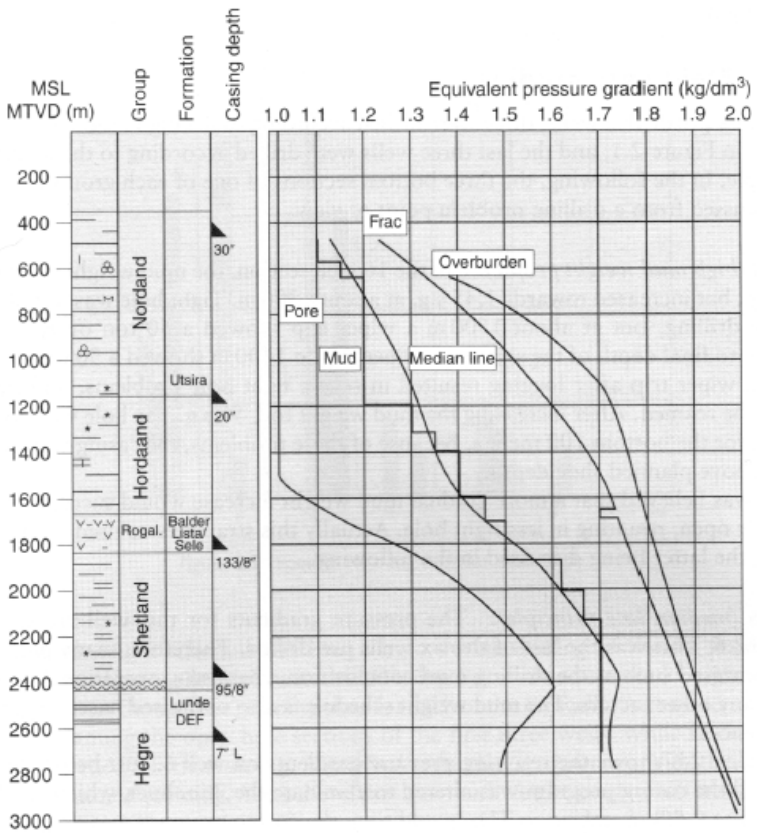

Figure 2.1: Gradient plot. [1]

The cost of lost circulation adds up to hundreds of millions of dollars annually for oil companies. It is costly to lose mud mostly because of non-productive rig time, but also because the reservoir can be severely damaged if lost circulation occurs in the pay zone. In the latter scenario, the estimated recoverable reserves might no longer be recoverable. It is also important to note that the drilling fluid itself could be expensive. A cost analysis was conducted for six wells in the North Sea. Figure 2.2 shows that bore hole stability problems accounts for a great amount of the non-productive time for these six wells. It also shows that lost circulation is one of the most time consuming problems. [1, 2]

Event	Time used (days)
Circulation losses	15
Tight hole	2
Squeeze cementing	15
Stuck casings	20
Fishing	2
Total	52 days
Per well	52/6 = 8.7 days

Figure 2.2: Time consumption related to bore hole stability. [1]

Lost circulation can occur during any operation that involves pumping of fluid into the well. In order for fluid loss to occur, there have to be a formation with flow channels that allow fluid in the well to flow into the formation, as well as pressure overbalance in the wellbore. There are four main circulation loss scenarios. These scenarios are listed in Table 2.1.[2]

	Description
Permeable zones	Drilling into permeable and porous rock might cause fluid to flow into the formation. Typically, unconsolidated formations cause circulation loss.
Natural fractures	Vertical or horizontal fractures that already exist in the rock. These fractures are flow paths that allow the fluid to escape into the formation.
Induced Fractures	Occurs if the well pressure exceeds the fracture pressure limit of the rock. This scenario might happen during various types of operations (i.e. drilling, cementing, gravel packing etc.).
Caverns	Void spaces of various sizes in the rock formation. Dependent on the void size, it might cause complete loss of mud return.

Table 2.1: Lost circulation scenarios. [2]

Due to the fact that the cost of circulation loss is very high, there is focus on preventing lost circulation to happen. Whenever fluid is circulated in the well, an additional pressure will be present due to the friction between the fluid and the wellbore wall. Equivalent circulation density is the static pressure from the fluid column plus the additional friction pressure (measured in specific gravity, s.g.). The equivalent circulation density (ECD) is always

monitored during drilling to ensure that the well pressure is inside the pressure window of the well, meaning that the well pressure must be within the pore/collapse pressure and the fracture pressure. In order to be able to drill deeper, casings are set at strategic depths and allows for heavier mud to be used in the following well sections. However, the most important prevention method for lost circulation is fluid design.[2] There are a few different theories on how to use drilling fluid in order to prevent or stop circulation loss. Some of these theories will be briefly explained in the following.

Generally speaking, mitigation of circulation loss can be categorized in two main categories. Preventive measures and remedial measures. In planning phase, the type of mitigation is chosen based on experience from nearby wells and the geology knowledge in the area. Also, the cost of the different mitigation methods should be considered.

2.1.1 Preventive Measures

The risk of lost circulation can be removed or at least reduced by using measures such as:[2]

- Properly designed mud systems
- Controlling ECD carefully
- Casing design
- Underbalanced drilling
- Managed pressure drilling

During drilling, casing design and ECD monitoring might not be enough to prevent circulation loss incidents, which is why mud design is important. In depleted reservoirs, the fracture gradient could be reduced to such extend that it is practically impossible to drill. The industry uses different methods to optimize drilling fluid and cement in order to increase the fracture pressure gradient of the well.

Studies have shown that by adding solid particles and chemicals to the mud, the fracture gradient could be increased. Sometime the wellbore is strengthened to such extend that it is possible to drill wells that were normally not drillable with traditional mud systems. In order to have a well working mud system, the mud has to be monitored and maintained continuously. The reason for this is that salts, cuttings and formation fluid will contaminate the return mud. Also, the shakers might remove the important particles that were added to the mud in the first place. When designing the mud, it is important to focus on the fracture healing properties of the mud, but also to make sure that the particle additives do not affect other mud properties such as rheology, density, etc.[2, 3]

Experiments in this thesis focus on circulation loss related to fractures. The Kirsch equation is widely used in the industry to predict the fracture pressure limit of the formation, but recent research at the University of Stavanger has led to another theory called the Elastoplastic fracture model. The new Elastoplastic model takes the filter cake's plastic behaviour into account in addition to the mechanical properties of the rock. One of the major advantages with the Elastoplastic model is that leak-off test (LOT) data from nearby wells could be used to predict the fracture gradient for a new well. However, in order to achieve an improved frature gradient, the drilling fluid has to be optimized for that purpose.[4]

2.1.2 Remedial Measures

When lost circulation has already occurred, different methods might be used to stop the fluid from escaping into the formation:[2]

- Allowing the formation to heal itself by removing the cause of circulation loss.
- Using Lost Circulation Materials (LCMs) to bridge off the interval (LCM pill)
- Spotting high-viscosity plug across the interval
- Squeeze cementing
- Setting pipe across the interval (casing)
- Abandon or sidetracking

Many of these techniques are time consuming, and might cost a lot both because of non-productive rig time and equipment cost. Also, as mentioned earlier, the cause of circulation loss might be unknown. It is therefore sometimes hard to choose the correct action to stop losses.

2.2 Rock Mechanics

This section is based to a great extend on the book "Petroleum Rock Mechanics" by Aadnøy & Looyeh[5]. Generally, rock mechanics is a specific use of solid mechanics theory, which is used in many industries. However, rock mechanics in this thesis refers to the stress and strain in subsurface rock formations, and the use of the analytical methods to evaluate well stability. The theory of rock mechanics will, however, only be explained briefly in this thesis, and the main focus is to add extra knowledge to understand the fracture theories in later sections. The following will be defined:

- In-situ stress
  - Maximum horizontal stress (σ_H)
  - Minimum horizontal stress (σ_h)
  - Vertical/overburden stress (σ_v)
- Near wellbore stresses
  - Radial stress
  - Hoop stress
  - Axial stress
  - Measuring methods

2.2.1 In-situ Stresses

The natural occurring stresses that exist in subsurface formations are referred to as "in-situ stresses" or "far field stresses". Any point below surface is exposed to these stresses, which

can be transformed/projected into three principal stresses[1], namely the minimum and maximum horizontal stresses and the vertical stress. The vertical stress is generally generated from the weight of the overlaying rocks, hence often referred to as the overburden stress. It might however be influenced by other geological phenomenon such as salt domes or magma intrusion. Due to Poisson's ratio, the overburden stress will usually spread and expand the underlying rock in lateral direction. This movement is restricted by adjacent material (rock) and horizontal stresses will therefore occur. The knowledge of the in-situ stress state helps the petroleum industry to understand and use methods like leak-off tests (LOT) to verify the wellbore stability.

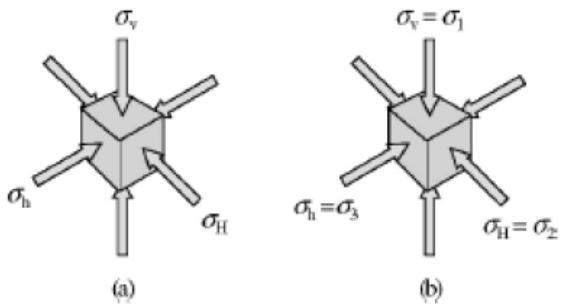

Figure 2.3: (a) Rock formation in-situ stresses. (b) In-situ stresses in drilled formation. [5]

2.2.1.1 Vertical Stress

The vertical stress can be defined as:

$$\sigma_v = \int_0^d \rho_b(h) g \, dh \qquad (2.1)$$

Where, d is the formation depth, g is the gravitational constant, h is the vertical thickness of the rock formation and ρ_b is the rock formation's bulk density. With the simplified equation below, one can obtain the vertical stress from a density log.

$$\sigma_v = 0.434 \gamma d \qquad (2.2)$$

Where σ_v is the vertical stress (psi), Υ is the rock formation's average specific gravity (s.g.) and d is the depth (ft.).

[1] If three in-situ stresses are plotted in a 3-dimensional coordinate system, the orientation of this coordinate system can be manipulated so that all shear stresses will be equal to zero. The remaining three stresses are called the principal stresses. [3]

2.2.1.2 Horizontal Stresses

It is fairly easy to determine the vertical stress, but the horizontal stresses can be dramatically more complex. However, by assuming that the horizontal stresses exist due to the vertical stress alone and that there are no tectonic movements, active faults or other geological activity, one can use the analytical relation in equation 2.3. By using this approach, both the horizontal stresses will be equal in magnitude to each other ($\sigma_h = \sigma_H$) and always perpendicular in direction. Note, equation 2.3 is only applicable where the horizontal stresses could be assumed equal.

$$\sigma_h = \sigma_H = \frac{\nu}{1-\nu}(\sigma_v - \beta P_o) + \beta P_o \quad (2.3)$$

Where ν is Poisson's ratio, β is Biot's constant and P_o is the pore pressure.

2.2.2 Near Wellbore Stresses

When a well is drilled, the in-situ stresses are disturbed and another stress regime is introduced near and at the wellbore wall. Rock structures might fall into one of two main categories, either statically determinate structures or statically indeterminate structures. Reactions and internal forces in the first category can be analysed solely with the use of equation of equilibrium. The second category is more complex and three sets of equations have to be solved simultaneously. These equations are (i) equation of equilibrium, (ii) equation of compatibility and (iii) constitutive relation / stress-strain equation. These equations are described in more detail by Aadnøy and Looyeh[5], but a quick synopsis follows.

2.2.2.1 Stress Transformation

Before the stress state at the wellbore wall can be predicted, one must transform the in-situ stresses into the direction of the wellbore. In other words, transform σ_h, σ_H and σ_v into the stresses in the wellbore direction, σ_x, σ_y and σ_z. Where z is the direction parallel to the wellbore path, and x is the direction towards the high side of the hole.

The stresses in Figure 2.4 are transformed by using the following equations:

$$\sigma_x = (\sigma_H cos^2\varphi + \sigma_h sin^2\varphi)cos^2\gamma + \sigma_v sin^2\gamma \quad (2.4)$$

$$\sigma_y = \sigma_H sin^2\varphi + \sigma_h cos^2\varphi \quad (2.5)$$

$$\sigma_{zz} = (\sigma_H cos^2\varphi + \sigma_h sin^2\varphi)sin^2\gamma + \sigma_v cos^2\gamma \quad (2.6)$$

$$\tau_{xy} = \frac{1}{2}(\sigma_h - \sigma_H)\sin 2\varphi \cos\gamma \quad (2.7)$$

$$\tau_{xz} = \frac{1}{2}(\sigma_H cos^2\varphi + \sigma_h sin^2\varphi - \sigma_v)\sin 2\gamma \quad (2.8)$$

$$\tau_{yz} = \frac{1}{2}(\sigma_h - \sigma_H)\sin 2\varphi \sin\gamma \quad (2.9)$$

Where, σ_x is the stress in the direction of the high side of the wellbore wall. σ_y is the stress in the horizontal direction. σ_z is the stress in the axial direction. τ are shear stresses.

2.2.2.2 Equations of Equilibrium

Equation of equilibrium is derived from a free body diagram and the fact that there is a relation between applied forces, reactions and internal forces (Newton's laws of motion). For the situation in Figure 2.4, the stress state in a Cartesian coordinate system is given by equations 2.10 – 2.12.

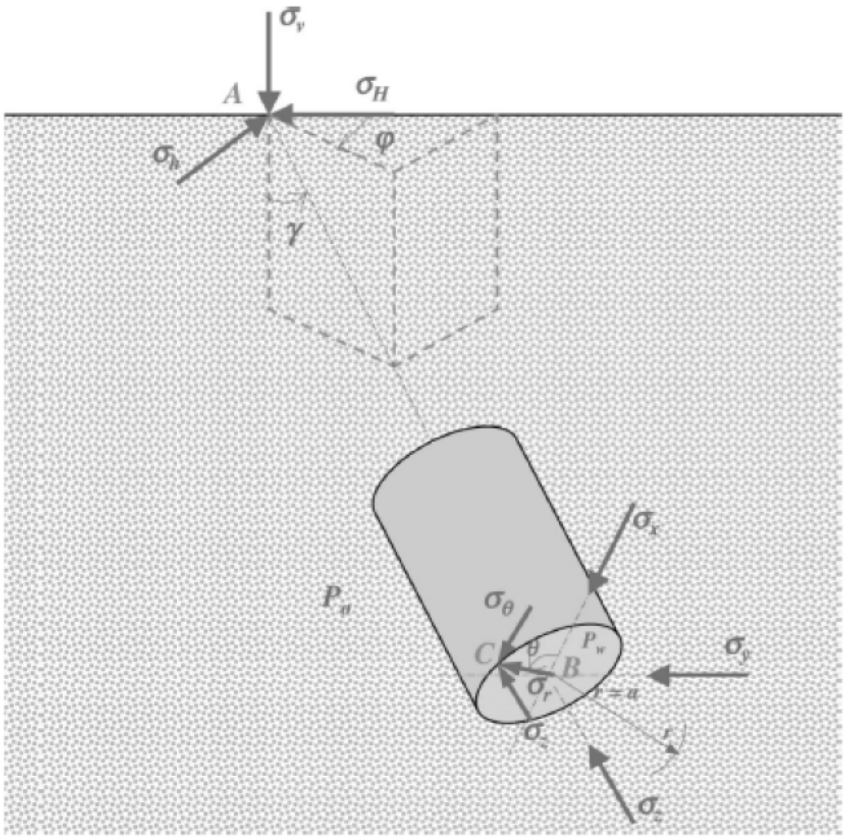

Figure 2.4: Stresses on a deviated well bore. [5]

$$\frac{\partial\sigma_x}{\partial x} + \frac{\partial\tau_{xy}}{\partial y} + \frac{\partial\tau_{xz}}{\partial z} + F_x = 0 \quad (2.10)$$

$$\frac{\partial\tau_{xy}}{\partial x} + \frac{\partial\sigma_y}{\partial y} + \frac{\partial\tau_{yz}}{\partial z} + F_y = 0 \quad (2.11)$$

$$\frac{\partial \tau_{xz}}{\partial x} + \frac{\partial \tau_{yz}}{\partial y} + \frac{\partial \sigma_z}{\partial z} + F_z = 0 \quad (2.12)$$

Where τ_{xy}, τ_{xz}, τ_{yz} are shear stresses. σ_x, σ_y, σ_z are normal stresses and F_x, F_y, F_z are forces applied to a unit volume in x,y and z direction. Sometimes it is more convenient to use a cylindrical coordinate system. Equations 2.10 – 2.12 are then given by:

$$\frac{\partial \sigma_r}{\partial r} + \frac{1}{r}\frac{\partial \tau_{r\theta}}{\partial \theta} + \frac{\partial \tau_{rz}}{\partial z} + \frac{\sigma_r - \sigma_\theta}{r} + F_r = 0 \quad (2.13)$$

$$\frac{\partial \tau_{r\theta}}{\partial r} + \frac{1}{r}\frac{\partial \sigma_\theta}{\partial \theta} + \frac{\partial \tau_{\theta z}}{\partial z} + \frac{2\tau_{r\theta}}{r} + F_\theta = 0 \quad (2.14)$$

$$\frac{\partial \tau_{rz}}{\partial r} + \frac{1}{r}\frac{\partial \tau_{\theta z}}{\partial \theta} + \frac{\partial \sigma_z}{\partial z} + \frac{\tau_{rz}}{r} + F_z = 0 \quad (2.15)$$

Where $\tau_{r\theta}$, τ_{rz} and $\tau_{\theta z}$ are shear stresses, and σ_r, σ_θ and σ_z are normal stresses in a cylindrical coordinate system. F_r, F_θ and F_z are body forces in r, θ and z direction.

2.2.2.3 Equations of Compatibility

The rock deformation has to be continuous, thus, compatibility equations have to be applied. This means that the stress has to be compatible with strain. The statement that the deformation has to be continuous is very important. In a situation where this statement is not true, continuum mechanics is no longer applicable. There are a total of six equations of compatibility. One of them is given by equation 2.16 for a cylindrical coordinate system.

$$\frac{\partial^2 \varepsilon_r}{\partial \theta^2} + \frac{\partial^2 \varepsilon_\theta}{\partial r^2} = \frac{\partial^2 \gamma_{r\theta}}{\partial r \partial \theta} \quad (2.16)$$

Where ε_r, ε_θ and $\gamma_{r\theta}$ are normal and shear strain respectively.

2.2.2.4 Constitutive Relations

Since it is impossible to measure stress, one needs an indirect way to determine it. One way is to measure deformation. The parameters obtained from laboratory experiments are called constitutive relations. The two follow equations gives the relationship between the normal stresses and normal strain (2.17), and shear stresses and shear strain (2.18) in a cylindrical coordinate system.

$$\begin{bmatrix} \sigma_r \\ \sigma_\theta \\ \sigma_z \end{bmatrix} = \frac{E}{(1+\nu)(1-2\nu)} \begin{bmatrix} 1-\nu & \nu & \nu \\ \nu & 1-\nu & \nu \\ \nu & \nu & 1-\nu \end{bmatrix} \begin{bmatrix} \varepsilon_r \\ \varepsilon_\theta \\ \varepsilon_z \end{bmatrix} \quad (2.17)$$

$$\begin{bmatrix} \tau_{r\theta} \\ \tau_{\theta z} \\ \tau_{rz} \end{bmatrix} = G \begin{bmatrix} \gamma_{r\theta} \\ \gamma_{\theta z} \\ \gamma_{rz} \end{bmatrix} \quad (2.18)$$

2.2.2.5 Kirsch Equations

The Kirsch equations are derived from the three sets of equations above. The process is quite complex. By following the methodology given by Aadnøy and Looyeh, one will end up with two solutions, namely, an isotropic solution and an anisotropic solution. Both solutions are given below.

2.2.2.5.1 Anisotropic solution

In this case, anisotropic means that the horizontal stresses are not equal. Also, shear stresses are present. With this assumption, the Kirsch's solution at the wellbore (r=rw) yield the following:

$$\sigma_r = P_w \tag{2.19}$$

$$\sigma_\theta = \sigma_x + \sigma_y - P_w - 2(\sigma_x - \sigma_y)\cos 2\theta - 4\tau_{xy}\sin 2\theta \tag{2.20}$$

$$\sigma_z = \sigma_{zz} - 2\nu(\sigma_x - \sigma_y)\cos 2\theta - 4\nu\tau_{xy}\sin 2\theta \text{ (Plane strain assumption)} \tag{2.21}$$

$$\sigma_z = \sigma_{zz} \text{ (Plane stress assumption)} \tag{2.22}$$

$$\tau_{r\theta} = 0 \tag{2.23}$$

$$\tau_{rz} = 0 \tag{2.24}$$

$$\tau_{\theta z} = 2(-\tau_{xz}\sin\theta + \tau_{yz}\cos\theta) \tag{2.25}$$

2.2.2.5.2 Isotropic solution

Unlike the anisotropic solution above, the isotropic solution assumes that horizontal stresses are equal ($\sigma_H = \sigma_h$) and that shear stresses are negligible. With these assumptions the Kirsch's solution at the wellbore (r=rw) is reduced to:

$$\sigma_r = P_w \tag{2.26}$$

$$\sigma_\theta = 2\sigma_a - P_w \tag{2.27}$$

$$\sigma_z = \sigma_{zz} \text{ (Plane stress/strain assumption)} \tag{2.28}$$

σ_r is known as the radial stress, σ_θ is known as circumferential/hoop stress and σ_z is the axial stress along the wellbore. Now, the essence of this is not to understand the derivation of the Kirsch equations, but to understand that there is a strong relation between the in-situ

stresses and the near wellbore stresses. The Kirsch equation is used in the petroleum industry for analysis of wellbore failure.

2.2.2.6 Measuring Methods

There are several ways to measure the horizontal stresses. In the North Sea, the most common method is a leak-off test (LOT) or extended leak-off test (XLOT) in combination with the inversion technique (Aadnøy, 1990). By using data from nearby wells as input in the inversion technique, all in-situ stresses can be determined for the well in interest. In order to get enough data for a stress state tensor, six individual tests have to be taken. There are other methods to measure the in-situ stresses such as a breakout analysis, cross dipole etc., but these are not relevant for this work.

Both tests described below are done the same way. As the pressure in the wellbore is increased, the rock formation in an open-hole section will break. The pressure that is measured surface is recorded, and usually has a profile like illustrated in Figure 2.5.

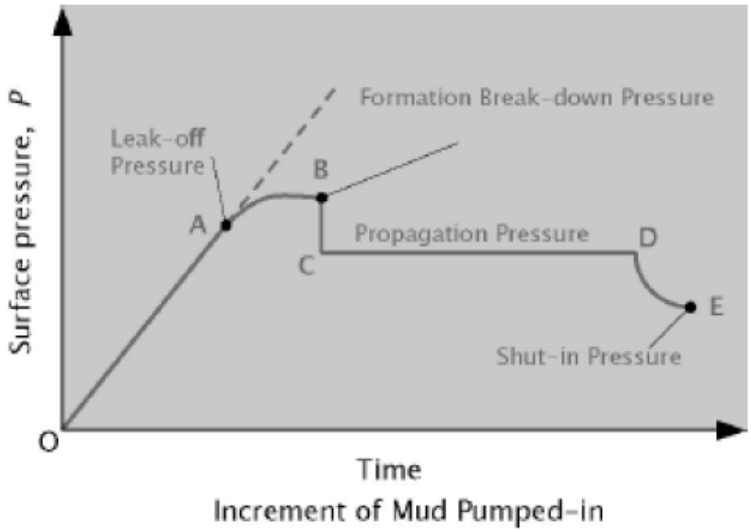

Figure 2.5: Surface pressure profile [5]

2.2.2.6.1 Leak-off test

Leak off tests are often ran a couple of meters below a newly cemented casing shoe. The well is shut in, and drilling fluid is pumped into the well to increase the well pressure. Pumping continues until the fluid starts to escape, either through permeable channels in the rock formation or through fractures. This will happen at the top of the linear pressure build-up, also referred to as the leak-off pressure (point A in Figure 2.5). The maximum allowable well pressure is the leak-off pressure minus a safety margin, i.e. slightly below the leak-off pressure.

2.2.2.6.2 Extended leak-off test

The extended leak-off test (XLOT) executed in the same way as the LOT, but during this test, the fluid is pumped into the well until fracture propagation pressure can be measured. This pressure is illustrated in Figure 2.5 (point C). The fracture propagation pressure is defined as the pressure at which a fracture will continue to grow.

2.3 Drilling Fluids

This section is mainly based on the book "Fundamentals of Drilling", ref [2].
The drilling fluid has many functions. Below is a list of the major purposes of using well-engineered drilling fluid: [2]

- Cutting transport
  - Clean under the drill bit
  - Transport drilled cuttings up the borehole
  - Release the cuttings at the surface without losing other beneficial materials
  - Hold cuttings and weighting materials when circulation is stopped
- Physicochemical functions
- Cooling and lubricating the rotating bit and drill string
- Fluid-loss control
  - Create a impermeable filter cake at the wellbore wall for borehole support
  - Reduce adverse and damaging effects on the formation around the wellbore
- Control surface pressure
- Support part of the drill string and casing weight
- Ensure maximum logging information
- Transmit hydraulic horsepower to the rotating bit

There are different types of drilling fluids. According to the fluid's continuous phase, these fluids can be categorized in the three following main categories: water based fluids, oil based fluids and or pneumatic (gas) fluids. Composition and properties of water-based – and oil-based mud will be covered in this section. Note that there is a lot of research within the area of drilling fluids, and specialised fluids could be designed for specific tasks.[2]

2.3.1 Water-based Drilling Fluids

There are three main types of water based drilling fluids:

- Inhibitive
- Non-inhibitive
- Polymer

In zones where reactive clays are present, inhibitive fluids are used to retard the clay swelling. Inhibitive fluids use native water to avoid reaction between clay and the drilling fluid. Polymer fluids may be either inhibitive or non-inhibitive. In these types of fluids, cations are added to achieve inhibitive effects.

Water based fluid consists of many types of additives such as brine, bentonite, barite, salts etc. Figure 2.6 shows a typical composition of a water-based fluid. In addition to the additives shown in the picture below, loss circulation materials (LCM) are added if needed. The main ingredient in WBM is either fresh water, brine or formation water. Type of water is often chosen based on the formation the mud is going to be used in. Reactive shale formations will be, somewhat, inhibited if formation water is used. In other situations, additives such as polymers or salts are used to inhibit shale swelling. Polymers are added both to gain some inhibitive properties, and also to control rheology. Oil is also used in WBMs to lubricate the drill string and bit. In addition to that, if oil is added to the mud used in a water wet formation filtration loss is sometimes reduced. Solids and clay are added to create a strong filter cake, and also to achieve the desired density of the mud. Fine particles might also affect the viscosity of the mud.[2] One of the major advantages of using WBMs is that these are more environmentally friendly than OBMs.

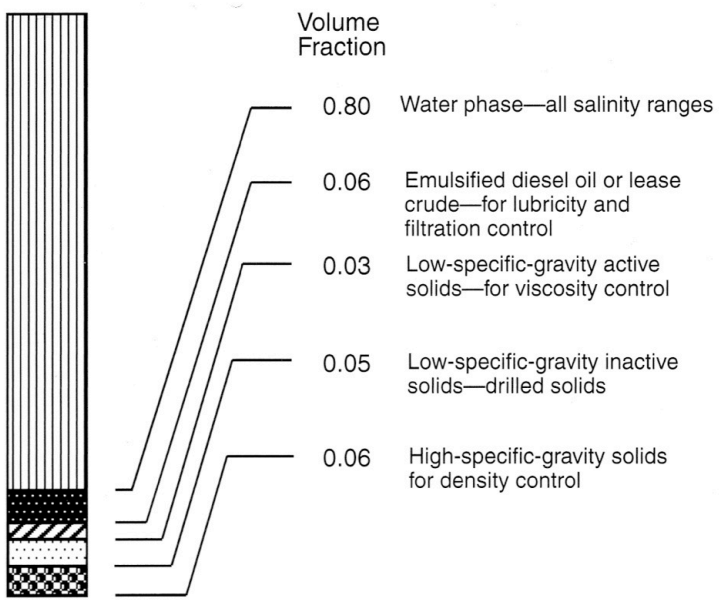

Figure 2.6: Typical composition of water-based mud. [2]

2.3.2 Oil-based Drilling Fluids

Oil-based mud is often preferred because it has better inhibitive properties, it lubricates the drill string, causes less corrosion and gives less friction between the drillstring and the wellbore wall. Clay swelling is caused by hydration of the clay. Water enters the inner layers of the clay due to attraction forces between O^{2-} ions (from water) and Na^{+} ions (in the clay), and attraction between H^{+} ions (water) and O^{2-} ions (clay). All-oil fluids do not cause this effect, because it does not contain water. However, most oil-based muds also contain water

and could cause some shale reactions. Typical oil/water ratio ranges from 90:10 to 60:40. Figure 2.7 shows a typical OBM composition.[2]

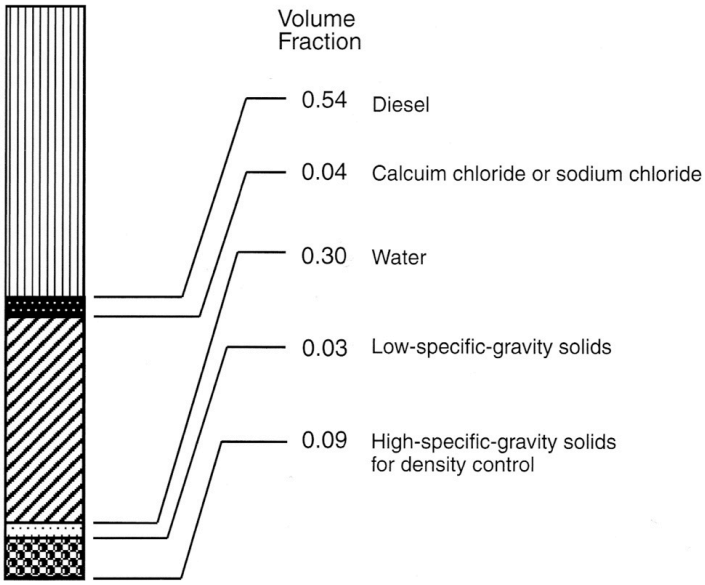

Figure 2.7: Typical composition of oil-based mud. [2]

There are different types of OBMs. Most commonly, there are diesel based mud systems, which are illegal to use in many countries because it is toxic. Better alternatives are often used such as synthetic based fluids or emulsion based fluids. Synthetic based fluid uses synthetic oil as base, which is a lot less toxic than diesel. These are almost exclusively used for drilling offshore. Emulsion based fluids are ester/IO blends, which have stable viscosity and gel properties in larger temperature ranges. Rheology and filtrate loss properties are maintain by adding fatty acids and surfactants.[2]

2.3.3 Drilling Fluid Additives

Different materials are added to the mud system in order to achieve desired properties of the mud. Solids are added for various reasons, which will be explained later. There are two types of solids, active and inactive solids. Active solids often referred to as hydrophilic solids, such as hydratable clays reacts with the water phase. These solids dissolve chemicals and make the mud more viscous. Inactive (hydrophobic) solids do not react with water or chemicals to any significant degree. Examples of hydrophobic solids are sand and shale.

In order to get the desired density of the mud, heavy solids are added. Barium sulphate (barite) is used most commonly as weighting agent. Barite has a density typically around 4.20 g/cm^3. Other important weighting agents are siderite (3.08 g/cm^3), calcium carbonate (2.7-2.8 g/cm^3), hematite (5.05 g/cm^3), limetite (4.6 g/cm^3) and galena (7.5 g/cm^3).

While drilling, a filter cake is formed at the wellbore wall. The filter cake is important to maintain a stable wellbore. When the filter cake is formed, some of the fluid in the well will

be lost into the rock formation. The lost fluid is referred to as filter loss. When designing a mud system, it is important to control the amount of filter loss. If too much is lost, the density of the mud will increase. If too little is lost, the filter cake will be thin and not strong enough. To achieve a good filter cake and control the filter loss, clay, dispersant and/or polymers are added to the mud. Mainly sodium montmorillonite is used as fluid loss additive. This is clay consisting of thin and sheet like particles with large surface area. These particles are known form a compressible filter cake.

Lost circulation materials are added to prevent major fluid losses through pores or fractures in the formation. The industry uses a variety of different materials to achieve this. Such material could be:[2]

- Fibrous materials
  - Wood fibre
  - Cotton fibre
  - Mineral fibre
  - Shredded automobile tires
  - Ground-up currency
  - Paper pulp
- Granular materials
  - Nutshells (fine, medium, coarse)
  - Calcium carbonate $CaCO^3$ (fine, medium, coarse)
  - Expanded perlite
  - Marble
  - Formica
  - Cottonseed hulls
- Flake like materials
  - Mica flakes
  - Shredded cellophane
  - Pieces of plastic laminate
- Graphite (LC-lube)

In order for the LCM to work properly, the concentration and particle size distribution have to be optimized. This could be done in the lab or by the use of information from nearby wells in the same geological area. Typical concentrations for a graphite/CaCO3 mix are[6]:

- Low risk of loss: 30-40 kg/m3
- Medium risk: 40-60 kg/m3
- High risk: 60-100 kg/m3
- Very high risk: 100-140 kg/m3

The maximum concentration of 140 kg/m3 is limited by measurement while drilling (MWD) equipment.

2.4 Fracture models

Through recent years, many fracture models have been developed. In general, these models describe the physics behind the deformation of subsurface rock formations. A joint industry project (DEA-13) was launched in the early 1990's (Morita et. al.). The scope of this project was to investigate the mechanism behind wellbore strengthening. Findings during this project was: [7]

- No significant difference in fracture initiation pressure between OBM and WBM.
- High density WBM has higher fracture extension pressure than OBM.
- WBM has better fracture healing properties than OBM.
- High-fluid-loss water-based-mud pill is the best lost-circulation treatment for OBM-induced fractures.
- The main difference between high density OBM and WBM is their reopening and propagation pressures.

OBM is often used in the North Sea, and it is therefore of interest to find a method to increase the fracture healing properties of OBMs. There have been a few models that describe the wellbore strengthening properties of different types of muds. Some of these models are presented in the following sections.

Fuh et. al. described the strengthening effect as a result of fracture tip isolation. Particles in the mud are transferred into the fracture until it reaches the tip of the fracture (a "screen-out effect"). When this is achieved, these particles create a "filter cake" inside the fracture and the fracture tip is then isolated and inhibits further fracture growth. During their work, a saw-tooth pattern on the pressure plot was observed. These saw-teeth were described as fracture growth, i.e. the point where the particle "filter cake" breaks. Tip isolation is illustrated in Figure 2.8. The pressure at which the particle "screen" breaks can be estimated by the equation below.[8]

$$P_{tip}^{c} = 0.87 \cdot \frac{k_p^c}{2} \sqrt{\frac{\pi}{0.5H}} - \sigma_H \tag{2.29}$$

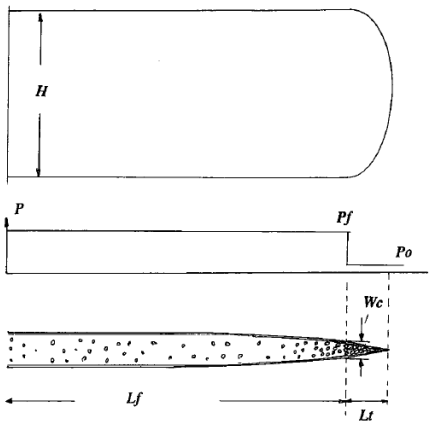

Figure 2.8: Fracture tip isolation. [8]

Later, another joint industry project was launched, the GPRI 2000 project. The main finding in this project was that different particle additives affect the wellbore strengthening differently. Resilient Graphite was the material that had most promising effect. The results from this project led to the many wellbore-strengthening theories known today. [9, 10]

Research at the University of Stavanger during the recent years has led to a fracture theory that differs from other theories. This theory is named the Elastoplastic fracture theory. Most wellbore-strengthening theories is based on change in the stress state near the wellbore, while the Elastoplastic theory states that a well could contain a higher pressure due to the strength of the particles that form the particle bridge.[3]

2.4.1 Linear Elastic Fracture Model

The linear elastic fracture model is a direct use of the Kirsch equations. The model assumes that the wellbore will fracture when the stress goes from compression into tension, which happens when the borehole pressure exceeds the smallest horizontal stress. At this point, the hoop stress around the wellbore goes from compression into tension.[5]

There are two types of fluids that can be analysed with this model. These are non-penetrating fluids and penetrating fluids. Non-penetrating fluids are fluids that will not flow into the rock formation, i.e. the filter cake seals the wellbore and the fluid is contained in the well. Penetrating fluids are fluids that do penetrate the wellbore wall, and fluid can flow into the rock formation.[5]

2.4.1.1 Fracture Pressure for Non-Penetrating Fluids

The general equation for the fracture pressure is given by equation 2.30. It is valid for wellbores in any direction.

$$P_{wf} = \sigma_x + \sigma_y - 2(\sigma_x - \sigma_y)\cos 2\theta - 4\tau_{xy}\sin 2\theta - \frac{\tau_{\theta z}^2}{\sigma_z - P_0} - P_o - \sigma_t \qquad (2.30)$$

The equation above assumes that the fluid is non-penetrating. Meaning that the filter cake is sealing and there is no fluid flowing into the rock formation. Further simplification of the equation yields:

$$P_{wf} = 3\sigma_x - \sigma_y - P_o \; for \begin{cases} \sigma_x < \sigma_y \\ \theta = 90° \end{cases} \qquad (2.31)$$

or

$$P_{wf} = 3\sigma_y - \sigma_x - P_o \; for \begin{cases} \sigma_y < \sigma_x \\ \theta = 90° \end{cases} \qquad (2.32)$$

Both equations above are valid when the borehole is aligned with the principal horizontal stresses.[5]

2.4.1.1.1 Fracture Direction

By using equation 2.30, there is no guarantee that the fractures are initiated in the direction of the highest principal horizontal stress. The direction of the fracture can be found by differentiate the equation. The result is presented in equation 2.33 below.[5]

$$\tan 2\theta = \frac{2\tau_{xy}}{\sigma_x - \sigma_y} \tag{2.33}$$

2.4.1.2 Fracture Pressure for Penetrating Fluids

For clean fluids, such as water, the fluid will penetrate the well bore wall. For this situation, the fracture pressure will be the same as the smallest horizontal stress.

$$P_{wf} = \sigma_h \tag{2.34}$$

The linear elastic model is almost exclusively used in the oil and gas industry. However, the non-penetrating equation often estimates a lower fracture pressure than what is shown by leak-off tests. On the other hand, the penetrating model gives good estimates for clean fluids, which indicates that the filter cake might have influence on the fracture pressure for non-penetrating fluids.[5]

This model underestimates the fracture pressure because it assumes that the fluid is either penetrating or non-penetrating. In the real world, there will always be some filtrate loss when unclean fluid is used. Meaning, what is assumed to be non-penetrating fluids actually are a little penetrating after all. There are no linear elastic models for “semi-penetrating” fluids. In order to make a filter cake, there have to be a certain amount of filter loss.

2.4.2 Wellbore Strengthening

Wellbore strengthening is an expression sometimes used to describe stress cage. In this work the expression will be used as a common expression for the fracture theories that describe the strengthening effect particles have on the wellbore.

After DEA-13 and GPRI 2000, researchers started to describe how particles in mud have a strengthening effect on the well bore. When a fracture is induced or reopened, particles in the mud will start to flow into the fracture. Unlike the early findings in DEA-13, researchers now believe that the wellbore strengthening effect does not come from tip isolation, but rather a change in the stress near the wellbore.[11-13]

2.4.2.1 Bridging

In order to achieve proper strengthening effect, the particles in the drilling fluid have to be small enough to get into the fracture. Once inside the fracture, these particles will form a bridge just inside the fracture mouth. The particle bridging is illustrated in Figure 2.9. It is important that the bridge seals the fracture so that the fluid behind it can dissipate through the formation pores and create pressure equilibrium between the area behind the fracture and the surrounding formation.[11, 13]

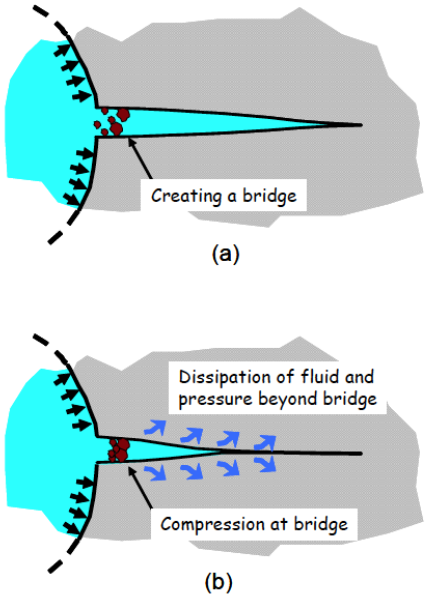

Figure 2.9: Bridging process. (a) Particles enter the fracture. (b) Particles form a bridge near the fracture mouth. [11]

2.4.2.2 Strengthening Process

The strengthening process is based upon the already established Kirsch equations. When the hoop stress around the circumference of the wellbore goes from compression into tension, the formation will start to crack. The pressure required to reopen an already existing or induced fracture is called fracture-reopening pressure. At this pressure, the fracture closure stress (FCS) is reached, and the fracture will start to gain width. In literature, the FCS is defined as the stress that is trying to close the fracture. For a fully closed fracture, the FCS is equal to the fracture-reopening pressure. However, as fracture width increases the FCS also increases. This is happening because the tension causing the fracture to widen up will cause the surrounding formation to compress. It might be thought of having springs on each side of the fracture. The more the fracture is opened, the more the springs will try to "push" the fracture back together.[13]

The idea behind wellbore strengthening is that particles will bridge the fracture, making it possible to gain fracture width. As the well pressure is increased, the particles will go further into the fracture. In order to achieve a good treatment, the BOP is usually closed, and mud pumps are used to increase the well pressure. When the pressure has increased to a desired

level, and the fracture bridge is in place, the pressure is decreased. Now the FCS has increased due to the compression in the surrounding formation. The particle bridge will keep the fracture open and sealed. Due to the higher FCS, drilling can proceed without losses as long as the pressure is below the new FCS. Figure 2.10 illustrates the bridging/strengthening process.[13]

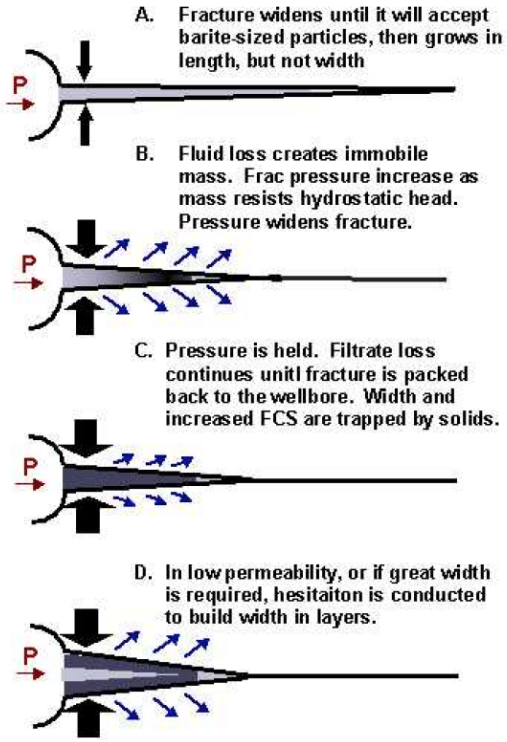

Figure 2.10: Wellbore strengthening mechanism. [13]

The fracture closure stress is referred to in literature by many names; stress cage, FCS, fracture sealing, artificial hoop stress, increased hoop stress, wellbore strengthening and more. A recent publication by Duffadar et. al. states that many of the different theories describe the same effect.[12]

2.4.2.3 Engineered Approach

In order to achieve proper treatment, mud companies have developed engineered approaches to estimate fracture width and best suited PSD. Firstly, the well has to be analysed and possible loss zones must be recognized. Hydraulic model software is used to estimate the ECD in the given intervals of the well. The results are fed into a fracture modelling software. The software will estimate fracture width, height and shape, and propose a PSD, which may be used as treatment to achieve a more stable well. The software can be used to design PSD for both LCM pills and for active drilling fluid.

Since the strengthening is a dynamic process and the near-wellbore stress state changes with fracture width, the software uses numerical estimation to predict the fracture width.

Different methods are used, and different softwares are used in the industry, but the main objective is to find the most suitable particle mix. Figure 2.11 and Figure 2.12 show two different types of fracture modelling software. The latter shows the PSD as percentiles.

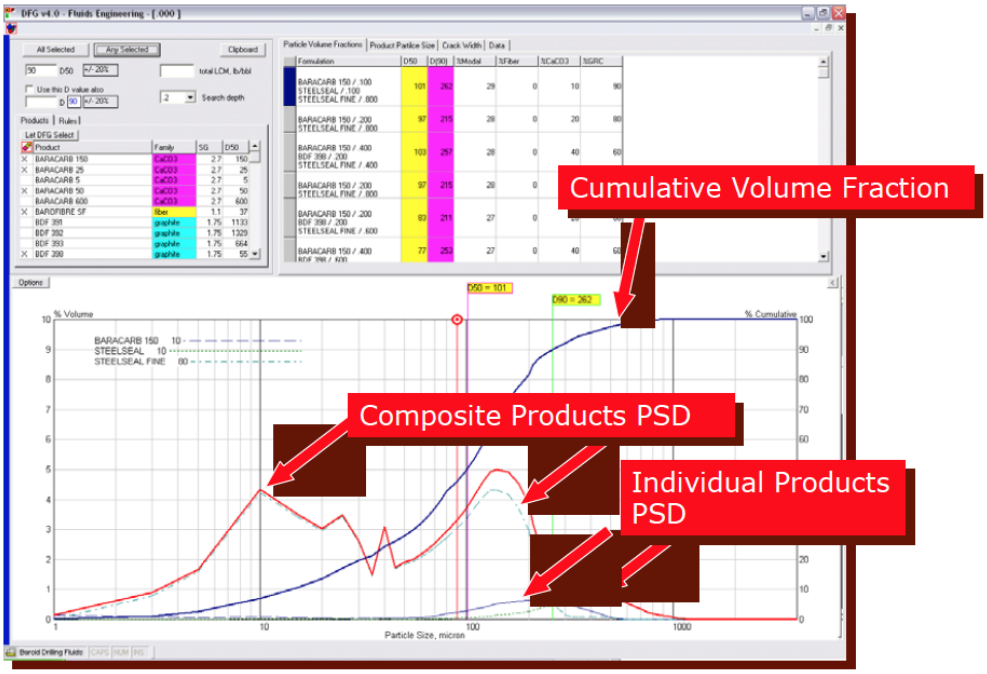

Figure 2.11: Screenshot of software used to estimate PSD. [14]

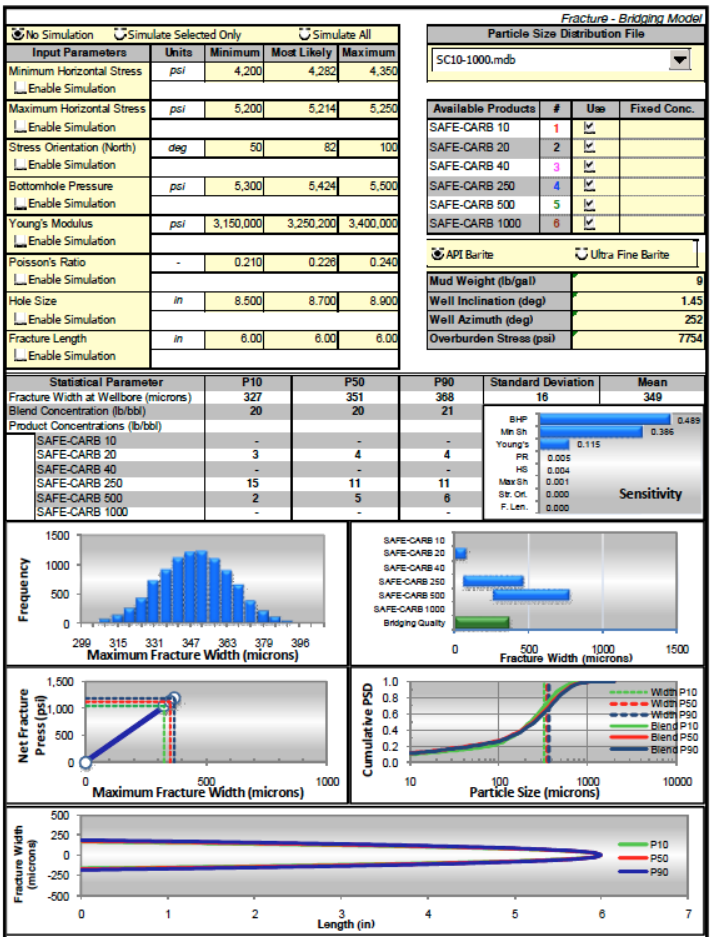

Figure 2.12: Fracture software, shows fracture width and PSD in a probabilistic manner.[15]

Another important engineering aspect is the logistics involved on rig site to maintain the right amount of LCM and PSD in the active drilling mud. If the treatment is based on pumping a LCM pill, the logistic is less important. The logistics will be covered in another section later in this work. [10, 14, 15]

2.4.3 Elastoplastic Fracture Model

The Stress Cage model explains the increase in wellbore strength as an increase in hoop stress. Aadnoy, Belayneh and Kaarstad had another view and developed the Elastoplastic Fracture model.

The Elastoplastic Fracture model assumes that the “extra wellbore” strength comes from the plastic behaviour of the filter cake. From LOTs, one can see that there is a non-linear pressure profile before the breakdown pressure is reached (between point A and B in Figure 2.5). When the pressure starts to build up, the formation behaves elastically, which is represented by the linear pressure profile. When the pressure reaches a certain point, the filter cake starts to deform plastically, which is represented by the non-linear pressure profile. Ultimately the filter cake and formation break down, and a fracture is created. This is

what happens when “non-penetrating”, or rather, “semi-penetrating” fluids are used. Penetrative fluids will have close to a linear profile until the formation breaks down. If the mud is optimized, one could reach a higher fracture pressure due to the plasticity of the filter cake.[3, 4]

The most optimal fluid would be a fluid that creates a filter cake with very low permeability. If this were achieved, the fracture would be sealed off at the fracture mouth. Hence, no pressure energy is transferred to the fracture tip and the fracture will not grow any further. Fracture growth will happen if the pressure inside the well increases to such extend that the filter cake collapses.[3]

2.4.3.1 Filter Cake Properties

When a fracture is initiated, the LCM in the drilling fluid will prop the fracture and build a stress bridge. By optimizing the mud, this bridge can increase the fracture reopening pressure. The formation of the stress bridge is described in Figure 2.13. The increased reopening pressure comes from the bridge’s mechanical strength. When a bridge is established on the fracture mouth, any increase in well pressure will cause the bridge to compress. As the fracture widens, the bridge become thinner and weaker. At a certain point the bridge will break. It is believed that the yield strength of the particles in the bridge governs when the bridge collapses.[3]

There are no good ways to estimate or know the yield strength of the particles, but Mohs scale can be used as quantitative characterization of yield strength. Experiments have been conducted, and the hardness of the particles plays an important role. The hardest particles (according to Mohs scale) gave the best results. Table 2.2 shows Mohs scale of hardness.[3]

Scale	Mineral	Test
1	Talc	(Softest)
2	Gypsum	
2.5		Fingernail
3	Calcite	Copper coin
4	Fluorite	
5	Apatite	
5.5-6		Knife blade
6	Orthoclase	
6.5-7		Steel file
7	Quartz	
8	Topaz	
9	Corundum	
10	Diamond	(Hardest)

Table 2.2: Mohs scale of hardness. [3]

Event	Fig	Main controlling parameters
Filter cake formation	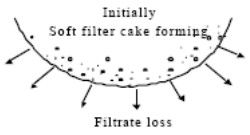	Filtrate loss
Fracture initiation	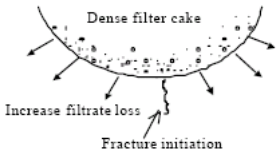	Filtrate loss, Stress
Fracture growth	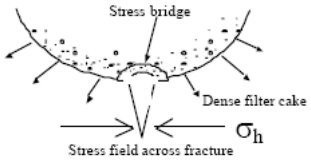	Bridge stress Rock stress
Further fracture growth	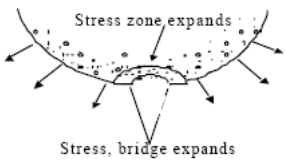	Bridge/rock stress Particle strength
Filter cake collapse	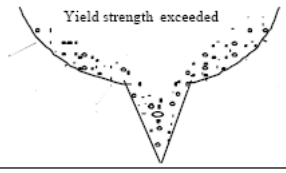	Particle strength

Figure 2.13: Descritpion of the fracture process. [3]

2.4.3.2 Elastoplastic Fracture Theory

As mentioned earlier, the non-penetrating kirsch equation underestimates the fracture pressure. Aadnoy et.al. investigated this and found that for certain fluids, the Kirsch approach was severely off the values measured in the lab. Figure 2.14 shows estimated values together with measured values for three different fluids. There is only one fluid that matches the Kirsch equation. During the study, the synergy between different additives was tested. It seemed that "less is more". Having too many different additives in the mud had a negative impact on the fracture healing properties of the mud.[4]

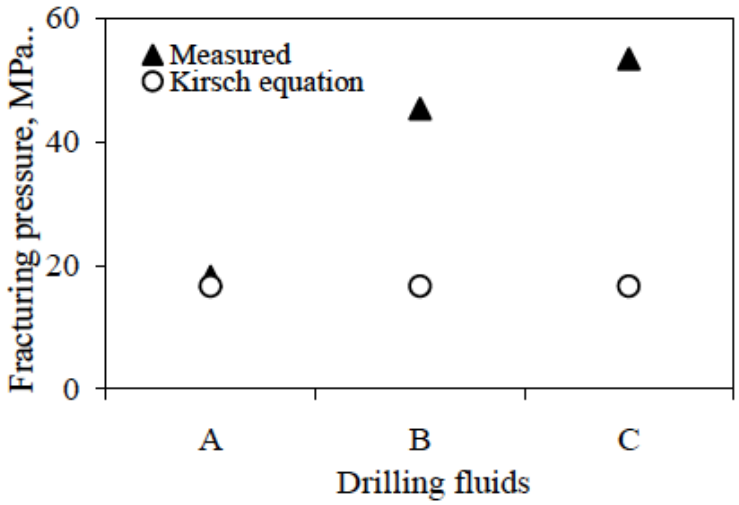

Figure 2.14: Measured pressure values vs. estimated pressure values. [4]

The equation for the Elastoplastic model matches the measured values in the figure above, and the simplest form looks like:

$$P_{wf} = 2\sigma_h - P_o + \frac{2\sigma_h}{\sqrt{3}} \ln\left(1 + \frac{t}{a}\right) \quad (2.35)$$

Here t is the filter cake thickness and a is the wellbore radius. By defining the Elastoplastic barrier as:

$$P_{ep} = \frac{2\sigma_y}{\sqrt{3}} \ln\left(1 + \frac{t}{a}\right) \quad (2.36)$$

the general fracture equation yield the following equation.

$$P_{wf} = P_{ep} + \sigma_x + \sigma_y - 2(\sigma_x - \sigma_y)\cos 2\theta - 4\tau_{xy} \sin 2\theta - \frac{\tau_{\theta z}^2}{\sigma_z - P_0} - P_o - \sigma_t \quad (2.37)$$

The fracture direction would be identical to equation 2.33. The term in equation 2.35 is the only difference from the linear elastic model, which means that the Elastoplastic fracture model can be used in early planning to estimate the fracture gradient. Equation 2.36 is also independent of the well direction.[4]

If used consistently, this model can be used to estimate the fracture gradient for new wells. For prediction of fracture gradient, it is very important to use the Elastoplastic model both to estimate the horizontal stresses and to predict the fracture gradient. The consistency in what model that is used is important to get reliable results. If the input data for the Elastoplastic model is based on data from the linear elastic model, the results could be severely off. Therefore, it is important to know where the input data comes from in order to use them correctly. [4, 16]

Equation 2.37 describes an ideal mud system that is optimized to heal fractures. Firstly, the mud system has to be tested in lab before it can be used in operation. Thereafter, the mud has to be monitored and the properties maintained during operation. On a rig, the contaminated drilling fluid can be tested different types of equipments, which will be covered in later sections.

2.4.4 Effect of Temperature

It is a fact that the wellbore temperature affects the near wellbore stress state. A study conducted by Chevron and Landmark shows that LOTs taken at different wellbore temperatures yield different results. As mud is circulated, the wellbore is cooled and weakened. Likewise, as the wellbore is being heated, the wellbore is strengthened.[17]

With this in mind, I. Gil et.al. proposed a method to increase the effect of stress caging. By first cooling the wellbore (decrease the hoop stress around the wellbore), fractures can be initiated at a lower pressure. If the wellbore is cooled, the stress cage can be "set" at lower pressures. As the wellbore then again heats to its original temperature, the treatment is locked in place.[18]

For the linear elastic fracture model, the temperature can be incorporated in the equation. Using Poisson's ratio and temperature to express strain (assuming plane stress), the following equations give the fracture pressure.[5]

Penetrating fluid:

$$P_{wf} = \frac{1}{2}(2\sigma_h - \sigma_H) + \frac{1}{2(1-\nu)} E\alpha\Delta T \qquad (2.38)$$

Non-penetrating fluid:

$$P_{wf} = \frac{(1+\nu)(1-\nu^2)}{3\nu(1-2\nu)+(1+\nu)^2}(3\sigma_h - \sigma_H - 2P_o) + P_o + \frac{(1+\nu)^2}{3\nu(1-2\nu)+(1+\nu)^2} E\alpha\Delta T \qquad (2.39)$$

Having equal normal stresses on the wellbore wall, the equation above simplifies to:

$$P_{wf} = \frac{(1+\nu)(1-\nu^2)}{3\nu(1-2\nu)+(1+\nu)^2}(2\sigma - 2P_o) + P_o + \frac{(1+\nu)^2}{3\nu(1-2\nu)+(1+\nu)^2} E\alpha\Delta T \qquad (2.40)$$

By assuming Poisson's ratio is zero and no temperature effect, the equation reduces to the simplest form of the linear elastic fracture equation:

$$P_{wf} = 2\sigma_h - P_o \tag{2.41}$$

2.5 Particle Size Distribution

The particle size distribution (PSD) says something about how much particles of different sizes the mud contains. There is a strong connection between the particle sizes and the bridging properties of the drilling fluid. It is also important to optimize the mud to avoid formation damage and formation invasion. The critical fracture pressure tends to increase for muds with good bridging properties. Numerous of models have been developed to find the optimized PSD. It is important to notice that by introducing solids into the mud, one may encounter sagging problems or affect the fluid rheology.

Material type is of importance when it comes to prevent or stop circulation loss. The two most common materials in the industry are sized calcium carbonate and graphite. The synergy between these two materials also seems to have a positive effect on bridging properties of the mud. Graphite is able to deform and create a more pressure resistant bridge while sized calcium carbonate is able to plug a variety of fracture sizes.[19]

2.5.1 Packing of Particles

In order to get as tight as possible filter cake, the packing of the lost circulation material has to be as dens and impermeable as possible. Through the history, many mathematicians have tried to solve and prove the theoretical maximum density of a sphere pack. This is referred to as Kepler's Conjecture, which asserts that the density of a packing of equal squares in three dimensions is never greater than $\pi/\sqrt{18} \approx 0.74048$. Or viewed differently, the porosity can never be less than $1 - \frac{\pi}{\sqrt{18}} \approx 0.25952$. Kepler's conjecture is considered proven by Thomas Callister Hales. There are though difficulties to verify Hales' proof.[20, 21] Figure 2.15 shows a 3-dimensional illustration of a hexagonal equal sphere pack from two different angles. It can be derived mathematically that the hexagonal pack has maximum density possible, namely, 0.74048.[22] There are two types of voids between the spheres in the figure, separated with different colours (blue and yellow).

Figure 2.15: Hexagonal packing of spheres.

By filling the voids with smaller spheres, the theoretical porosity might be smaller. However, for lost circulation applications, the more relevant parameter is the permeability of the pack. Studies have been conducted within this area in order to determine size of particles in gravel packs. In a gravel pack, the permeability should be high and the density low to let the reservoir fluid flow through. These studies have shown that for gravel packs, the particle size distribution of the gravel used should be well sorted. Meaning, the gravel should contain particles nearly equal in size and shape in order to get a permeable pack.[23] In a well, the filter cake should be as tight and impermeable as possible, i.e. the opposite of gravel packs. In the petroleum industry this is implemented, but the procedures does not say anything about the optimal particle size distribution. The procedures do, on the other hand, say that there should be a wide size distribution and that coarse particles should be present.[6]

The packing in Figure 2.15 can be viewed in 2-dimensions. Dependent on the view-angle, two different cross sections can be drawn. These two cross sections represent a cubic packing (a) and hexagonal packing (b) in a 2D-space, and are shown in Figure 2.16. The void between the spheres in the cubic arrangement is the same void as the blue coloured void in Figure 2.15. Likewise, the void between the spheres in the hexagonal arrangement corresponds to the yellow coloured void in Figure 2.15.

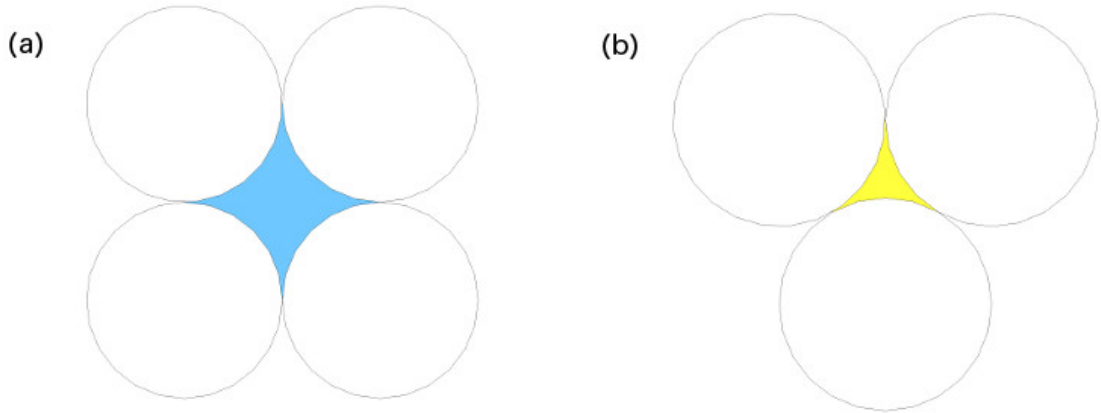

Figure 2.16: 2D-cossection of packing. (a) Cubic packing (b) Hexagonal packing.

Calculating the size of the spheres that would fit inside these voids is not too difficult. For the case where the spheres are in a cubic arrangement, the diameter of the sphere that fits inside the void is:

$$d = \left(\sqrt{2} - 1\right)D = 0.4142D \quad (2.42)$$

Where d is the diameter of the smaller sphere and D is the diameter of the bigger sphere (see Figure 2.17)

For the hexagonal arrangement, the diameter of a sphere that fits inside the void would be:

$$d = \frac{2-\sqrt{3}}{\sqrt{3}}D = 0.1547D \quad (2.43)$$

Where D is the diameter of the bigger sphere and d is the diameter of the smaller sphere.[24]

The diameter of the spheres that fit in the even smaller voids is more difficult to find, but an approximation can be found by drawing the spheres in scale and measure the sizes. By doing so, relationships between the spheres were found. The number of spheres in the 3D-packing shown in Figure 2.15 and the sizes are listen in Table 2.3.

Number of spheres in the packing	Diameter
13	D1 = fracture opening/biggest pore diameter
6	D2 = 0.4142 x D1
8	D3 = 0.1547 x D1
24	D4 = 0.138 x D1
24	D5 = 0.112 x D1

Table 2.3: Size relation and number of spheres in pack.

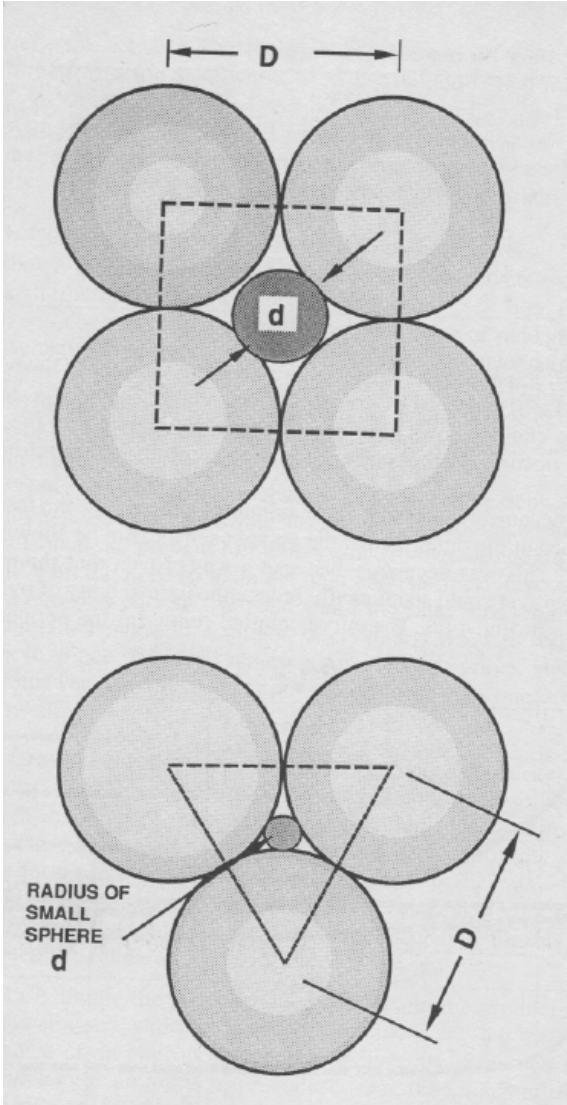

Figure 2.17: Fitting of spheres. [24]

From size relations and by counting the numbers of voids for each size, a theoretical size distribution can be made. The result is shown in Figure 2.18, where the largest diameter is set to 1mm. This theoretical particle size distribution could be tested, but there are a few concerns that should be highlighted. Most importantly, this theory builds upon a hexagonal 3-dimension packing of particles. In a real situation where fluid is pumped into a well, there is no guarantee that the particles will be arranged in a hexagonal order. The particles will take a random arrangement, which is impossible to predict. Nevertheless, random packing of particles of different sizes can be simulated. Secondly, the approximation of the sphere sizes is based upon a 2-dimensional cross-section. It may or may not be possible to fit the smaller spheres into the same 3-dimensional void, which introduce an error/uncertainty in the theory.

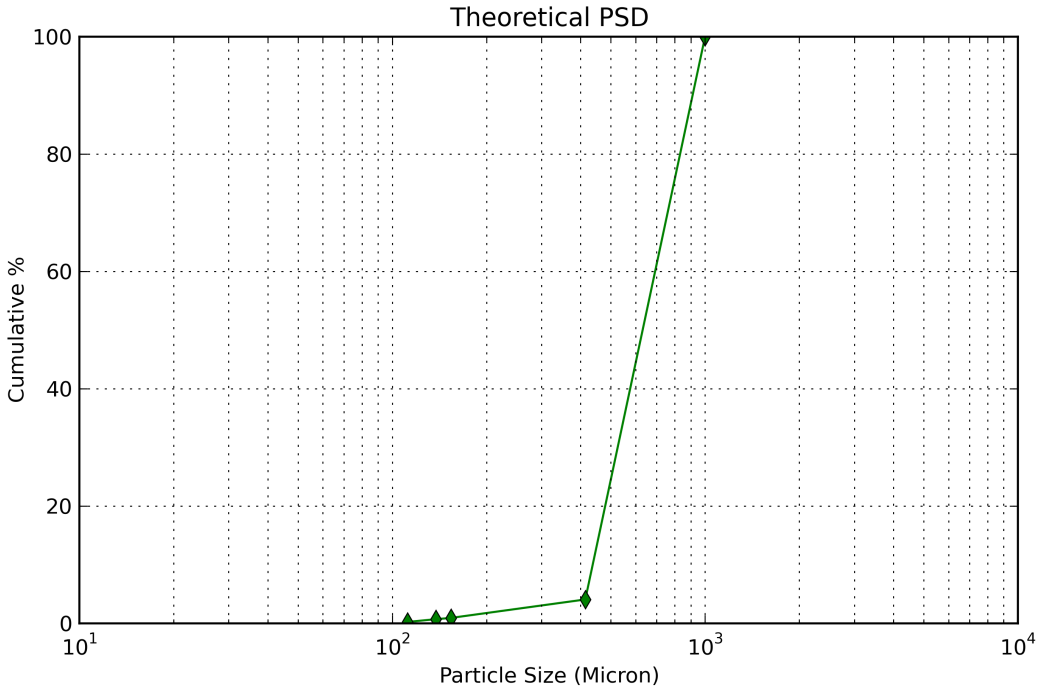

Figure 2.18: Theoretical PSD

2.5.1.1 Permeability of packed spheres

Gravel packs are used as sand control down hole. Proppant (sand) is pumped into the well with specialized equipment. The downhole pressure is increased to a level at which the formation cracks open. The proppant flow into the induced fracture, and keep the fracture open. Now, the fractures itself generates a flow channel, which makes it possible for reservoir fluid to flow into the well. The proppants inside the fractures and around the tubing creates a restriction for formation sand to flow into the production tubing. A properly made gravel pack is permeable enough to allow reservoir fluid to flow through the pack, but is also tight enough to restrict formation sand to enter.[23, 24]

When drilling a well, solids and clay material will settle on the wellbore wall. This creates what is called a filter cake. The filter cake is tight, causing the drilling fluid to stay inside the well, which is important. It is important in order to have pressure control in the well.[2]

For gravel packs, well-sorted particles are used to achieve permeable packing, which generates a quite steep particle size distribution. With this in mind, the opposite (a wide distribution) should result in a more impermeable packing of particles.[23]

In 1991, M. J. MacDonald et. al. tested the permeability and porosity of particle mixes with different PSD. There were two interesting results from this study. Firstly, the tests showed that a mixture of particles with large difference in size gave best results regarding both permeability and porosity. Secondly, the weight percent ratio that gave lowest porosity did not necessarily give the lowest permeability. A 25% fine – 75% coarse mix gave minimum porosity, while a 75% fine – 25% coarse mixture gave minimum permeability. This indicates

that there should be excess of finer particles in order to get low permeability. A third interesting result is that absence of coarse material gave poor porosity and permeability results opposed to mixtures that contained coarse material.[25]

Sandaband uses particles to plug and abandon wells. This technology is based upon the fact that a wide size distribution results in an impermeable pack of particles. Figure 2.19 shows an example of Sandaband particle size distribution together with a typical gravel pack distribution.[26, 27]

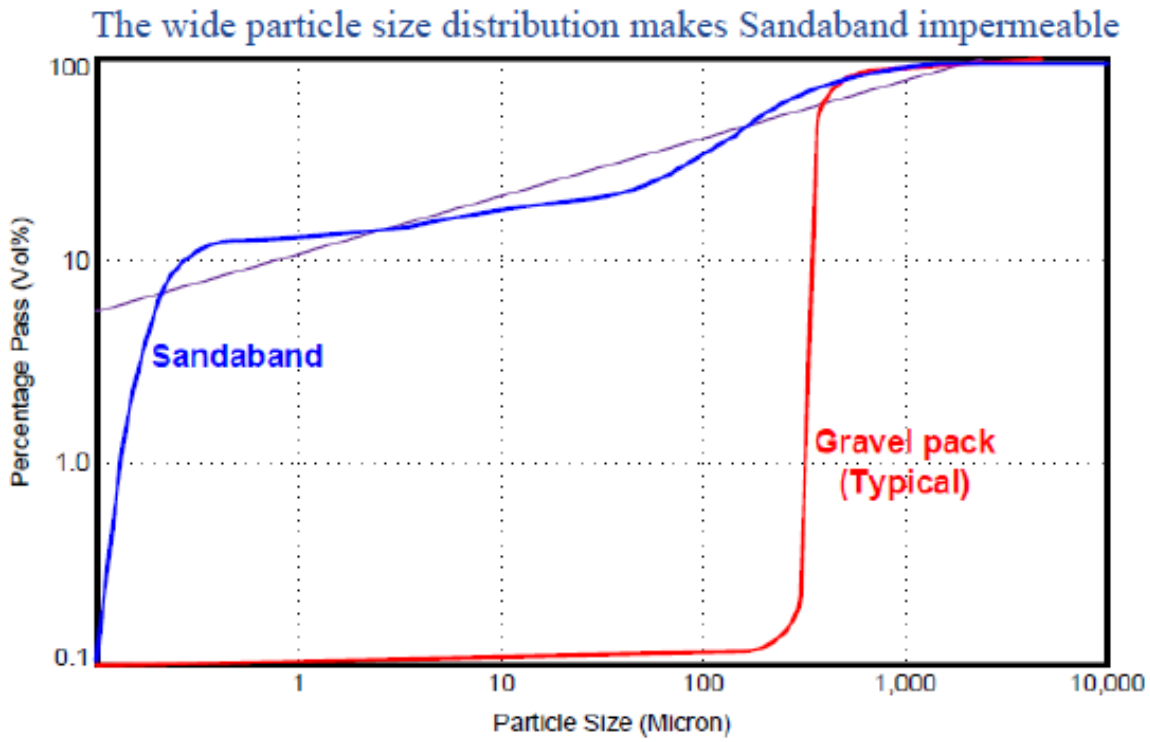

Figure 2.19: Sandaband PSD vs. gravel pack PSD. [27]

Comparing the gravel pack distribution and the theoretical distribution, small differences can be seen. Expectedly, the theoretical PSD there are higher amount of smaller particles. The comparison is shown in Figure 2.20 below.

Generally looking at PSD, it is important to understand that these plots looks like continuous curves, but in reality these are scattered plots. This might cause misinterpretations of PSDs made with only a few grain sizes included.

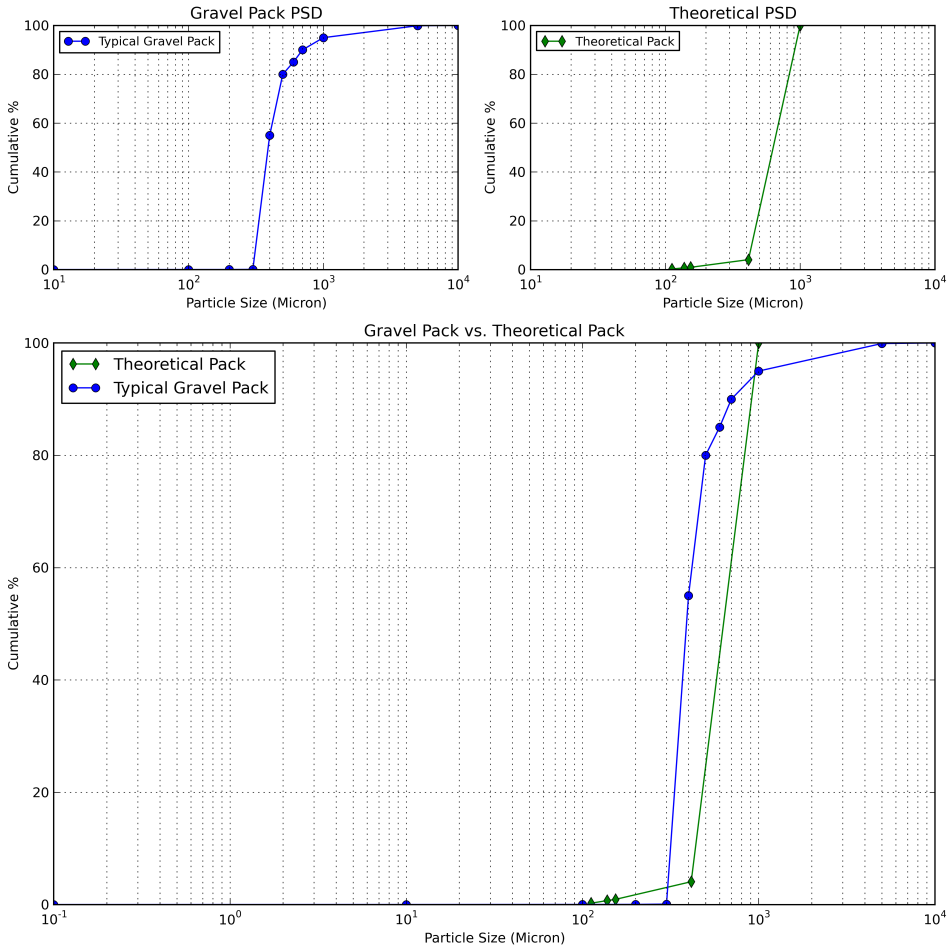

Figure 2.20: Comparison of a typical gravel pack PSD and theoretical PSD.

2.5.2 Abrams' 1/3 rule

From laboratory experiments, Abrams found that the median particle size has to be greater than 1/3 of the median pore size. Also, the concentration of the particles has to be minimum 5-volume-percent of the solids. By calculating the median pore size, a PSD can be developed according to this rule.[28]

2.5.3 Vickers Method

The Vickers method suggests that the PSD should match five parameters. One needs to know the D90, D75, D50, D25 and D10 of the pore sizes. If these parameters are known, the PSD could be designed as following:

D90 = largest pore throat.
D75 < 2/3 of largest pore throat.
D50 +/- 1/3 of the mean pore throat.

D25 1/7 of the mean pore throat.
D10 > smallest pore throat.

By following this method, the mud will form a strong and sealing filter cake.[29] This method is however optimized to avoid formation damage/invasion, not to heal fractures.

2.5.4 Ideal Packing Theory

The ideal packing theory (IPT) uses the pore size or permeability together with PSD to determine the ideal packing sequence. Preferably, the pore size should be known, but permeability information can also be used to estimate the pore size distribution.

The PSD itself does not tell anything about the sealing capability of the filter cake. The PSD can, however, be used to generate a basic ideal packing for the filter cake. The $D^{1/2}$ (square root of the particle diameter) plotted against the percent of cumulative volume. If the plot shows a straight line, the particle packing is ideal. Figure 2.21 and Figure 2.22 show PSD and $D^{1/2}$ plot respectively. The orange line in Figure 2.22 shows the ideal mixture of the particle agents.[30]

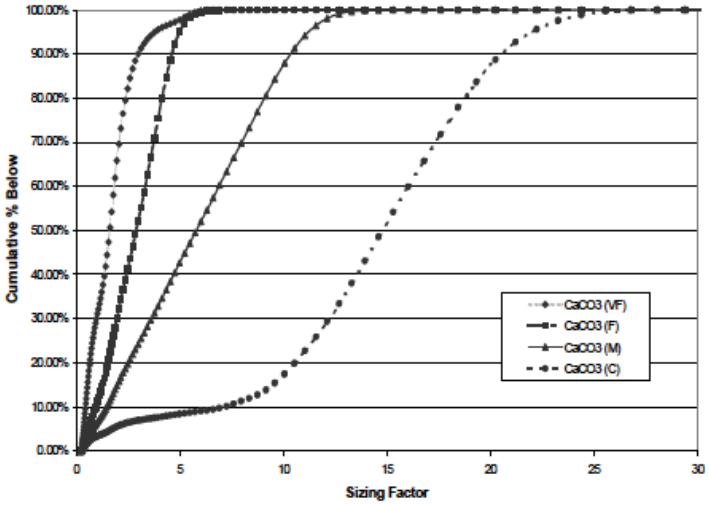

Figure 2.21: PSD of some commercially available bridging agents. [30]

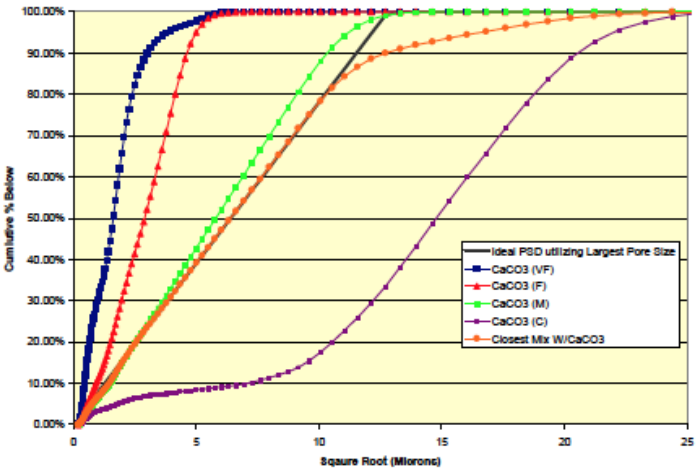

Figure 2.22: $D^{1/2}$ plotted against percent cumulative volume. [30]

2.5.5 Halliburton Method

Don Whitfill studied the particle size distribution together with fracture width. When the fracture width is known, a PSD can be developed and optimized to create a bridge. The d50 particle size distribution should equal the fracture with. That way there should be enough particles smaller and bigger than the estimated fracture with to seal off the fracture. In other words, the d50 is set to be equal to the fracture width in order to account for the uncertainty in the fracture with estimation. For this model, the following equation is used to estimate the fracture width.

$$\Delta P = \frac{\pi}{8} \cdot \frac{w}{R} \cdot \frac{E}{(1-\nu^2)} \qquad (2.44)$$

Where,

- ΔP is exess pressure within the fracture
- W is fracture width
- R is fracture radius
- E is Young's modulus of elasticity
- V is Poisson's ratio[14]

2.6 Logistics

The mud treatment system on the rig site consists of the following components in its simplest form:[2]

- Mud pumps
- Diverter
- Mud pits
- Shakers
- Monitoring equipment (such as temperature sensors, flow meters, etc.)

As the well is drilled, different materials such as formation fluid, cuttings and salts contaminate the mud. Ultimately this could cause the mud to change properties regarding rheology, PSD and density. It is therefore important to monitor the mud during the operation, and continuously add additives to maintain the properties. Another consideration is that the mud is loosing some particles when the filter cake is forming; hence, the mud will change during drilling as a result of the filter cake build up. In addition, during drilling, the particles in the mud tend to be ground down into smaller particles.

2.6.1 Real-time monitoring

At the time being, there is no reliable continuous PSD monitoring of the drilling fluid on the rigs. Samples are taken during drilling, but these samples do not say too much about the PSD or produced solids. Controlling drilling parameters is important to obtain proper drilling performance. The performance is also dependent on formation knowledge in order to add the right drilling fluid additives. It is also important to get information about the produced solids to know whether the solids are cuttings or originates from caving.

A series of laboratory devices have been tested offshore to see if these can be used to monitor PSD, cuttings and particles in real-time. The study gave good indications that by implementing a few devices, live monitoring can be achieved. With some modifications, these measurements could also be done automatically.[31]

2.6.1.1 Monitoring PSD

In order to monitor the PSD of the return drilling fluid, a photo-optical fluid analyser can be used. By taking samples after the shakers, a particle distribution can be established. During testing of this equipment offshore, the change in PSD was monitored. Figure 2.23 shows how the PSD changes during drilling of a well. The PSD shifted towards finer particles, except at one point where coarser particles were added to the drilling fluid (sample 5). Sample 1 in the figure is the oldest.

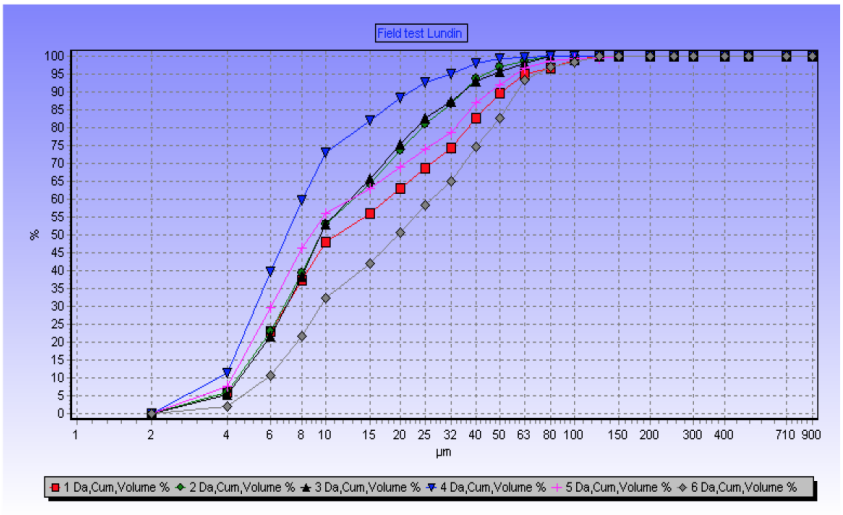

Figure 2.23: Real-time monitoring of PSD. [31]

The photo-optical device makes analyses based on real-time measurements of the drilling fluid. Lasers are used, and when the beam hits a particle, it is scattered in a manner dependent on the size and shape of the particle. The angular intensity is recorded by a series of photo detectors. A typical "picture" that the photo-optical analyser will give is shown in Figure 2.24. Both the shape and size of the particles can be analysed.[31]

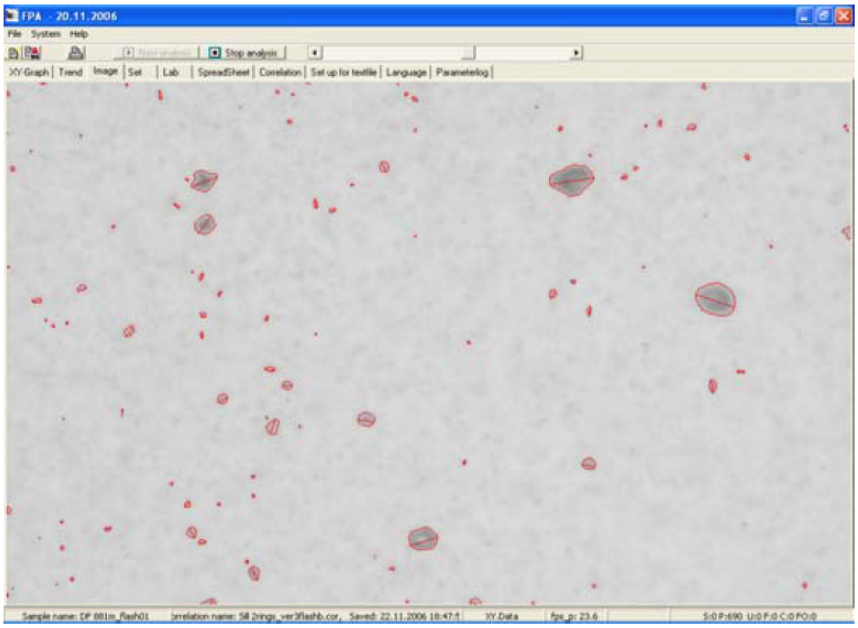

Figure 2.24: Picture from a photo-optical analyser. [31]

2.6.1.2 Monitoring cuttings

By using the same photo-optical analyser, the shape of the cuttings can be analysed. This measurement is useful to detect cavings. By plotting the aspect ratio of the cutting, i.e.

monitoring the Length/Thickness ratio, indications of cavings can be discovered at an early stage.

Figure 2.25 shows a plot of aspect ratio of cuttings. Note that the smallest particles are too small to get a reliable result. The apparatus is optimized to measure typical cuttings size range. In the figure, the cuttings have the same aspect ratio for particles over 0.3mm. This indicates that the particles have not originated from cavings. For the even larger particles, there is some variability in the measurements. This is because the amount of particles are lower, and the individual particle shapes become more notable.[31]

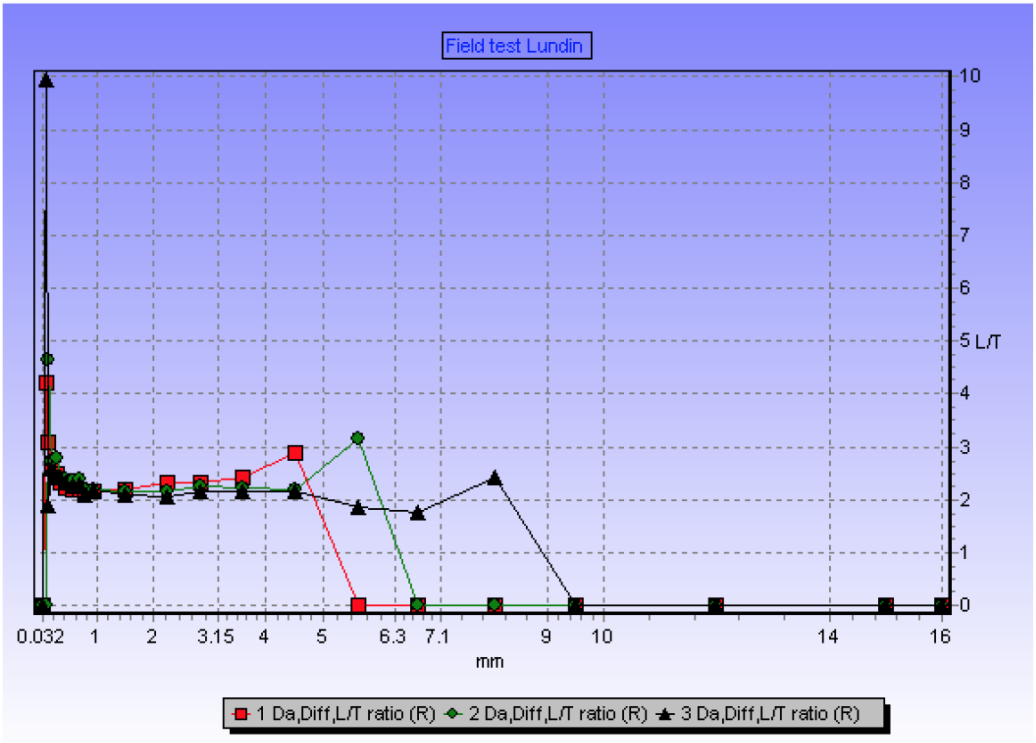

Figure 2.25: Aspect ratio of cuttings. [31]

2.6.1.3 Mineralogical monitoring

In addition to the two previous measuring techniques, it is also important to get information about the formation mineralogy. This information can be used to determine if the drilling has processed into a new formation. It can also determine if the drill bit is about to enter a formation with hole stability problems.

A method to determine the mineralogy of the return particles is to use a Raman Spectroscopy. Raman spectroscopy is a well-established chemical analysis device, which can describe both minerals and fluids (such as hydrocarbons). It is based on laser-induced excitation of chemical bonds. Individual bonds emit distinct frequencies of light, which defines “fingerprints” characteristics of different chemical phases.

Figure 2.26 shows an example of the spectrum from a field test. Here calcite can be distinguished from other organic materials. In addition to the mineral characterisation, one could also use this equipment to gain information about the formation fluid if there are measurable volumes of formation fluid in the drilled cuttings.[31]

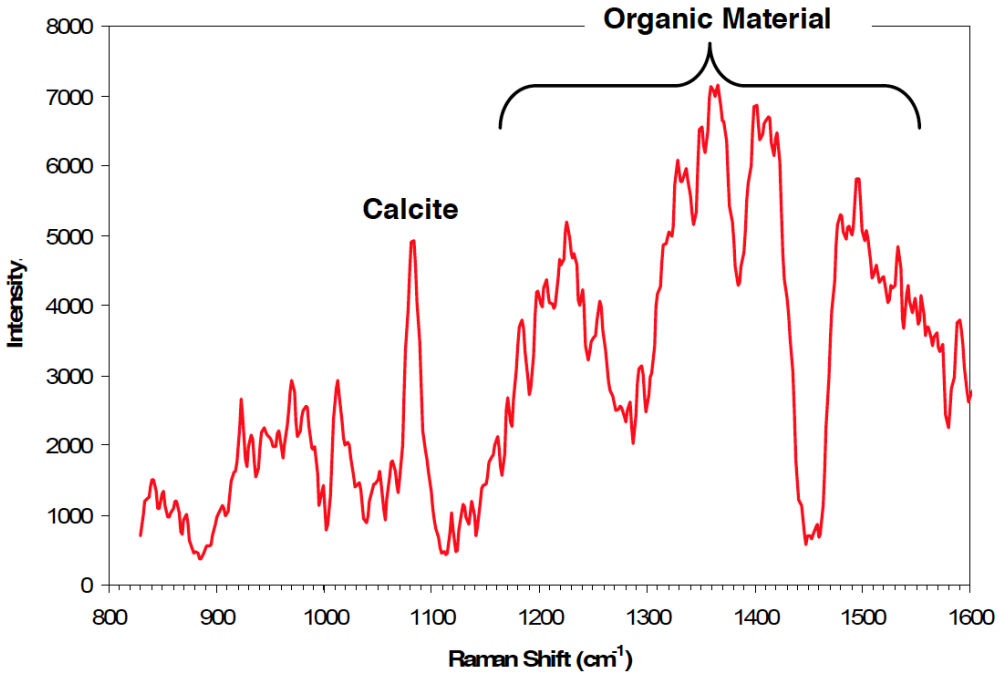

Figure 2.26: Example of Raman spectra from limestone cuttings. [31]

2.6.2 Solids Control

During drilling, cuttings are transported out of the hole with drilling fluid. The drilling fluid itself is designed to be able to carry cuttings, as well as keeping cuttings in suspension when circulation is stopped. At surface, the mud passes through shakers in order to remove cuttings. This is done to maintain the mud properties.

As mentioned in earlier sections, lost circulation prevention is based on adding particles to the mud. These particles introduce some challenges when it comes to hole cleaning and maintaining mud properties. If the shaker screens are too fine, all the coarse particles (and cuttings) will be removed from the active drilling fluid, and the mud will no longer be able to heal fractures. If the screens are too coarse, the density and rheology of the drilling fluid will be compromised. This implies that in order to prevent circulation loss, the mud treatment system has to be optimized for the task. This includes proper monitoring of PSD and proper screen selection.

2.6.2.1 Size, Conductivity and Strength of Screens

Shaker screens cloths are made of warp wires running along the cloth and weft wires running across. The opening between the wires is measured in mesh size, and the opening might vary dependent on how the screen cloth is made. Figure 2.27 shows the different definitions used to classify screens.[32]

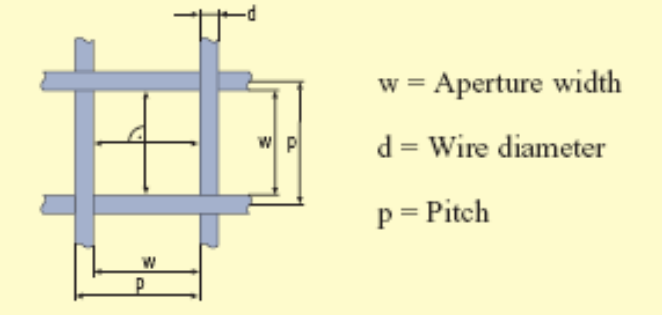

Figure 2.27: Screen cloth definitions. [32]

Mesh size is defined as number of apertures per inch. This could be problematic, because it does not reflect the aperture width. Figure 2.28 shows two screen cloths where the pitch is made different for the warp and wrap wires to get an oblong aperture. Note that the parameters in Figure 2.27 could be different for screens with the same Mesh number, and therefore filter out different particles sizes. This is illustrated in Figure 2.29. On the left side, the mesh number is kept constant and the aperture width is varying. The right side of the figure shows how the flow area is affected if aperture width and mesh number is kept constant.[32]

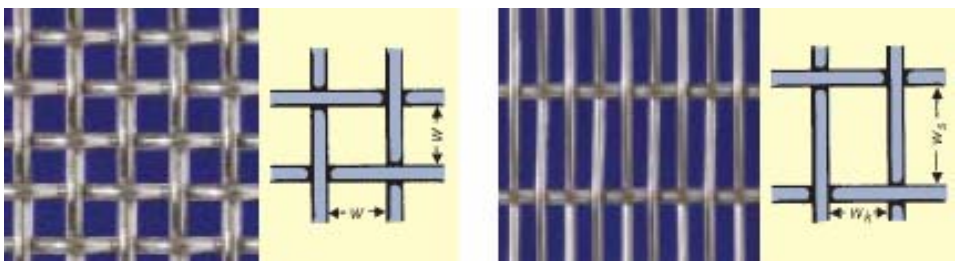

Figure 2.28: Screen cloth with carying pitch. [32]

Multilayer screens are often used in drilling operations. It is especially difficult to predict the aperture opening if oblong screens are used in a multilayer setup, because there is no simple connection between mesh and cut point. This is due to the fact that screens are often superpositioned manually, leading to different aperture openings.[32]

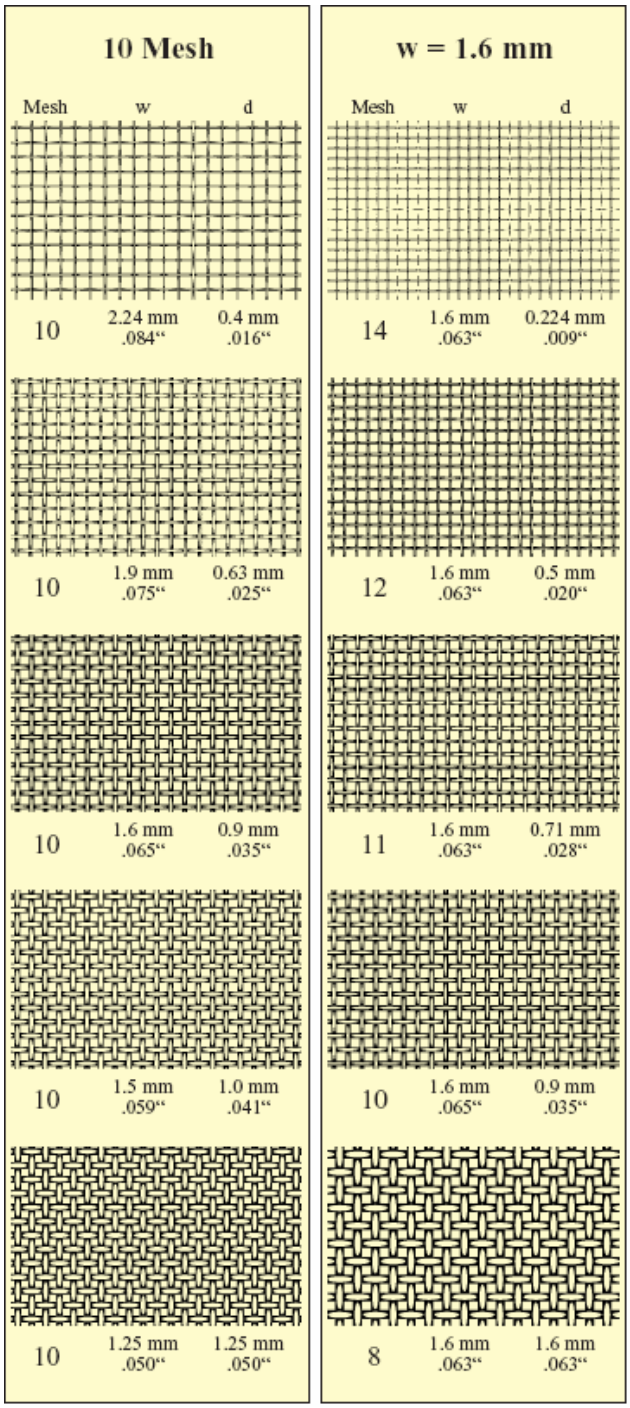

Figure 2.29: Left: Screens with similar mesh number have varying aperture width. Right: Constant Mesh number and aperture width affect flow area. [32]

Another important aspect to consider when selecting screens is the conductivity of the screen. The conductivity is related to the aperture width. Figure 2.30 shows the relative conductance as a function of wire thickness for a 200 Mesh cloth. Here the relative conductance is the flow area given wire thickness divided by flow area of a cloth with aperture width of 75 microns. This is a very crude estimate. Flow through screens is also dependent on the viscosity of the drilling fluid and the extensional viscosity.[32]

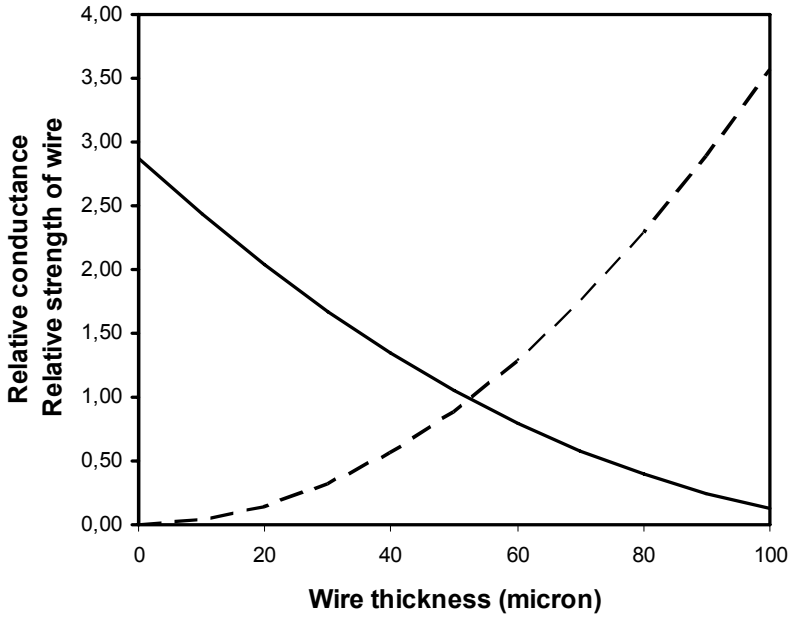

Figure 2.30: Solid line shows relative conductivity. Dashed line shows relative strength. [32]

Figure also shows relative strength of the screen. Relative strength is crudely estimated as cross sectional area of the wire divided by wire thickness of a 200 Mesh screen with 75 microns aperture. Screens should be selected based on strength rather than conductivity, because most shale shakers today can handle large flows without optimizing conductivity.[32]

2.6.2.2 Screen Wear

It is a common belief that screen wear origins from the friction between particles and the screen cloth. In other words, the wear happens from topside of the screen. Research does, however, show that in multilayer screen setups, the wear happens in between the layers. The weight from drilled cuttings presses the upper cloth onto the middle en lower cloth, causing more friction due to relative motion between the different cloths. For single layer screens, the wear is, in fact, generated from particles sliding on the top of the screen.[32]

For multi-layered screens, it is often hard to know to which extend the wear is. Since the wear is happening in between layers, it is impossible to see the wear before wires are starting to tear holes. In the North Sea it is normal practice to run coarse single layer screens as scalping screens (to remove coarse particles), before the drilling fluid enters the finer main screen. Some configurations with very coarse scalping screen (10 Mesh) and much finer main screens (200-300 Mesh) cause extremely high screen consumption.[32]

In order to reduce the screen consumption, the weight of solids on the main screens has to be minimized. Meaning, the scalping screen should be finer than 10-Mesh. Done correctly, wear on primary screens could be reduced by 90%. To achieve this, scalping screen should be as fine as possible to reduce the weight of particles on primary screens.[32]

Another way of reducing screen wear has been tested by Dahl et. al. By using a device that modifies the direction at which the fluid enters the screens had significant effect on the following: [33]

- Increase flow capacity of the shakers
- Reduce screen wear
- Reduce volume of drilling fluids on cuttings
- Reduce low gravity solids in drilling fluids
- Reduce the need for personnel exposure in the shaker room.

2.6.2.3 Field Case

Statoil conducted a field test where coarse shakers were used to let coarse particles re-enter the well. These particles acted like lost circulation material, and strengthened the wellbore. The well that was drilled had depleted by 100bar and the fracture gradient was reduced during the depletion period. Other wells previously drilled in the reservoir suffered severe losses. Initially, multiple shakers were planned to have different screen configurations, and the flow into each shaker could be controlled with valves. However, issues regarding controlling the flow into the shakers resulted that this concept was abandoned. Coarse shaker screens were ultimately chosen to let coarse particle pass and re-enter the well. The cut point of the shaker screens was analysed in order to select the best fitting screens for the task. Also, shaker wear was closely monitored; damaged screens were replaced accordingly as soon as possible. To control the PSD a laboratory sieve stack was used offshore.[34]

The fluid's bridging capabilities was tested using a production screen tester (PST). This test reviled that even though the shakers removed some of the coarse particles, the fluid was still able to create bridge effectively for fractures up to 1000 micron. Another discovery was that during drilling, the PSD shifted to finer particles rapidly. This indicates that continuous monitoring of the PSD is necessary in order to achieve a strengthened wellbore.[34]

3 Experiments

3.1 Description of Experimental Setup

The experimental work of this thesis consists of two parts. The same experimental procedure is used for both Part I and II, i.e. a static bridge apparatus was used to test the bridging properties in both parts.

3.1.1 Part I

Part I is aimed to determine whether or not the theoretical PSD in section 2.5 is valid. In order to test it, a water based polymer fluid was mixed. The fluid composition is only water and polymer. Four different PSDs were tested, and the polymer kept the particles in suspension during the tests.

3.1.2 Part II

Contaminated oil based mud from the Gudrun field in the North Sea was tested in the lab. As a reference, the rheology and bridging properties of the mud were tested in the lab beforehand. The contaminated mud samples where taken both from before and after the shakers. These two samples are listed below:

- Oil based WARP from before the shakers
- Oil based WARP from after the shakers

Composition and properties of the fluids are presented in section 3.2.

3.1.3 Static Bridge Apparatus

In order to test the mud's bridging properties, a static bridge apparatus was used.

A schematic overview of the static bridge apparatus is shown in Figure 3.1. The system consists of a steel cylinder. At the bottom of this cylinder, steel slots are inserted to simulate fractures. The slots can be configured to make different fracture openings. Figure 3.2 shows a picture of slots used in the experiments. The cylinder is filled with mud and the top is sealed. A high-pressure Gilson pump is used to pressurize the cylinder by pumping water into the cylinder. Maximum pressure for the system is 50MPa (500 bar). Pressure is measured by the pump and recorded on a computer. Flow rate was set to 2 ml/min for all experiments and each experiment lasted about 60 minutes. After an hour, water-breakthrough could be observed. However, for some tests, the particles created a bridge that could withstand the 50MPa pressure limit of the system, and those tests were therefore stopped before 60 minutes.

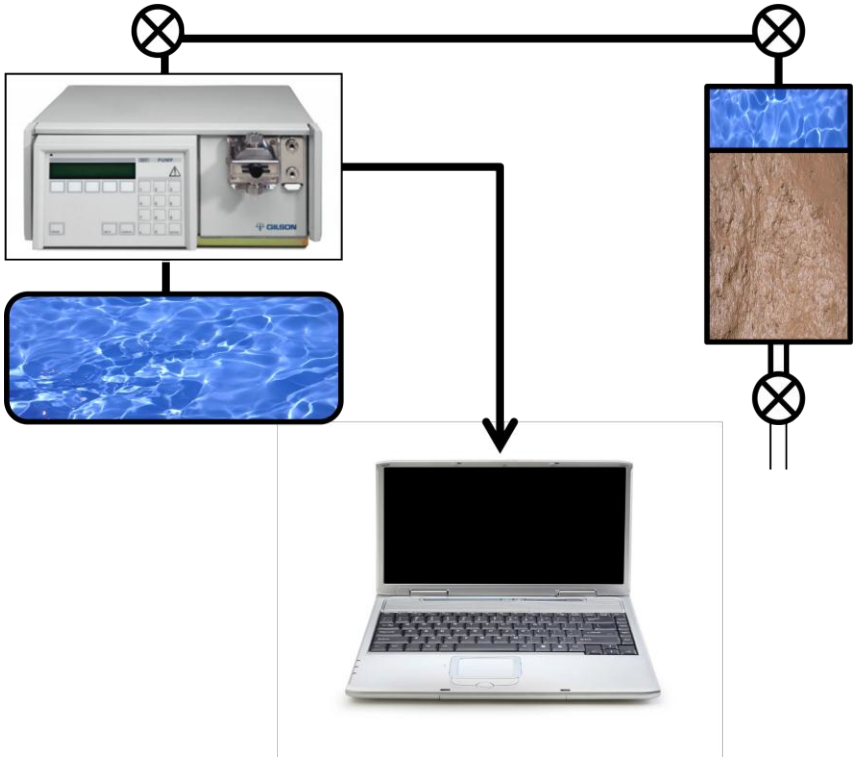

Figure 3.1: Static bridge apparatus. [35]

Figure 3.2: Slots made up of two "half-circles" used to simulate fracture.

3.2 Description of Mud Preparation and Properties

Rheological properties of the mud were analysed with a viscometer at 50 deg. C. Also, the density and filtrate loss were recorded before bridging experiments were started. Filtrate

loss was tested with a HPHT filtrate press at 95 deg. C and 500 Psi. Results are listed in Table 3.1 and Table 3.2.

Mud sample before shaker	
θ_{600}	140
θ_{300}	78
θ_{200}	55
θ_{100}	31
θ_{6}	5.5
θ_{3}	4.7
Gel strength	5.4/9.7
Plastic viscosity	62 cP
Apparent viscosity @ 600rpm	70 cP
Yield point	16 lbf/100ft^2
Filtrate loss	6.4ml
Density	1.98sg @ 20 deg. C

Table 3.1: Properties for mud sample before shaker.

Mud sample after shaker	
θ_{600}	143
θ_{300}	78.8
θ_{200}	57.6
θ_{100}	33
θ_{6}	4.8
θ_{3}	4
Gel strength	4.9/9.9
Plastic viscosity	64.2 cP
Apparent viscosity @ 600rpm	71.5 cP
Yield point	14.6 lbs/100ft^2
Filtrate loss	5.8ml
Density	1.98sg @ 20 deg. C

Table 3.2: Properties for mud sample after shaker.

The drilling fluid recipe is shown in Table 3.3. A PSD analysis was taken on the samples in order to determine the amount and size of particles already in the mud. This was done at MI-Swaco's laboratory at Forus. Result from the analysis is attached in Appendix A, and the two figures below shows the concentration of barite particles. It can be seen from the figures that the two samples have almost equal amounts of particles and pretty much the same size distribution. A visual inspection of the fluid before the shaker screens reviled that there were very little cuttings. As there were very small amounts of cuttings in combination

with the similar particle size distribution discussed above, it was decided that bridging tests were to be run only on the fluid sample from after the shakers.

Composition of drilling fluid

Additive	Unit	Amount
OBWARP Concentrate	g/l	1540
EDC 99 DW	g/l	129.1
One-Mul	g/l	6.0
VG Supreme	g/l	3.5
Lime	g/l	29.0
EcoTrol RD	g/l	3.0
Versatrol HT	g/l	19.0
Water	g/l	58.2
$CaCl_2$ Salt	g/l	13.5
G-Seal Fine (Graphite)	g/l	50.0
VK-150 ($CaCO_3$)	g/l	50.0

Table 3.3: Composition of drilling fluid.

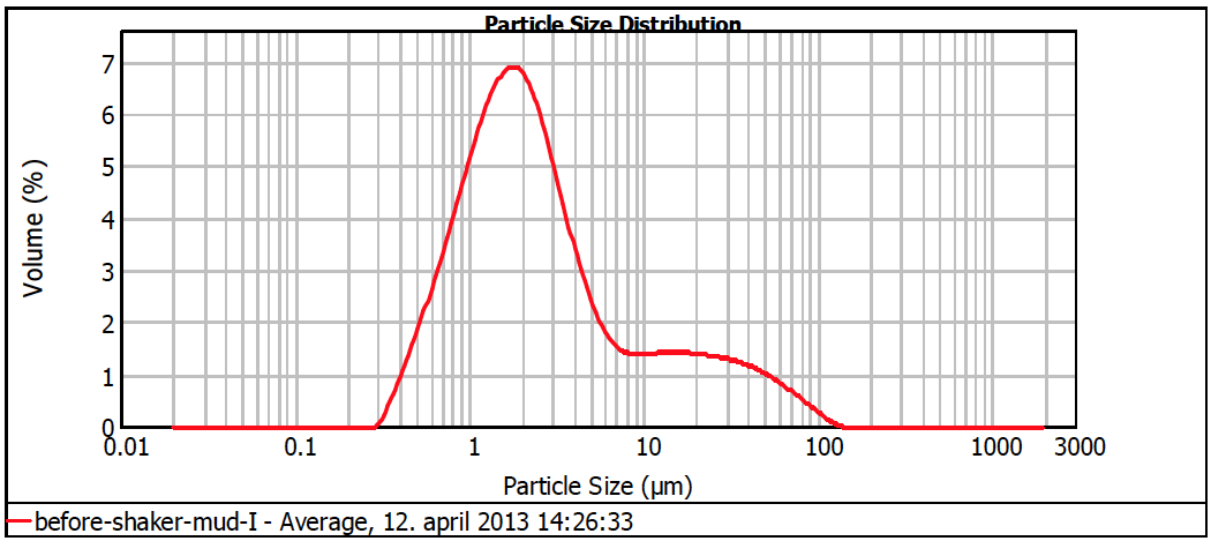

Figure 3.3: Particle size distribution of particles before shaker. Mud unmodified.

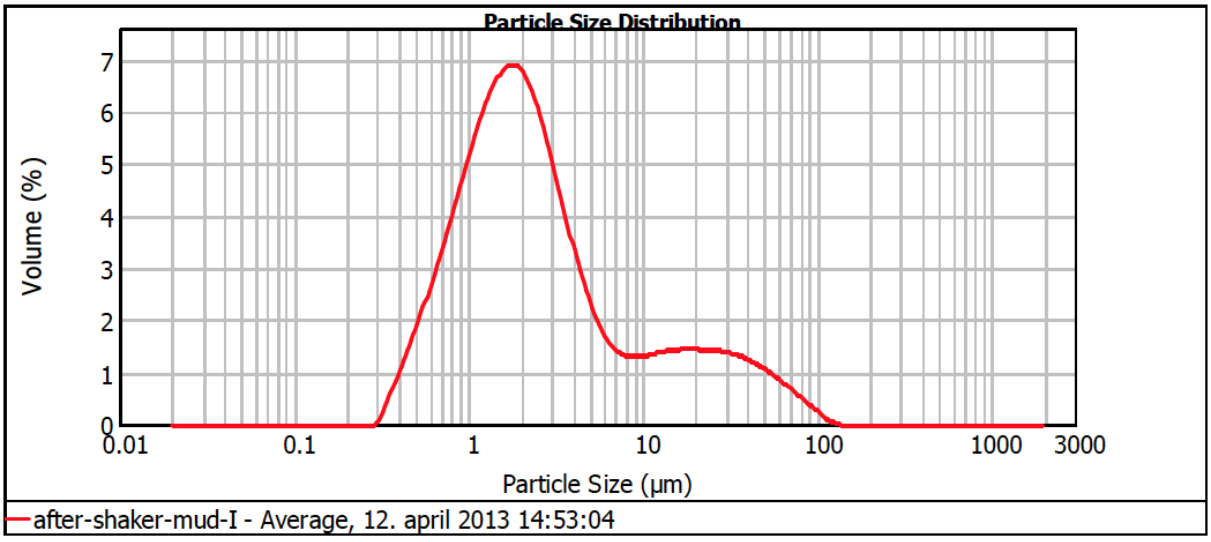

Figure 3.4: Particle size distribution of particles after shaker. Mud unmodified.

3.3 Description of the Experiments

The experimental part of the thesis consists of testing four different types of materials as lost circulation material. These four materials are as follows:

- Quartz
- Feldspar
- CaCO3
- LC-Lube (Graphite)

Adding these particles introduces some changes to the fluid's properties. Firstly, adding CaCO3 or LC-Lube will affect the rheology of the fluid. Quartz and Feldspar are harder particles. These particles will not dissolve in the fluid, hence, not affect the rheology. On the other hand, Quartz and Feldspar could introduce more severe sagging.

3.3.1 Part I

Quartz particles were used to test the bridging capabilities of a polymer water-based fluid. Four tests were run with the static bridging apparatus. The four tests are described in the following sub sections. The PSDs used were optimised to bridge a 250-micron fracture, and a 250-micron slot was used for all four tests. Test results are presented in section 4.

3.3.1.1 Test #1

39 kg/m3 of 250-280 micron quartz particles was added to the polymer mud sample.

3.3.1.2 Test #2

39 kg/m3 of quartz was added to the mud sample. The PSD in Figure 3.5 was used, which has D3 = 100micron. This is the PSD most similar to the theoretical PSD discussed in section 2.5.1.

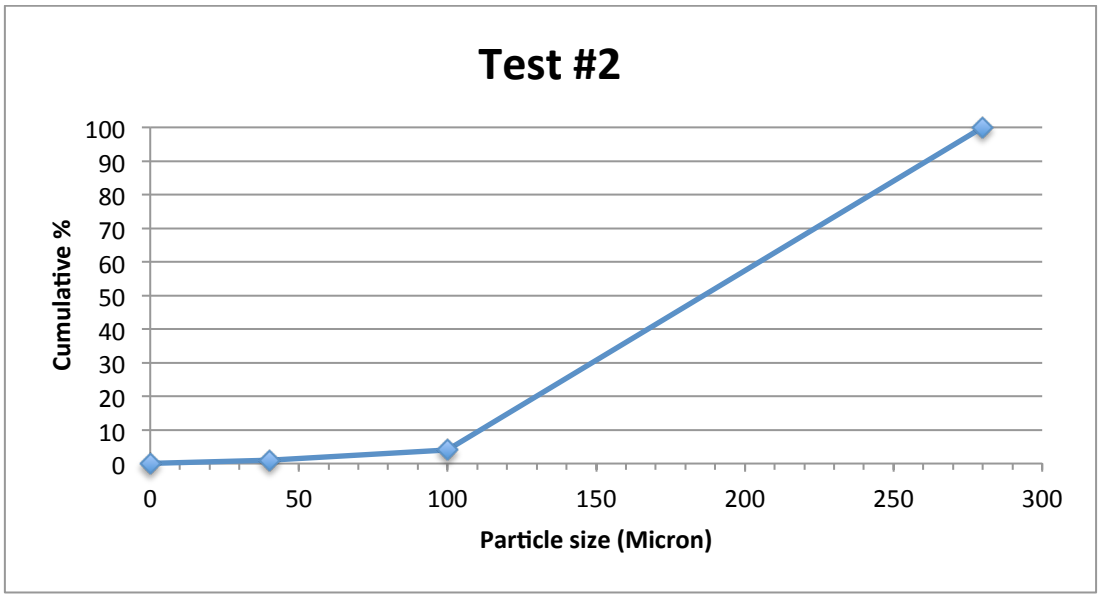

Figure 3.5: PSD for Test #2 (part I)

3.3.1.3 Test #3

39 kg/m3 of quartz was added to the mud sample. PSD in Figure 3.6 was used, which has D10 = 100 micron. i.e. more small particles added.

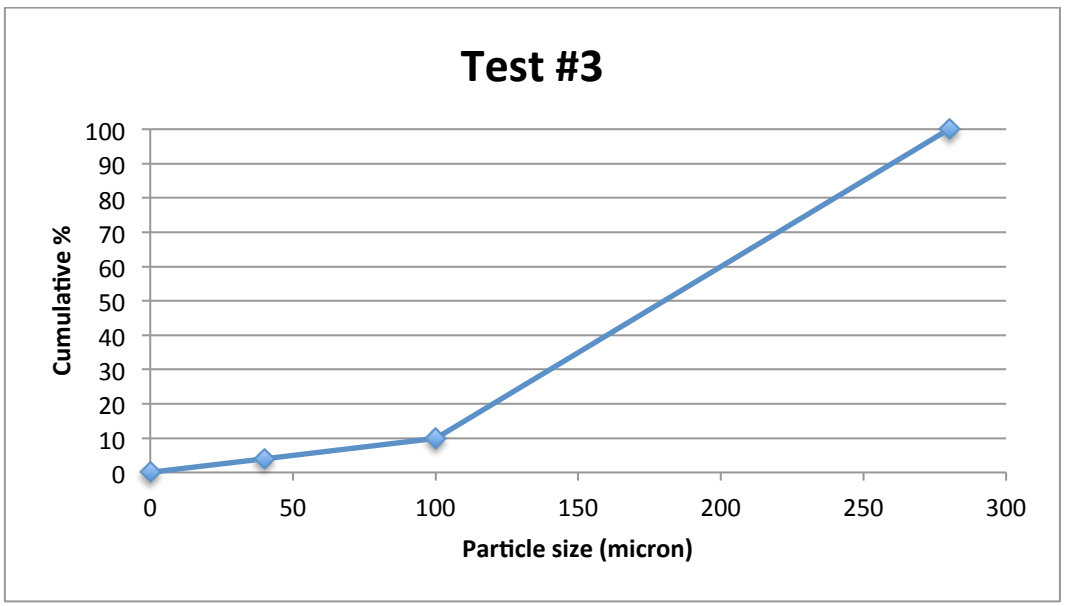

Figure 3.6: PSD for Test #3 (part I)

3.3.1.4 Test #4

39 kg/m3 of quartz was added to the mud sample. PSD in Figure 3.7 was used, which has D20 = 100 micron. i.e. even more small particles added.

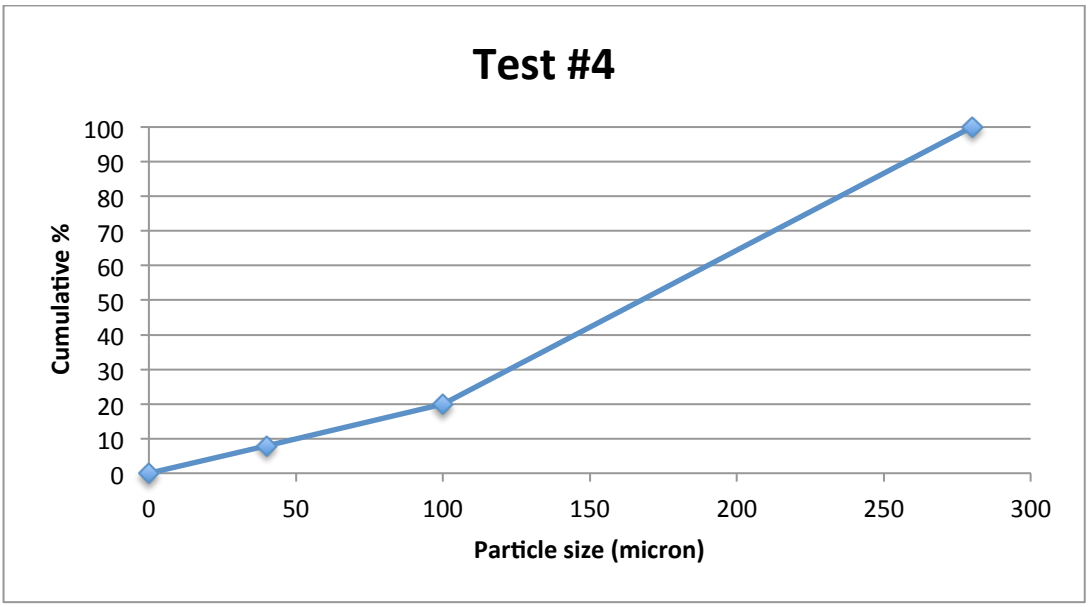

Figure 3.7: PSD used for Test #4 (part I)

3.3.2 Part II

Four different materials were used as LCM in the experimental work. Also, mixture of any two materials was tested to see the synergy between the different kinds.

Table 3.4 shows a list of particles used in the experiments.

Material	Trademark	Producer
Quartz	SI-700	North Cape Mineral AS
Feldspar	K-600	North Cape Mineral AS
CaCO3	Flow-carb	Baker Hughes
Graphite	LC-Lube	Baker Hughes

Table 3.4: LCM used in experiments. (part II)

Sieves with different aperture openings were used to sort the particles, and a PSD was created with these sorted particles. The PSD in Figure 3.8 was used for all materials in all experiments. D50 is approximately 245 microns for the chosen PSD. During the tests, a concentration of 39 kg/m3 of particles was added to the mud sample, which is similar to 2 weight-% for the specific drilling fluid used in this thesis.

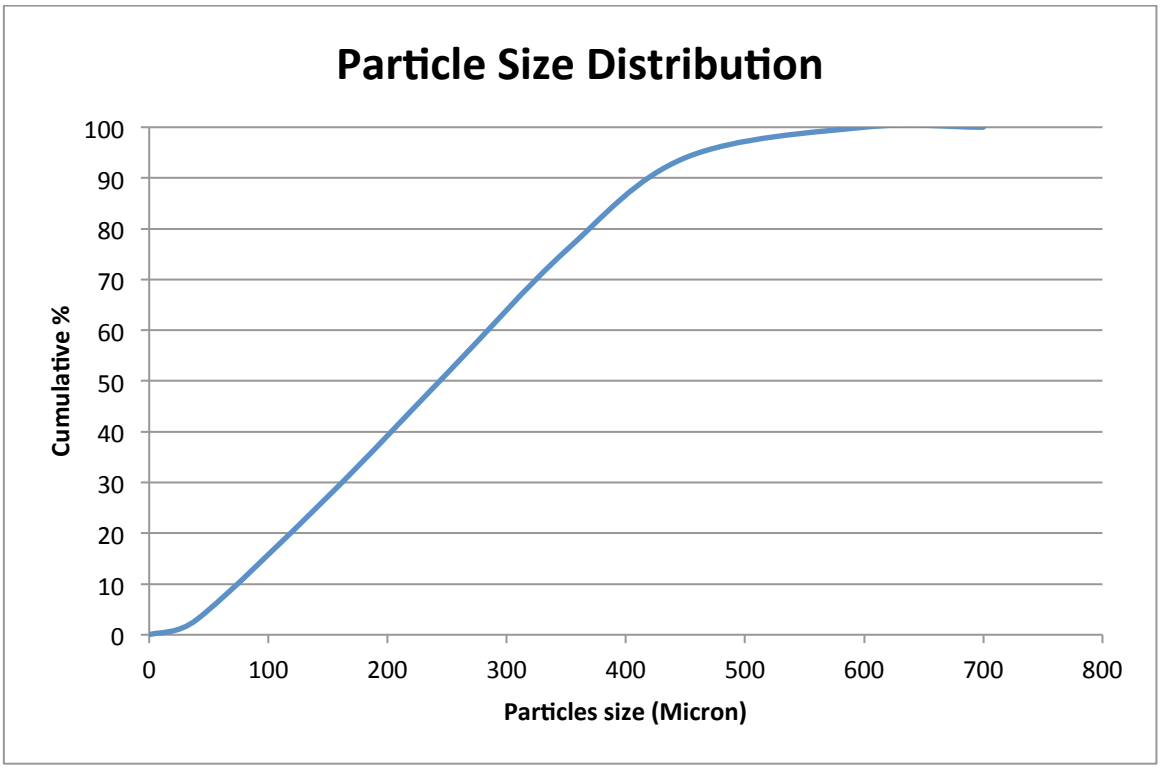

Figure 3.8: Particle size distribution used in experiments for part II.

100, 250, 300, 400, 500 and 600 microns slots were used in the experiments.

3.3.2.1 Synergies

The following synergies were tested with the same PSD as above. Slot opening for synergy tests was 400 microns.

Materials	Ratio	Concentration
Quartz / Feldspar	50 / 50	39 kg/m3
Quartz / CaCO3	60 / 40	39 kg/m3
Quartz / LC-Lube	60 / 40	39 kg/m3
CaCO3 / Feldspar	40 / 60	39 kg/m3
CaCO3 / LC-Lube	40 / 60	39 kg/m3
LC-Lube / Feldspar	40 / 60	39 kg/m3

Table 3.5: Synergy tests.

4 Results and Discussion

4.1 Part I

All tests were run with a slot size of 250 micron in the experimental part I. Different size distributions were used as described in section 3.3.1. Quartz was used as LCM.

4.1.1 Test #1

Particles were sieved into a range of 250-280 microns. These sorted particles were added to the polymer water based fluid. Concentration: 39 kg/m3. Result is shown in Figure 4.1.

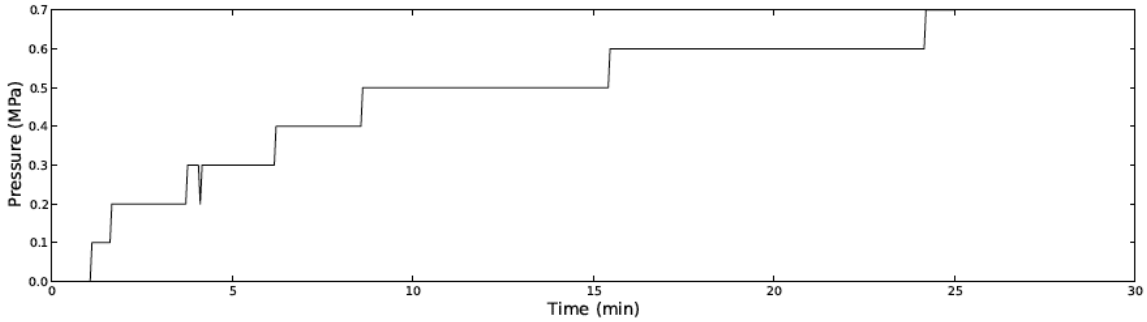

Figure 4.1: Pressure plot Test #1. Quartz with size range 250-280u, slot 250u. Polymer fluid.

It is clear from the figure above that the particles were not forming a sealing bridge. Maximum pressure was only 7bar, and it took about 25 minutes to build that pressure.

4.1.2 Test #2

39 kg/m3 of LCM with D3=100micron (shown in Figure 3.5) was added to the polymer water based fluid. Results of the test are shown in Figure 4.2. This particular PSD is close to equal to the theoretical PSD presented in section 2.5.1.

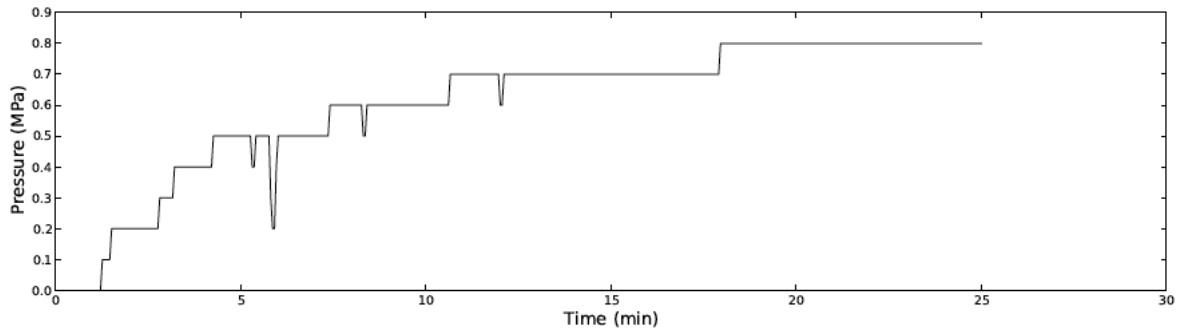

Figure 4.2: Pressure plot Test #2.

By adding smaller particles to the fluid, the bridging properties were slightly better, but not significantly. Test #2 had a particles size distribution where the biggest particles were 250-280 micron and D10=100micron. Maximum pressure recorded was 8bar, which is not good enough for fracture healing purposes. Another interesting observation is that the time to build up the pressure of 8bar was shorter than Test #1. This is also an indication that smaller particles will improve the bridge.

4.1.3 Test #3

Based on the results in Test #1 and #2, a new mixture of particles was made. 39 kg/m3 of LCM with PSD shown in Figure 3.6 was added to the polymer water based fluid. Results of the test are shown in Figure 4.3. D10 of the particles in this experiment was 100 micron and the bigger particles were in the size range of 250-280micron.

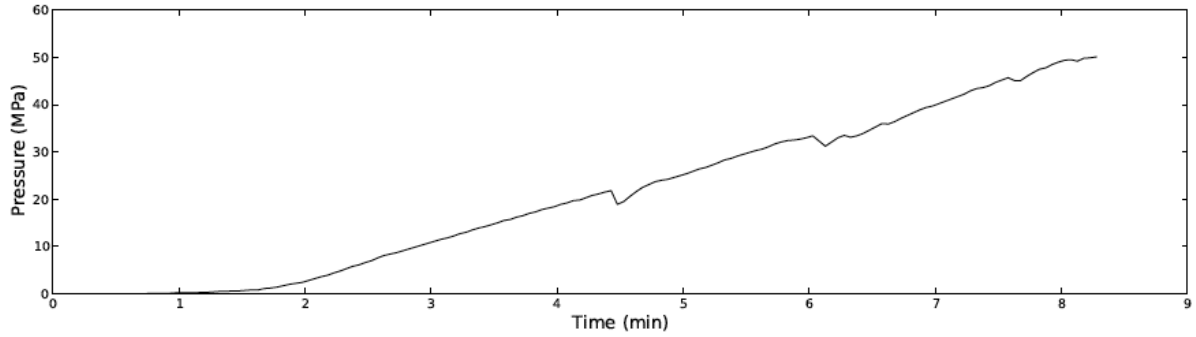

Figure 4.3: Pressure plot Test #3

The figure above shows that the increased concentration of smaller particles enhanced the bridging properties of the fluid. In this experiment, the fluid created a bridge in 8 minutes, which held a pressure of 500bar. During the experiment, fluid loss of 9.1 ml was observed as the pressure built up, indicating that the bridge was not sealing. This observation is interesting because it shows that a bridge could withstand high pressures even though it is not sealing.

4.1.4 Test #4

In order to further investigate the relationship between the LCM's bridging capability and its PSD a new mixture was mixed. 39 kg/m3 of LCM with PSD shown in Figure 3.7 was added to the polymer water based fluid. Results from the experiments are shown in Figure 4.4. D20 was set to 100 micron and the bigger particles were still kept in range of 250-280 micron.

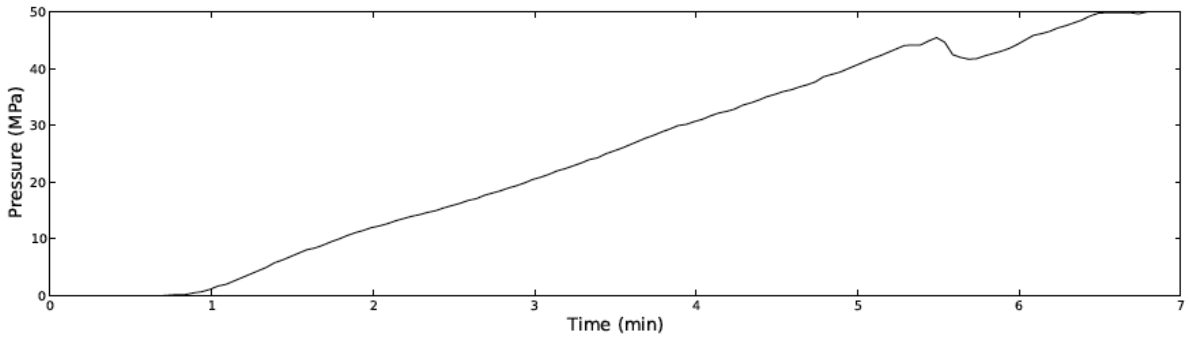

Figure 4.4: Pressure plot Test #4

It is interesting to compare Test #3 and #4. Firstly, the time to build a bridge was shorter for Test #4, meaning that the slope of the pressure curve is larger. The two pressure plots are shown in Figure 4.5. A large slope indicates low amounts of filtrate loss through the bridge, and these two experiments show that the sealing capability of the bridge is improved when the concentration of smaller particles is increased.

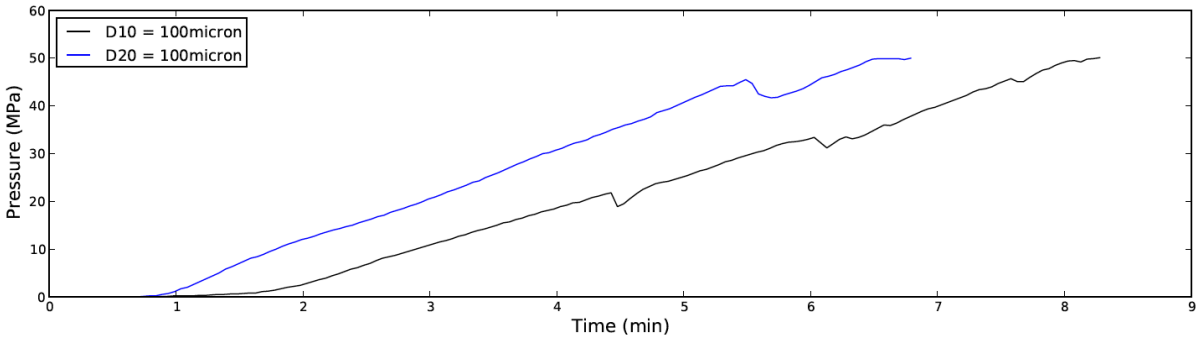

Figure 4.5: Comparison of Test #3 and #4.

Results from part I reviled that the theoretical PSD did not behave as expected, but the bridging capability of the fluid was dramatically improved by increasing the concentration of smaller particles. However, better results would be expected if the fluid contained filtrate loss controlling particles, such as clay. Table 4.1 shows the amount of filtrate loss that was recorder for test #3 and #4.

Test	Filtrate loss	Time until bridge formed
No. 3	9.1 ml	8.28 min
No. 4	6.1 ml	6.78 min

Table 4.1: Recorded filtrate loss and test time for Test #3 and #4.

From the four tests above, it seems that the smaller particles in the mixture plays an important role in terms of bridging properties of a fluid.

4.2 Part II

As mentioned earlier, the field mud was tested with slots of sizes 100, 250, 300, 400, 500 and 600 microns. The pressure was measured and recorded on a computer. The analytical approach is the same as Toroqi used for similar experiments, see ref [35]. The following parameters were recorded:

- Number of peaks (N)
- Average peak value ($P_{p\text{-}avg}$)
- Average pressure (P_{avg})
- Maximum pressure (P_{max})
- Test time (t)
- Number of peaks per minute (N/t)

Each of these parameters is described in more detail in the following sections.

4.2.1 Number of Peaks (N)

The peaks in the pressure plots indicates when the bridge collapses. Therefore, the peaks are somewhat a measure of the fluid's capability of forming a bridge in the fracture.[35] Figure

4.6 shows a pressure plot for quartz, using a 400-micron slot opening. The peaks are marked with black dots. Number of peaks also says something about the stability if the bridging, a low number represents a stable and strong bridge. However, this parameter is strongly dependent on the concentration of particles added to the fluid.

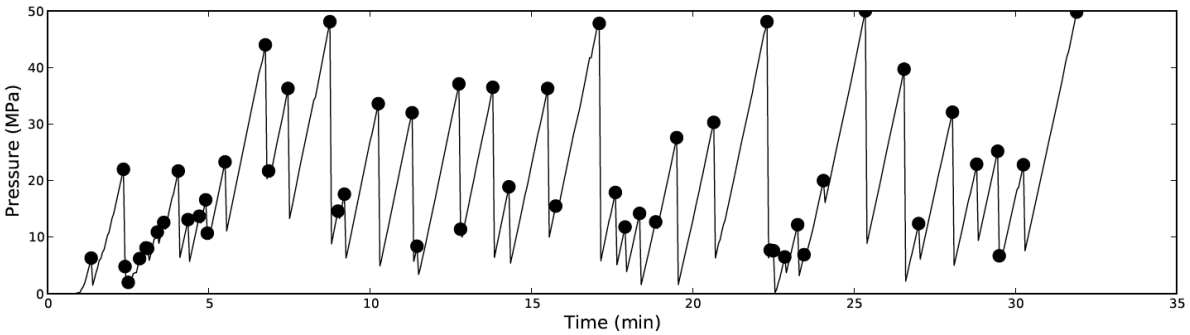

Figure 4.6: Peaks on pressure plot. Quartz used as LCM with 400-micron slot opening.

4.2.2 Average Peak Pressure ($P_{p\text{-}avg}$)

Average peak pressure indicates the average strength of the bridge formed in the fracture. It is a measure of the differential pressure over the bridge. The pressure inside the cylinder has a maximum of 50MPa and the pressure at the other end (outside the cylinder) is atmospheric pressure.[35] A high average peak pressure means that the fluid is strong and capable of holding high pressures. It also says something about how well designed the fluid is to form a bridge at the fracture.

4.2.3 Average Pressure (P_{avg})

Average pressure is also used to compare the different fluid samples as it tells something about the average strength of the bridge.[35] High average pressure indicates better bridge performance and strength. Borth average pressure and average peak pressure describe the bridge's strength. However, since there are less data points for average peak pressure, the $P_{p\text{-}avg}$ tends to be more scattered.

4.2.4 Maximum Pressure (P_{max})

The maximum pressure recorded during an experiment tells something about how particles are distributed in the fluid.[35] If the fluid creates a bridge unreasonably quick, it might be a sign that the particles are distributed unevenly in the fluid, and that there is a higher concentration of particles near the bottom of the cylinder (where the slot is). It also says something about the maximum pressure the bridge can withhold. However, the test system used in the experimental work has a maximum pressure of 500bar (50MPa). The experiments were stopped if the pressure reached 50MPa. It is still possible that the bridge could withhold a higher pressure, but it is hard to tell due to the pressure limitation of the system.

4.2.5 Test time (t)

Time (t) represents the time elapsed from start of the experiment until a bridge is formed or until water-breakthrough. In this work, a bridge formed when the pressure in the cylinder reaches 50MPa.

4.2.6 Number of Peaks per Minute (N/t)

Number of peaks normalized could be used to compare experiments of different time lengths.[35]

4.2.7 Analysis of Results

Table 4.2 shows the results from the experimental work.

Material	Slot (micron)	Peaks (N)	$P_{p\text{-}avg}$ (MPa)	P_{avg} (MPa)	P_{max} (MPa)	t (min)	N/t
Quartz	100	2	44.95	21.08	50.1	2.54	0.79
	250	6	38.18	26.305	50.1	5.02	1.2
	300	2	49.5	28.07	50.1	3.79	0.53
	400	53	21.22	18.7	50	31.95	1.66
	500	24	22.68	17.73	50.1	14.24	1.69
	600	45	3.66	0.59	21.8	58.66	0.77
Feldspar	100	1	49.9	19.3	50.1	2.91	0.34
	250	17	38.99	29	50.1	7.72	2.2
	300	5	28.34	19.23	50.1	3.48	1.43
	400	121	15.8	12.79	46.3	57.24	2.11
	500	70	13.08	10.66	50	33.09	2.12
	600	104	9.44	5.48	39.7	59.44	1.75
CaCO3	100	2	34.5	21.74	50	3.58	0.56
	250	148	23.65	19.48	45.6	59.80	2.47
	300	137	20.916	16.5	43.9	57.16	2.4
	400	171	8.64	6.2	27.1	58.74	2.91
	500	132	6.325	3.52	21	54.09	2.44
	600	119	3.6	1.32	16.9	53.85	2.2
LC-Lube (Graphite)	100	1	49.8	22.46	50.1	2.19	0.46
	250	207	12.23	10.32	30.4	59.53	3.48
	300	223	8.64	7.37	30.3	60.50	3.69
	400	206	4.11	2.82	22.1	61.06	3.37
	500	162	6.067	3.68	23.1	61.96	2.61
	600	114	2.27	0.68	11.5	55.79	2.04
Synergies							
CaCO3/Feldspar 40/60	400	135	14.58	11.18	45.2	56.92	2.37
LC-Lube/Feldspar 40/60	400	153	12.79	11.77	50.1	57.51	2.66
LC-Lube/CaCO3 60/40	400	223	6.23	4.65	26.9	60.27	3.7
Quartz/CaCO3 60/40	400	48	15.98	14.05	50.1	20.01	2.4
Quartz/Feldspar 50/50	400	13	29.18	20.75	50	9.70	1.34
Quartz/LC-Lube 60/40	400	110	15.87	14.21	50.1	48.73	2.26

Table 4.2: Results from bridge testing experiments on field mud.

The results in Table 4.2 are plotted in graphs below. Each parameter is plotted against slot opening size. A concentration of 39 kg/m3 was mixed into the field mud for all experiments. One interesting observation was that fluid with Quartz and Feldspar formed a bridge very quickly for slot size from 100-300 micron, whereas the CaCO3 and LC-Lube never really formed a bridge for slot sizes over 100 micron. This is a good indication that materials with a higher Mohs number perform better as LCM than materials with lower Mohs number.

A reference test of the mud system was run without any particles added. The fluid did not create any bridges when a 250-micron slot was used. This was as expected, since most of the particles in the fluid was smaller than 100 micron.

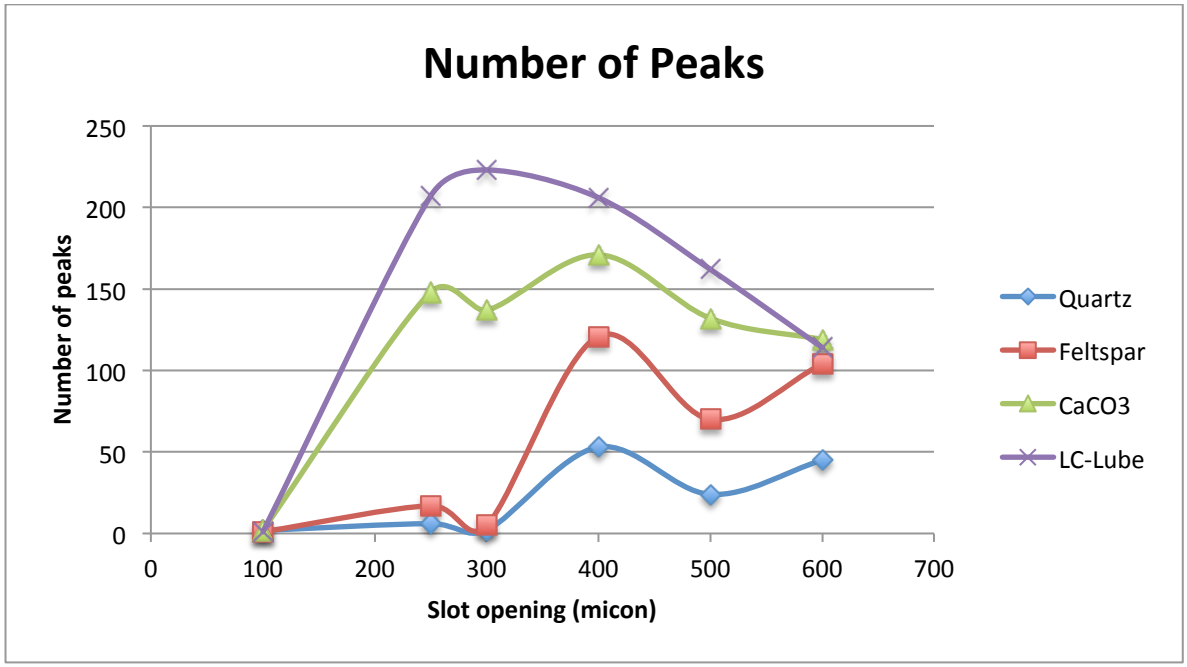

Figure 4.7: Number of peaks plotted for all materials as a function of slot opening.

From Figure 4.7 it can be observed that all materials had very good performance for the experiment with a slot opening of 100 micron. All four fluids created a bridge effectively and was capable of withstand high pressure during experiments with a slot opening of 100 micron. Another observation is that the number of peaks tends to decrease between slot size 250 and 300 micron. Same behaviour is observed between 400 and 500 micron. The reason for this observation is unclear and need further investigation. Tests from part I show that coarse particles not necessarily create better bridges. For this test LCM with a D50=245-micron could be suitable to bridge 250-micron fractures, but not necessarily 300-micron fractures. Since this effect is consistent for all materials except LC-Lube, the reason could be that the slot opening is less than 300 micron even though it was marked as 300 micron. The decrease in number of peaks between 400 and 500-micron could happen because two 250-micron particles could enter the fracture simultaneously (2x250=500micron). The concentration of 250micron particles probably higher than the concentration of 200 and 400 micron particles.

The general observation is that judging by the number of peaks, Quartz and Feldspar performed better than CaCO3 and LC-Lube. Quartz and Feldspar tend to create a stronger and more stable bridge. The strength of the bridges is easier to judge from Figure 4.8, and will be discussed below.

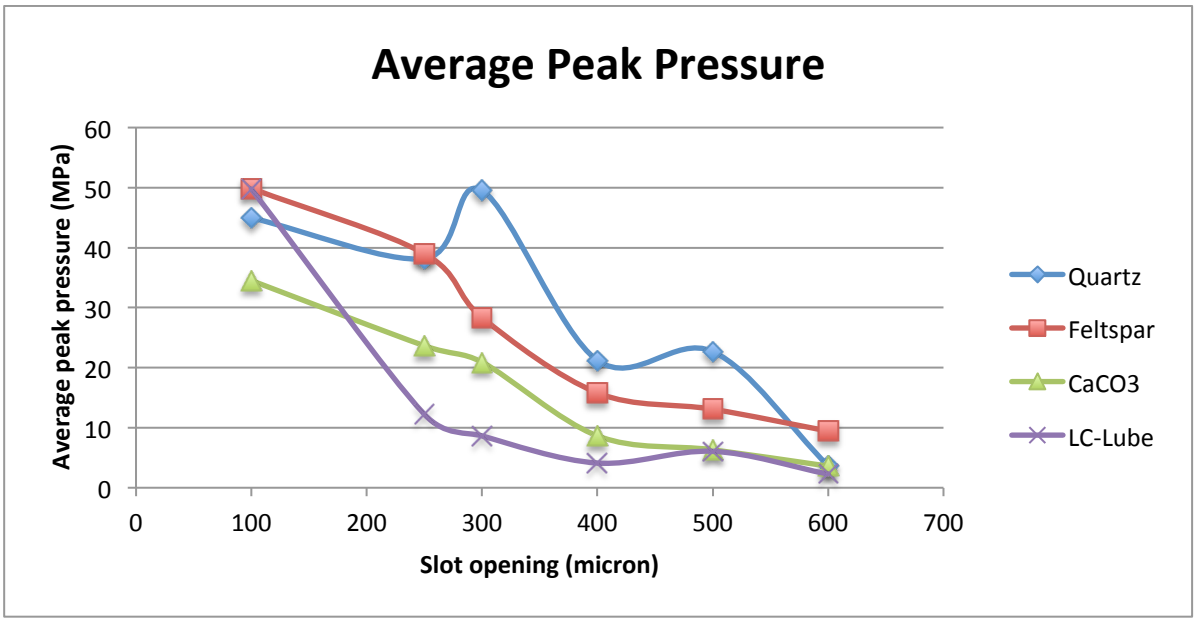

Figure 4.8: Average peak pressure for all materials plotted against slot size.

In general, the average peak pressure is higher for Quartz and Feldspar. However, for Quartz the plot is somewhat scattered, and could be misleading. The plot is still showing that particles that are higher up on the Mohs scale have better results. For a slot opening of 300 micron, Quartz is showing an unreliably high average peak pressure. This is because the fluid formed a bridge in only 3 minutes. Thus, that particular point might not be representative for comparing the different materials. If the point were removed, Quartz would have curve pretty similar to Feldspar, shown in Figure 4.9.

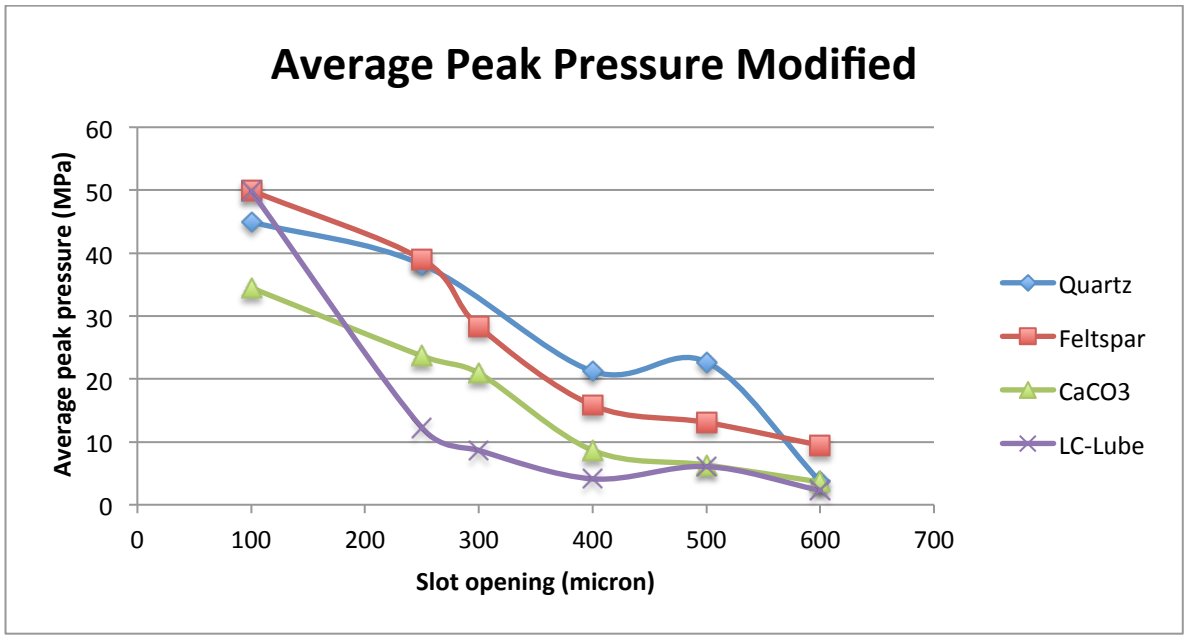

Figure 4.9: Modified average peak pressure plot.

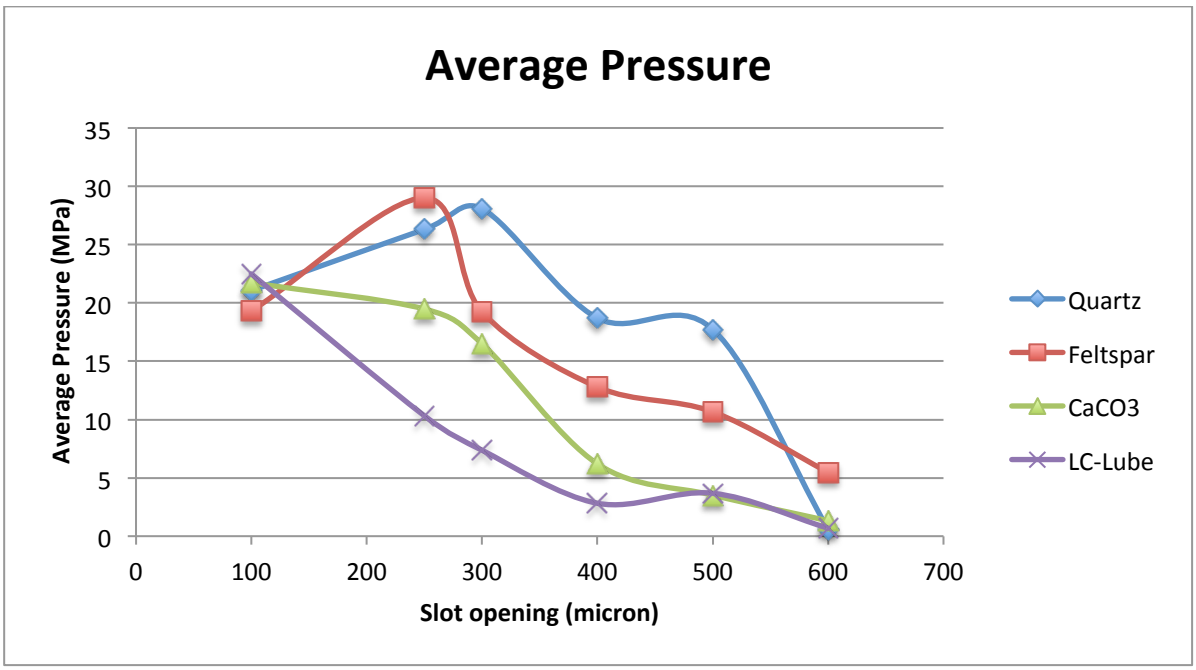

Figure 4.10: Average pressure plotted against slot opening.

The average pressure is clearly higher for Quartz. In general, average pressure is probably the one parameter that could tell something about the overall strength of a bridge. As the slot size increase, the average pressure is decreasing. Quartz and Feldspar show an increasing trend for slots from 100-300 micron in size. Again, this could be due to the fact that a bridge was formed very quickly for these materials at those particular slot sizes. Hence, also less data recordings to calculate averages. However, if the average pressure is divided by the test time (t), values that are more representative could be generated to get a better view. Figure 4.11 shows P_{avg}/t. This shows the LCM's ability to form a bridge at all.

Values close to zero indicates that the fluid forms bridges poorly, and that the filtrate loss is higher opposed to fluids that have greater normalized average pressure.

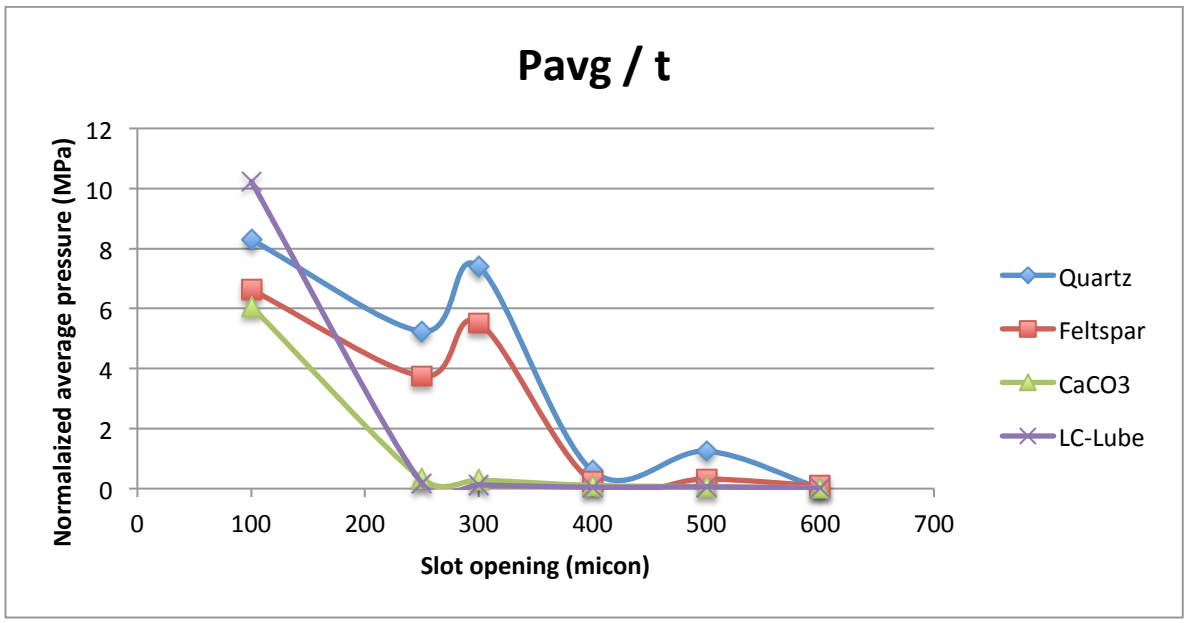

Figure 4.11: Normalized average pressure (Pavg/t).

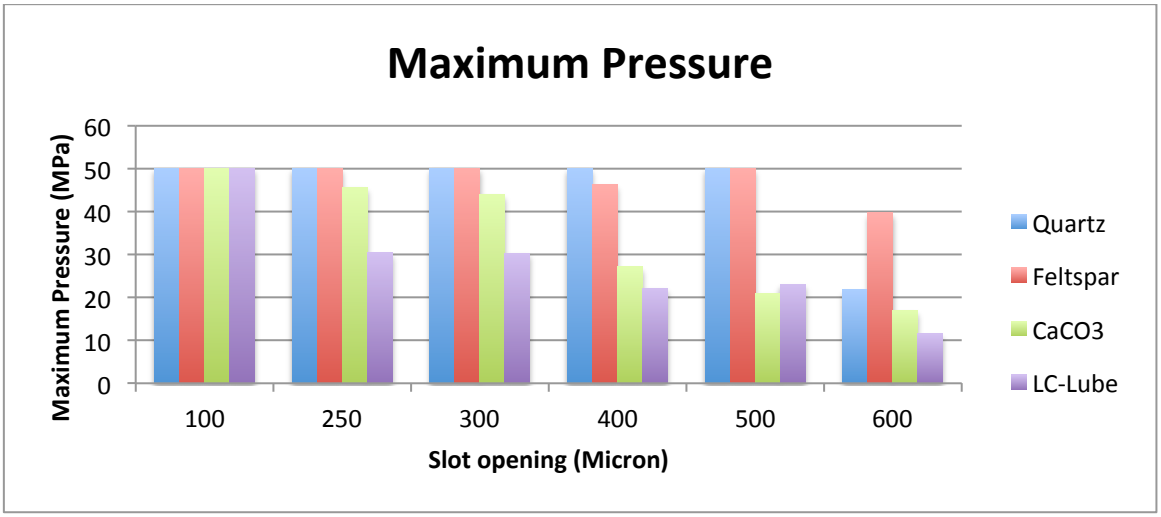

Figure 4.12: Maximum pressure for the different lost circulation materials.

Figure 4.12 shows the maximum recorded pressure for the different mixtures. The ones with a maximum pressure of 50MPa (500bar) have formed a bridge. Undoubtedly, Quartz and Feldspar show best performances, and creates bridges for fractures up to 500 micron.

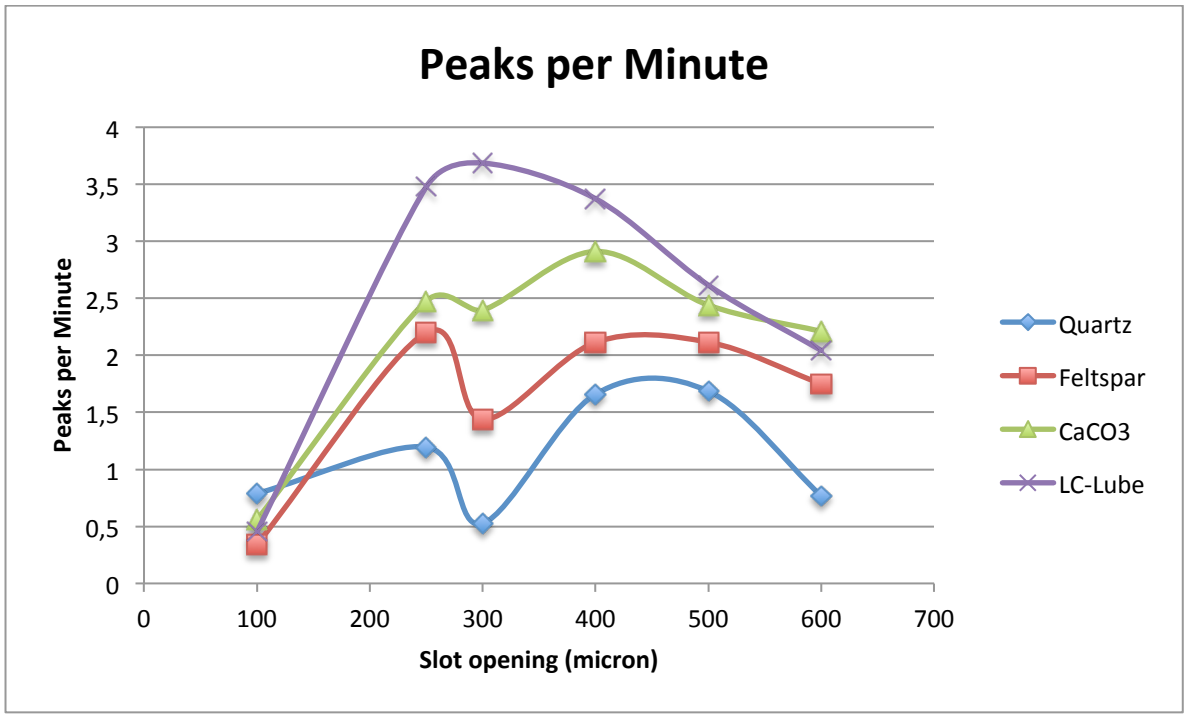

Figure 4.13: Peaks per minute plotted against slot opening.

It can be observed from Figure 4.13 that Quartz was the most stable material used in the experiments. However, CaCO3 and Feldspar also show relatively stable bridge forming. LC-Lube had the poorest results of all the materials.

4.2.7.1 Synergies

Synergy tests were conducted by mixing any two materials together. Table 3.5 at page 51 show the ratio that was mixed. The graphs below show the results and will be commented and discussed in the following. For these tests a slot opening of 400-micron was used.

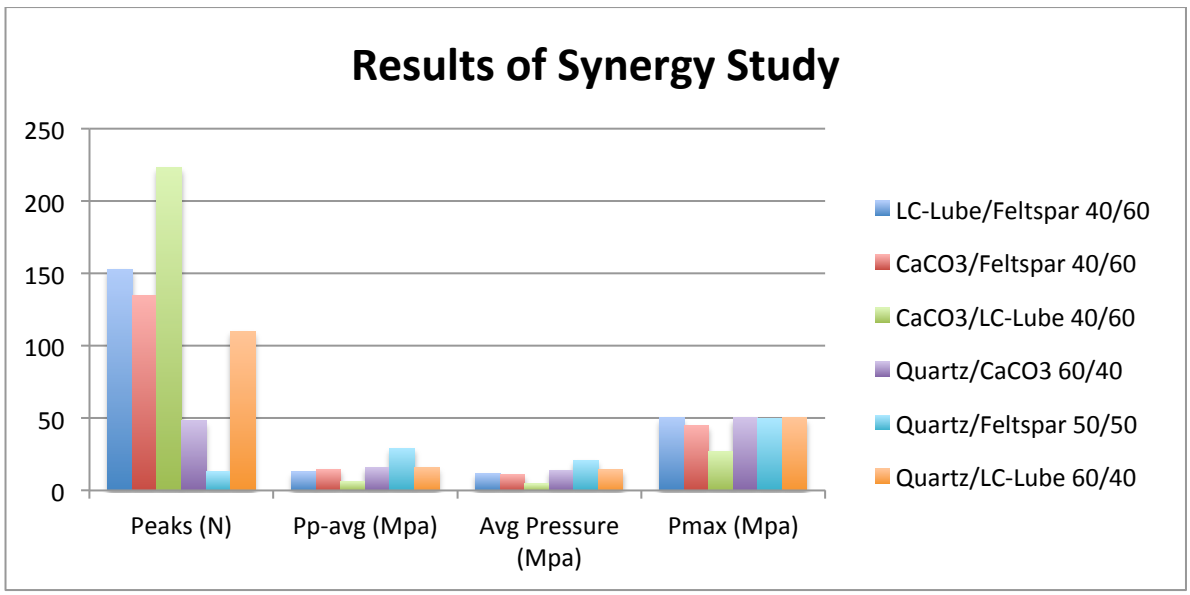

Figure 4.14: Results from the synergy experiments.

In the figure above, the results from the synergy tests are shown as columns. Best performance was observed for Quartz and Feldspar in a 50/50 mix. These two particles scored best on every parameter. Worst out was CaCO3 and LC-Lube (graphite), which is an interesting observation because these two materials are heavily used together in the industry as LCM. However, since CaCO3 dissolves in HCl, it is profitable to use these two materials in the pay zone, where skin could become a problem. This will be discussed further, later in this section.

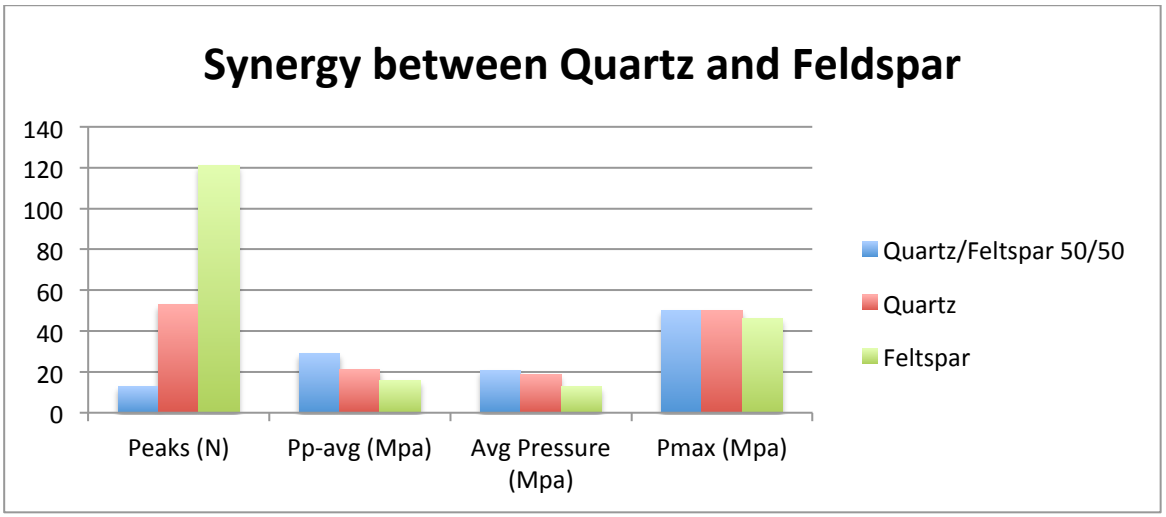

Figure 4.15: All parameters for synergy between Quartz and Feldspar

As discussed earlier, mixing 50/50 of Quartz and Feldspar had the best results when comparing all synergy experiments. However, Quartz performed better alone, as could be seen from Figure 4.15. Feldspar on the other hand seemed to be improved when mixed with Quartz.

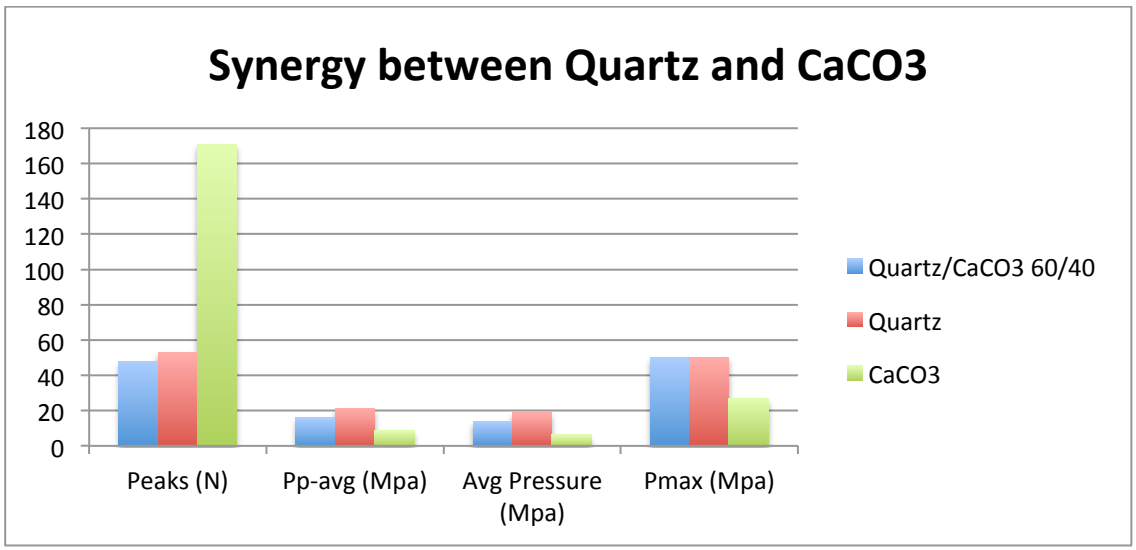

Figure 4.16: All parameters for synergy between Quartz and CaCO3.

As could be seen from Figure 4.16 CaCO3 combined with Quartz gave poorer results than Quartz or CaCO3 alone. However, CaCO3 did not seem to have a too negative effect on Quartz. The Quartz/CaCO3 mix and Quartz alone had very similar results, meaning that Quartz and CaCO3 could be used together in drilling fluid without compromising the fluid's ability to form a fracture bridge. The abrasiveness of Quartz is significantly higher than for CaCO3. During circulation, CaCO3 could reduce significantly in size when combined with Quartz particles due to the Quartz's abrasive properties.

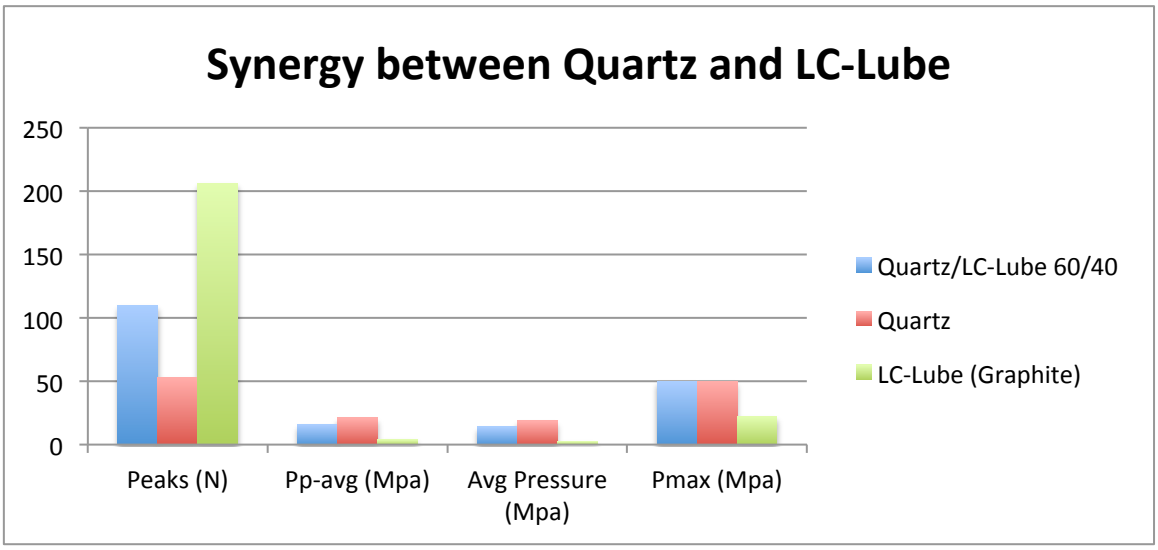

Figure 4.17: All parameters for synergy between Quartz and LC-Lube.

Unlike CaCO3, LC-Lube seemed to weaken the fluid's bridging capability. The mixture had poorer results for all parameters except Maximum recorded pressure. This indicates that even though the results were poor; the fluid still has the capability of forming strong, but unstable bridges.

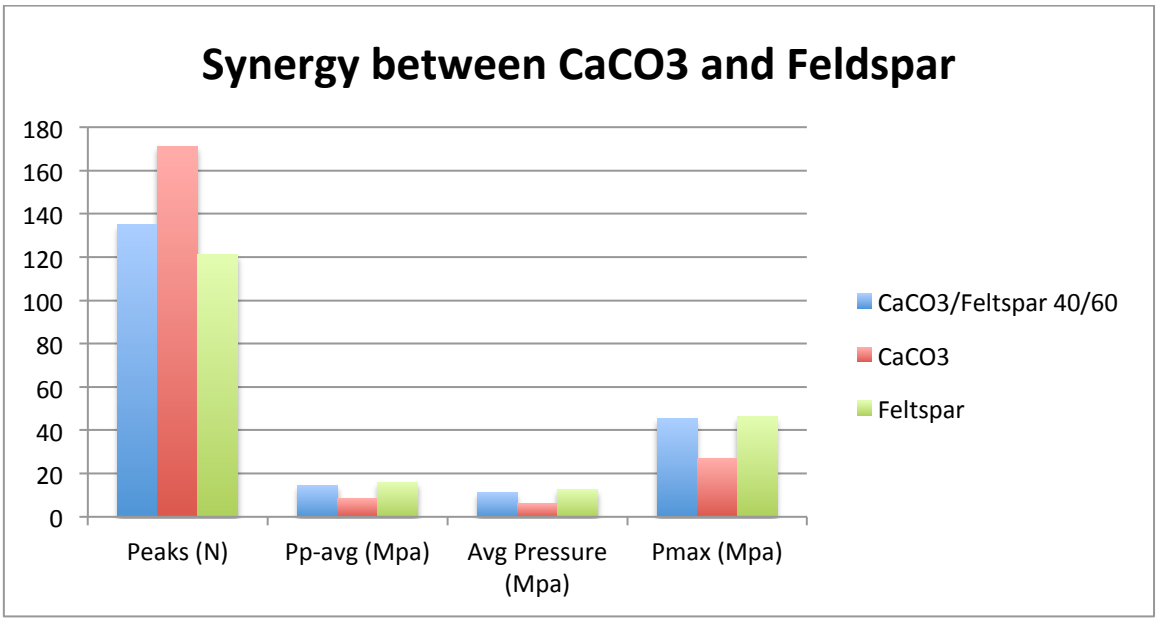

Figure 4.18: All parameters for synergy between CaCO3 and Feldspar.

Figure 4.18 shows that having both Feldspar and CaCO3 in the fluid would aggravate the fluid opposed to using Feldspar alone. Nevertheless, Pavg and Pp-avg are almost the same for Feldspar alone and the mixture. This indicates that the mixture will still be able to heal fractures and increase the fracture gradient.

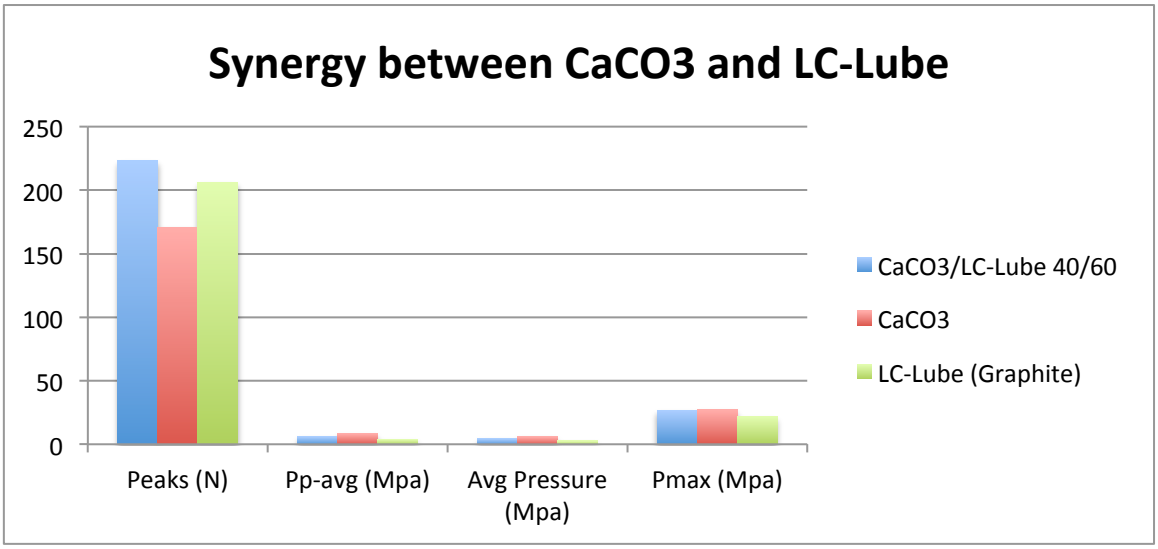

Figure 4.19: All parameters for synergy between CaCO3 and LC-Lube.

The most interesting observation during the synergy experiments was seen for a mixture of CaCO3 and LC-Lube (graphite). These two materials are used as LCM in the industry, but showed poor results in this experiment. Figure 4.19 shows how the combination of CaCO3 and LC-Lube had worse results than CaCO3 alone. The reason for this could be a badly mixed fluid, which leads to badly distributed particles. Another reason could be that the concentration of LC-Lube is too high. This matter requires additional testing and further investigation.

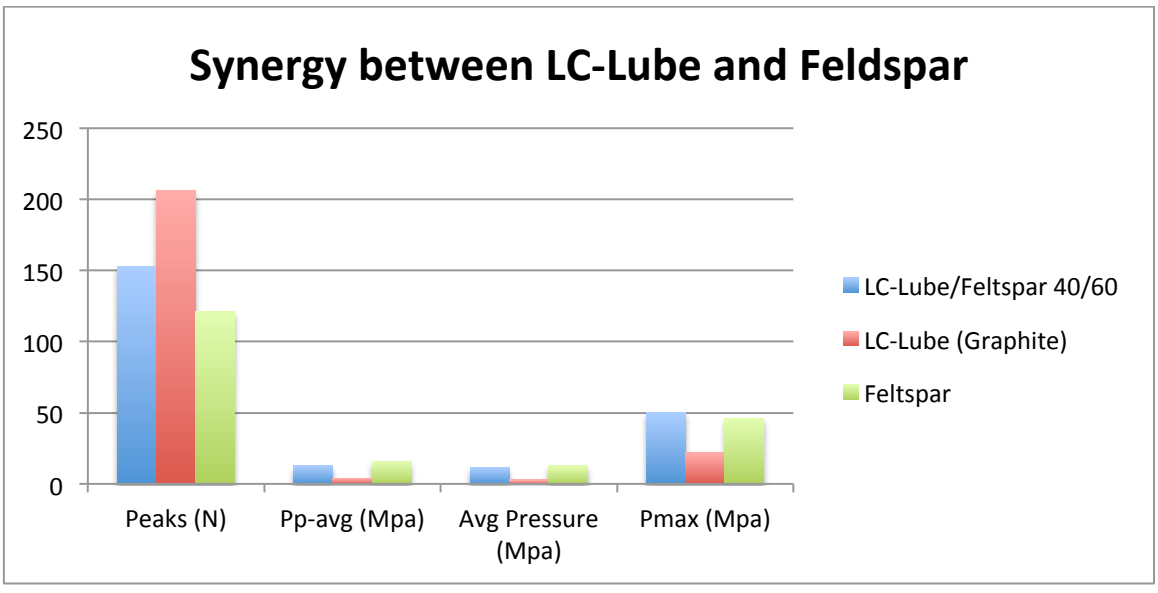

Figure 4.20: All parameters for synergy between LC-Lube and Feldspar.

The figure above shows that Feldspar is capable of holding higher pressures than both LC-Lube and the mixture of LC-Lube/Feldspar. Feldspar alone seemed to create a more stable bridge, but the mixture of LC-Lube and Feldspar had a higher maximum recorded pressure. This is somewhat an inconsistency in the results. No other significant improvement from mixing these materials was observed.

From all tests, the general perception is that particles high up on the Mohs scale performed better. It is assumed here that these materials have a higher yield strength opposed to the ones that are lower down on Mohs scale. This fact supports the Estaoplastic frature theory, which states that the bridge's strength is a function of the particles yield strength. No positive synergies were found between the four materials that were tested, with regards to bridging strength. For water based mud systems, the combination of CaCO3 and Graphite usually has a positive effect. It is not possible to tell why the CaCO3/LC-Lube mix did not perform as expected. A reason could be that the friction between particles is less for oil based mud systems opposed to water based systems. This lower friction might cause the bridge to collapse at a lower pressure than for WBM systems.

Looking at the average pressure for 250 and 500-micron slot, it is possible to see that both Quartz and Feldspar have a stronger bridge. Table 4.3 and Table 4.4 below show the difference in average pressure, also shown as percentage where CaCO3 is used as reference pressure. Feldspar has the highest average pressure for the 250 micron slot test, 48.9% higher than the average pressure of CaCO3. All materials show decreasing average pressure as the slot opening increases. Quartz and Feldspar does, however, show a much better performance for bigger slot openings compared to CaCO3 and LC-Lube. For the 500 micron slot test, Quartz has a average pressure 400% higher than CaCO3, which is significant.

	Avg. Pressure 250µm	%-difference
CaCO3	19.48	0
Quartz	26.30	35.04
Feldspar	29	48.87
LC-Lube	10.32	-47.02

Table 4.3: Average pressure compared for 250 micron test.

	Avg. Pressure 500µm	%-difference
CaCO3	3.52	0
Quartz	17.73	403.7
Feldspar	10.66	202.8
LC-Lube	3.68	4.545

Table 4.4: Average pressure compared for 500 micron test.

4.3 Practical Considerations

The results discussed above are giving insight in how the different materials act as lost circulation materials. Nevertheless, it is important to remember that all experiments were conducted with a static apparatus, and does not fully reflect how the different fluids behave in a dynamic environment where the fluid is circulated.

Below are some uncertainties and consideration discussed, and also thoughts around how to use results from this thesis in field-test are reflected on.

4.3.1 Dynamic Versus Static Tests

During drilling, the drilling fluid is circulated. The circulation causes particles in the drilling fluid to form a filter cake at the wellbore wall as well as it introduces an additional pressure due to friction. Also, circulation of fluid will introduce erosion on the filter cake at the wellbore wall. It will also cause erosion on the bridges that are being formed in the fracture mouths. These effects are not present in a static bridge test. It is therefore important to find a circulation rate that is high enough to avoid sagging, and low enough to maintain stable and strong fracture bridges. Dynamic bridge testing should be investigated in the future for OBMs.

Also, Quartz and Feldspar are abrasive particles. As a result of their abrasiveness, these particles are not very suitable to mix into the active drilling fluid. The particles could damage the drillstring and surface equipment when the drilling fluid is circulated in the well.

4.3.2 Sagging and Rheology

It was earlier mentioned that CaCO3 and Graphite tend to affect the fluid's rheology. When CaCO3 are used, it might be necessary to monitor the fluid's rheological properties. A too high viscosity could result in a too high ECD during the drilling operation, due to higher friction higher friction between the drillstring and the wellbore wall. If the fluid's viscosity is too low, the particles tend to settle out at the low side of the wellbore wall. This is referred to as sagging in the upstream branch of the petroleum industry. By using Quartz or Feldspar, sagging and erosion problems could be introduced. Thus, the concentration of the particles should be as low as possible, but still high enough to effectively form bridges. Also, particles with low bulk density should possibly be used. In the pay zone, CaCO3 is better suited because it can be removed with acid treatment.

4.3.3 Screen Selection and Wear

In the theoretical part of this thesis, the screen selection and wear were slightly introduced. When drilling offshore, the shakers must be optimized to maintain a PSD that is suitable to create bridges. This include analysis of the cut point of the different screens, since the Mesh number evidently does not say anything about the wire thickness and the aperture opening

of the screens. As a general practice, the PSD should be monitored continuously during the drilling operation since the shakers will sort out the coarsest particles. This could be done with the use of laboratory sieves or a photo-optical fluid analyser.

4.3.4 Concentration of Particles

The concentration of particles plays a role when it comes to bridging properties. Higher concentrations tend to make the fluid more suitable to create bridges more effectively and quicker. This study shows that Quartz and Feldspar creates bridges effectively also at low concentrations, 39 kg/m3 in this thesis. Sagging has not been analysed in this work, but since Quartz and Feldspar does not dissolve in the fluid the same way CaCO3 does, a sag analysis should be done to determine maximum concentration of these types of materials. In the case of very high loss rates, the concentration could be increased in order to create bridges quicker and more effectively.

4.3.5 Water-based - vs. Oil-based fluid Systems

There are not many studies done on LCM in oil based mud system. The ones that have been done are showing that bridges formed by LCM in OBM are less stable than bridges formed by LCM in WBM. This could be because the friction between the particles that form the bridge is less in oil-based systems opposed to water-based systems. The oil-based fluid used in this work has not been compared to similar studies for water based fluid because the water-based fluid in previous experiments had very different properties, regarding rheology and density. Differences in bridging capability for water-based – and oil-based fluid systems should be investigated further in order to understand why oil-based fluids tend to form less stable bridges.

4.3.6 Field Testing

As the yield strength of these particles is overcome, the bridge will collapse and the fracture will be able to grow further (losses occur).
In this thesis work, two fracture theories have been introduced. The wellbore strengthening theory and the Elastoplastic theory have been explained. These two theories are fundamentally different as these describe the forming of bridges differently. Mainly, the Elstoplastic fracture theory requires particles sizes to be the same as the fracture opening. The fluid must also be able to form bridges that are tight and able to seal the fracture. When this is achieved, the strength of the particles in the bridge will govern the fracture gradient. There are many different wellbore-strengthening theories, but all of them generally describe the same effect. For these models, the particles have to be slightly smaller than the fracture opening in order to form a bridge just inside the fracture mouth. As the well pressure is increased, the fracture width will increase. When this is happening, an additional stress will be introduced (referred to as increased hoop stress or fracture closure stress). The pressure is increased to a predetermined pressure, and then the pressure is bled off. Now, when the pressure decrease, the bridge in the fracture will keep the fracture open, and the additional

stress will still be present. In order to re-open the fracture, the well pressure has to exceed the fracture closure stress (the additional stress that has been introduced).

If a field test will be conducted, it would be interesting to use an optimized active drilling fluid. If both fracture theories are used to predetermine the fracture gradient, these models could be analysed and put against each other. Results from a study like this could be valuable information for further development of the theories and also for future drilling operations. A field-test like this could use methods mentioned in the theory part of this thesis to control and maintain the particles in the drilling fluid. This implies proper planning and selection of shaker screens before hand. And maybe even more laboratory of the drilling fluid. Quartz does not affect the rheology of the drilling fluid, but it could introduce sagging and erosion problems. Since Quartz and Feldspar are potentially damaging to the drillstring and surface equipment, other materials might be better suited. In zones known for having circulation loss problems, Quartz could be used as LCM pill. If the oil-based WARP fluid used in this experimental work is used as active drilling fluid, a LCM pill could be designed by adding Quartz (preferably) or Feldspar to the drilling fluid. The pill should be designed as following:

- Use the oil-based WARP as basis
- Add minimum 35-45 kg/m3 of Quartz (preferably) or Feldspar to fluid.
- Use a wide size distribution. Both coarse and fine particles.

The concentration of particles depends on the severity of losses, and should be known before the pill is designed. LCM with CaCO3/Graphite usually has a concentration of 350 kg/m3 of particles.[6] It is hard to predict the optimal concentration for a pill containing Quartz or Feldspar based on the results from this thesis. Quartz and Feldspar did however perform better than CaCO3 and Graphite; hence, a lower concentration would be expected to be necessary.

5 Summary and Conclusion

In this thesis work, different lost circulation materials have been tested in the lab. The following were done:

- A static bridge apparatus was used in order to see the differences of the materials.
- Synergy between the materials has been studied.
- Packing of spheres has been studied to create a theoretical particle size distribution.
- A literature study has been conducted and discussed.
- Four materials were tested as lost circulation materials.
    - Quartz
    - Feldspar
    - CaCO3
    - LC-Lube (Graphite)

This experimental study resulted in the following findings:

- A theoretical particle size distribution (PSD) was proposed. This PSD was tested in the lab, and the results were not promising. However, increasing the concentration of smaller particles improved the bridging capability of the fluid. The strength of the bridge increased as concentration of smaller particles increased. Smaller particles in the particles mix seemed to be important in order to achieve good bridging properties. As the concentration of smaller particles increased, the filtrate loss during the bridging test decreased.

- Wellbore strengthening theories rely on the fact that the near wellbore stress field is changed. However, this study shows that the fracture pressure is also governed by the bridges' strength.

- Particles in the upper part of the Mohs scale preformed better than particles in the lower part of the Mohs scale. However, harder particles could erode the drillstring and surface equipment.

- Quartz and Feldspar showed the best results. It is assumed that these particles have larger yield strength larger than CaCO3 and LC-Lube. This fact supports the elstoplastic fracture theory, which states that the fracture pressure increases if particles with high yield strength are used.

- In terms of average pressure measured during the bridge testing, all materials had a decreasing trend. The decrease in average pressure was significantly higher for CaCO3 and LC-Lube compared to Quartz and Feldspar. For the 250-micron slot test, Feldspar had an average pressure 48.8% higher than CaCO3, whereas Quartz had 35% higher average pressure. The difference in average pressure was more significant for bigger slot openings. The average pressure for the 500-micron slot test

reviled that fluid with Quartz or Feldspar was more capable of forming bridges. At this test, Quartz had an average pressure 400% higher than $CaCO_3$. Quartz and Feldspar were able to form bridges for a wide spectrum of slot openings, with a concentration of 39 kg/m3.

- No positive synergies were found between the four materials, with regards to bridging strength. Water based fluids with a particle mix containing $CaCO_3$ and Graphite usually have good bridging properties. The synergy effect of $CaCO_3$ and LC-Lube did show a negative effect for the particular fluid tested in this study. Reason for this might be that the WARP fluid used in this study is oil-based, hence, the friction between the particles in the bridge is less than in a water based fluid. Due to this fact, the bridge might collapse at a lower pressure than for water-based systems.

- A field test has been proposed, and practical considerations have been discussed. However, other particles than Quartz and Feldspar should probably be used due to the abrasive properties of these materials. However, in known loss zones, Quartz or Feldspar could be used to design a LCM pill. The oil-based WARP fluid would in that case be used as base fluid, with a minimum concentration of 35-45 kg/m3 of Quartz or Feldspar mixed in the fluid. The size distribution should be wide, including both coarse and fine particles.

References

1. Aadnoy, B.S., *Modern well design*. 2nd ed. 2010, CRC Press/Balkema. 9780415884679

2. Mitchell, R.F., et al., *Fundamentals of drilling engineering*. SPE textbook series. 2011, Society of Petroleum Engineers. 9781555632076

3. Aadnoy, B.S., et al., *Design of Well Barriers To Combat Circulation Losses.* SPE Drilling & Completion, 2008. **23**(3): p. pp. 295-300.

4. Aadnoy, B.S., E. Kaarstad, and M. Belayneh, *Elastoplastic Fracture Model Improves Predictions in Deviated Wells*, SPE-110355-MS, 2007, Society of Petroleum Engineers

5. Looyeh, R. and B.S. Aadnoy, *Petroleum rock mechanics : drilling operations and well design*. 1st ed. 2011, Gulf Professional Pub. 9780123855466

6. *Wellbore Stability and Lost Circulation GL3504*: Statoil ASA.

7. Onyia, E.C., *Experimental Data Analysis of Lost Circulation Problems During Drilling With Oil-Based Mud.* SPE Drilling & Completion, 1994. **9**(1): p. 25-31.

8. Fuh, G.-F., et al., *A New Approach to Preventing Lost Circulation While Drilling*, 00024599, 1992, 1992 Copyright 1992, Society of Petroleum Engineers Inc.

9. Collins, N., et al., *Comprehensive Approach to Severe Lost Circulation Problems in Russia*, SPE-135704-MS, 2010, Society of Petroleum Engineers

10. Halliburton. *Engineered WellSET™ Treatment Service Helps Prevent Lost Circulation by Strengthening the Wellbore*. 2007 [cited 2013 17. May]; Available from: http://www.halliburton.com/public/bar/contents/Data_Sheets/web/Sales_Data_Sheets/SDS-058.pdf.

11. Alberty, M.W. and M.R. McLean, *A Physical Model for Stress Cages*, 00090493, 2004, Society of Petroleum Engineers

12. Duffadar, R., F. Dupriest, and S. Zeilinger, *Practical Guide to Lost Returns Treatment Selection Based on a Holistic Model of the State of the Near Wellbore Stresses*, SPE-163481-MS, 2013, 2013, SPE/IADC Drilling Conference and Exhibition

13. Dupriest, F.E., *Fracture Closure Stress (FCS) and Lost Returns Practices*, 00092192, 2005, SPE/IADC Drilling Conference

14. Whitfill, D.L., D.E. Jamison, and H. Wang, *Lost Circulation Material Selection, Particle Size Distribution and Fracture Modeling with Fracture Simulation Software*, SPE-115039-MS, 2008, IADC/SPE Asia Pacific Drilling Technology Conference and Exhibition

15. Barrett, S., et al., *Wellbore Strengthening: Where Field Application Meets Theory*, SPE-139167-MS, 2010, Society of Petroleum Engineers

16. Aadnoy, B.S., *Quality Assurance of Wellbore Stability Analyses*, SPE-140205-MS, 2011, SPE/IADC Drilling Conference and Exhibition

17. Gonzalez, M.E., et al., *Increasing Effective Fracture Gradients by Managing Wellbore Temperatures*, 00087217, 2004, IADC/SPE Drilling Conference

18. Gil, I.R., J.-C. Roegiers, and D. Moos, *Wellbore Cooling as a Means To Permanently Increase Fracture Gradient*, SPE-103256-MS, 2006, Society of Petroleum Engineers

19. Vickers, S.R., et al., *The Application of Specifically Formulated Bridging Materials To Successfully Reduce Pore Pressure Transmission To Enable Depleted Fractured Reservoirs To Be Drilled and Produced Without Incurring Formation Damage*, SPE-107753-MS, 2007, Society of Petroleum Engineers

20. Weisstein, E.W. *Kepler Conjecture.* [cited 2013 23. April]; Available from: http://mathworld.wolfram.com/KeplerConjecture.html.

21. Hales, T.C. *An overview of the Kepler conjecture*. 1998 [cited 2013 22. April]; Available from: http://arxiv.org/pdf/math/9811071v2.pdf.

22. Weisstein, E.W. *Hexagonal Close Packing.* MathWorld - A Wolfram Web Resource. [cited 2013 22. April]; Available from: http://mathworld.wolfram.com/HexagonalClosePacking.html.

23. Ott, W.K. and P.E. Woods, *Modern Sandface Completion Practices Handbook*. 2nd ed. 2003, Gulf Publishing Company.

24. Schechter, R.S., *Oil well stimulation*. 1992, Prentice Hall. 0139499342

25. MacDonald, M.J., et al., *A Generalized Blake-Kozeny Equation for Multisized Spherical Particles.* AlChE Journal, 1991. **37**(10): p. 1583-1588.

26. Saasen, A., et al., *Permanent Abandonment of a North Sea Well Using Unconsolidated Well-Plugging Material.* SPE Drilling & Completion, 2011. **26**(3): p. pp. 371-375.

27. Grannes, I. *Sandaband Presentation*. 2011 [cited 2013 23. April]; Available from: http://www.norskoljeoggass.no/PageFiles/10706/7 Sandaband - Non consolidating plugging material.pdf

28. Abrams, A., *Mud Design To Minimize Rock Impairment Due To Particle Invasion.* Journal of Petroleum Technology, 1977. **29**(5): p. 586-592.

29. Vickers, S.R., et al., *A new methodology that surpasses current bridging theories to efficiently seal a varied pore throat distribution as found in natural reservoir formations*, AADE-06-DF-HO-16, 2006, American Association Of Drilling Engineers

30. Dick, M.A., et al., *Optimizing the Selection of Bridging Particles for Reservoir Drilling Fluids*, 00058793, 2000, Copyright 2000, Society of Petroleum Engineers Inc.

31. Omland, T.H., et al., *Improved Drilling Process Control Through Continuous Particle and Cuttings Monitoring*, SPE-107547-MS, 2007, Society of Petroleum Engineers

32. Dahl, B., A. Saasen, and T.H. Omland, *Successful Drilling of Oil and Gas Wells by Optimal Drilling-Fluid Solids Control A Practical and Theoretical Evaluation*, SPE-103934-MS, 2006, Society of Petroleum Engineers

33. Dahl, B.r., A. Saasen, and T.H. Omland, *Optimised solids control in arctic environments*, SPE-160574-MS, 2012, Society of Petroleum Engineers

34. Omland, T.H., et al., *Optimisation of Solids Control Opens Up Opportunities for Drilling of Depleted Reservoirs*, SPE-110544-MS, 2007, Society of Petroleum Engineers

35. Toroqi, S.V.M., *Experimental Analysis and Mechanistic Modeling of Wellbore Strengthening*, in *DEPARTMENT OF CHEMICAL AND PETROLEUM ENGINEERING*2011, UNIVERSITY OF CALGARY.

Appendices

A Particle Size Distribution of Unmodified Drilling Fluid

MALVERN INSTRUMENTS

MASTERSIZER 2000

Result Analysis Report

Sample Name: after-shaker-mud-I - Average	**SOP Name:** OB WARP Barite	**Measured:** 12. april 2013 14:53:04	
Sample Source & type: Supplier	**Measured by:** BBleie	**Analysed:** 12. april 2013 14:53:05	
Sample bulk lot ref:	**Result Source:** Averaged		
Particle Name: Barium Sulphate avg	**Accessory Name:** Hydro 2000SM (A)	**Analysis model:** General purpose	**Sensitivity:** Enhanced
Particle RI: 1.643	**Absorption:** 0.1	**Size range:** 0.020 to 2000.000 um	**Obscuration:** 18.43 %
Dispersant Name: Xylene/2Propanol	**Dispersant RI:** 1.410	**Weighted Residual:** 0.934 %	**Result Emulation:** Off
Concentration: 0.0050 %Vol	**Span :** 10.320	**Uniformity:** 3.01	**Result units:** Volume
Specific Surface Area: 3.63 m²/g	**Surface Weighted Mean D[3,2]:** 1.655 um	**Vol. Weighted Mean D[4,3]:** 7.627 um	

d(0.1): 0.744 um **d(0.5):** 2.129 um **d(0.9):** 22.717 um

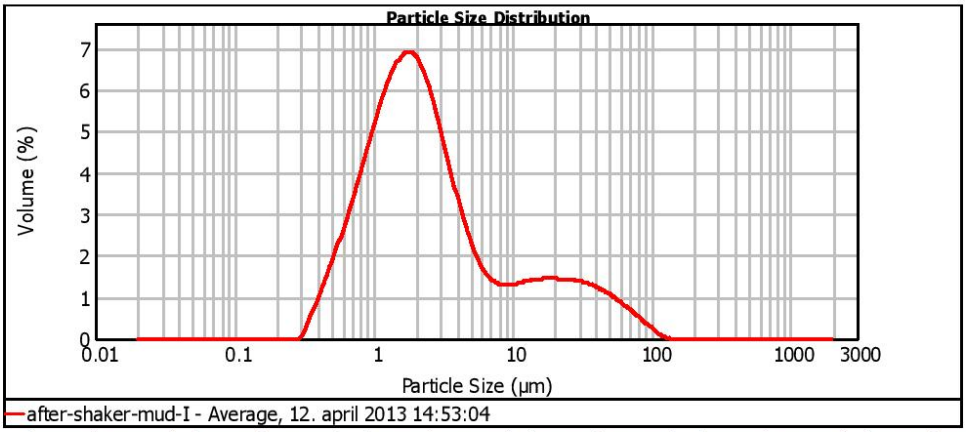

Size (µm)	Volume In %	Size (µm)	Volume In %	Size (µm)	Volume In %	Size (µm)	Volume In %	Size (µm)	Volume In %	Size (µm)	Volume In %
0.010	0.00	0.105	0.00	1.096	5.29	11.482	1.25	120.226	0.02	1258.925	0.00
0.011	0.00	0.120	0.00	1.259	5.77	13.183	1.28	138.038	0.00	1445.440	0.00
0.013	0.00	0.138	0.00	1.445	6.11	15.136	1.30	158.489	0.00	1659.587	0.00
0.015	0.00	0.158	0.00	1.660	6.23	17.378	1.31	181.970	0.00	1905.461	0.00
0.017	0.00	0.182	0.00	1.905	6.10	19.953	1.30	208.930	0.00	2187.762	0.00
0.020	0.00	0.209	0.00	2.188	5.72	22.909	1.29	239.883	0.00	2511.886	0.00
0.023	0.00	0.240	0.00	2.512	5.14	26.303	1.26	275.423	0.00	2884.032	0.00
0.026	0.00	0.275	0.02	2.884	4.44	30.200	1.22	316.228	0.00	3311.311	0.00
0.030	0.00	0.316	0.39	3.311	3.69	34.674	1.16	363.078	0.00	3801.894	0.00
0.035	0.00	0.363	0.79	3.802	2.97	39.811	1.08	416.869	0.00	4365.158	0.00
0.040	0.00	0.417	1.26	4.365	2.34	45.709	0.98	478.630	0.00	5011.872	0.00
0.046	0.00	0.479	1.76	5.012	1.84	52.481	0.86	549.541	0.00	5754.399	0.00
0.052	0.00	0.550	2.30	5.754	1.49	60.256	0.71	630.957	0.00	6606.934	0.00
0.060	0.00	0.631	2.87	6.607	1.28	69.183	0.56	724.436	0.00	7585.776	0.00
0.069	0.00	0.724	3.48	7.586	1.18	79.433	0.40	831.764	0.00	8709.636	0.00
0.079	0.00	0.832	4.10	8.710	1.17	91.201	0.26	954.993	0.00	10000.000	
0.091	0.00	0.955	4.71	10.000	1.20	104.713	0.10	1096.478	0.00		
0.105		1.096		11.482		120.226		1258.925			

Operator notes:

Malvern Instruments Ltd.
Malvern, UK
Tel : = +[44] (0) 1684-892456 Fax +[44] (0) 1684-892789

Mastersizer 2000 Ver. 5.60
Serial Number : MAL100477

File name: student-project-sigurd-lund
Record Number: 28
12.04.2013 15:27:37

MASTERSIZER 2000

Result Analysis Report

Sample Name: before-shaker-mud-I - Average
SOP Name: OB WARP Barite
Measured: 12. april 2013 14:26:33
Sample Source & type: Supplier
Measured by: BBleie
Analysed: 12. april 2013 14:26:34
Sample bulk lot ref:
Result Source: Averaged

Particle Name: Barium Sulphate avg	**Accessory Name:** Hydro 2000SM (A)	**Analysis model:** General purpose	**Sensitivity:** Enhanced
Particle RI: 1.643	**Absorption:** 0.1	**Size range:** 0.020 to 2000.000 um	**Obscuration:** 16.93 %
Dispersant Name: Xylene/2Propanol	**Dispersant RI:** 1.410	**Weighted Residual:** 0.990 %	**Result Emulation:** Off
Concentration: 0.0045 %Vol	**Span :** 9.838	**Uniformity:** 2.96	**Result units:** Volume
Specific Surface Area: 3.59 m²/g	**Surface Weighted Mean D[3,2]:** 1.669 um	**Vol. Weighted Mean D[4,3]:** 7.579 um	

d(0.1): 0.752 um **d(0.5):** 2.143 um **d(0.9):** 21.836 um

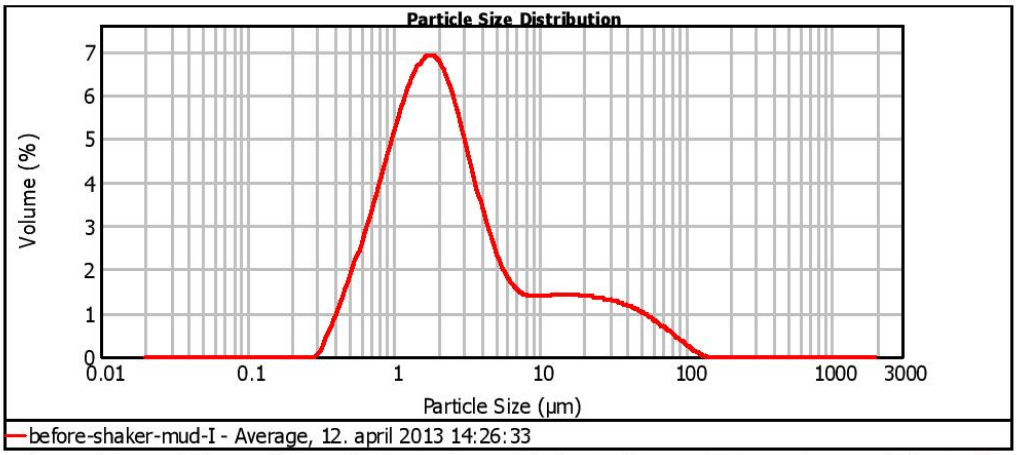

Size (µm)	Volume In %	Size (µm)	Volume In %	Size (µm)	Volume In %	Size (µm)	Volume In %	Size (µm)	Volume In %	Size (µm)	Volume In %
0.010	0.00	0.105	0.00	1.096	5.29	11.482	1.27	120.226	0.04	1258.925	0.00
0.011	0.00	0.120	0.00	1.259	5.77	13.183	1.29	138.038	0.00	1445.440	0.00
0.013	0.00	0.138	0.00	1.445	6.11	15.136	1.28	158.489	0.00	1659.587	0.00
0.015	0.00	0.158	0.00	1.660	6.23	17.378	1.27	181.970	0.00	1905.461	0.00
0.017	0.00	0.182	0.00	1.905	6.10	19.953	1.25	208.930	0.00	2187.762	0.00
0.020	0.00	0.209	0.00	2.188	5.73	22.909	1.22	239.883	0.00	2511.886	0.00
0.023	0.00	0.240	0.00	2.512	5.16	26.303	1.19	275.423	0.00	2884.032	0.00
0.026	0.00	0.275	0.01	2.884	4.47	30.200	1.15	316.228	0.00	3311.311	0.00
0.030	0.00	0.316	0.33	3.311	3.73	34.674	1.10	363.078	0.00	3801.894	0.00
0.035	0.00	0.363	0.75	3.802	3.03	39.811	1.03	416.869	0.00	4365.158	0.00
0.040	0.00	0.417	1.22	4.365	2.41	45.709	0.94	478.630	0.00	5011.872	0.00
0.046	0.00	0.479	1.72	5.012	1.93	52.481	0.83	549.541	0.00	5754.399	0.00
0.052	0.00	0.550	2.27	5.754	1.59	60.256	0.70	630.957	0.00	6606.934	0.00
0.060	0.00	0.631	2.85	6.607	1.38	69.183	0.56	724.436	0.00	7585.776	0.00
0.069	0.00	0.724	3.46	7.586	1.27	79.433	0.41	831.764	0.00	8709.636	0.00
0.079	0.00	0.832	4.08	8.710	1.24	91.201	0.28	954.993	0.00	10000.000	
0.091	0.00	0.955	4.71	10.000	1.25	104.713	0.13	1096.478	0.00		
0.105	0.00	1.096		11.482		120.226		1258.925	0.00		

Operator notes:

Malvern Instruments Ltd.
Malvern, UK
Tel : = +[44] (0) 1684-892456 Fax +[44] (0) 1684-892789

Mastersizer 2000 Ver. 5.60
Serial Number : MAL100477

File name: student-project-sigurd-lund
Record Number: 16
12.04.2013 15:27:19